Structure-based Design and Synthesis of Novel Akt Inhibitors for Pre-clinical Evaluation in Lung Cancer Cell lines

THESIS

Submitted in partial fulfilment

of the requirements for the degree of

DOCTOR OF PHILOSOPHY

by

VENKATA SAKETH SRIRAM D

ID No 2011PHXF419H

Under the Supervision of
Prof. P. YOGEESWARI

Co-Supervisor
Dr. Srikant Viswanadha

BITS Pilani
Pilani | Dubai | Goa | Hyderabad

BIRLA INSTITUTE OF TECHNOLOGY AND SCIENCE, PILANI

2014

BIRLA INSTITUTE OF TECHNOLOGY AND SCIENCE, PILANI

CERTIFICATE

This is to certify that the thesis entitled "**Structure-based Design and Synthesis of Novel Akt Inhibitors for Pre-clinical Evaluation in Lung Cancer Cell lines**" submitted by **VENKATA SAKETH SRIRAM D**, ID No. **2011PHXF419H** for award of Ph.D. of the Institute embodies original work done by him under my supervision.

Signature of the Supervisor: Co-supervisor

Name in capital letters   : **P.YOGEESWARI**   **SRIKANT VISWANADHA**

Designation   : **Professor**   **Vice-President, Drug Discovery**

Incozen Therapeutics Pvt. Ltd.

Date:

"Medicine, the only profession that labours incessantly to destroy the reason for its existence"

James Bryce, British jurist, historian and politician

ACKNOWLEDGEMENTS

I express my gratitude to Dr. Shrikant Charde, HOD, Department of pharmacy and other faculty members Dr. Punna Rao Ravi, Dr. Vamsi Krishna Venuganti, Dr. Swati Biswas, Dr. Balaram Ghosh, Dr. Onkar Kulkarni, Dr. Arti Dhar and past faculty Dr. AV Ramani, Mr. Aditya and Mr. Rahul Vats for their help during my doctoral thesis.

I would like to thank Mr. Sateesh M, Mr. Sridhar V, Dr. Kasi Viswanath, Mr. Uday S, Mr. Prashant B and Dr. Prajak B and all my other collegues at Incozen for their support during my stay there. Special thanks to Vasanth, Garima, Srinivas, Ratnajee and Sathish for their endless discussions and arguments, both scientific and non-scientific.

I am grateful to have a lot of friends and fellow Ph.D. students at BITS including Praveen, Gangadhar, Poorna, Shailender, Brahmam Suman, Mahesh and Srikanth. A special thanks to Madhu, Reshma, Radhika and Ganesh S for helping me with my research work and shaping my thesis.

Most importantly, I would like to acknowledge my parents Sai Rama Rao and Vani along with my sister Saranya for being a constant support and making me who I am today. No words can express how grateful I am for your love and support and how much I appreciate and love you.

*Finally, I would like to dedicate this work to my grandfather, **Mr. V Krishna Rao,** a wise man and a visionary who made me take the road not taken. Being a scientist rather than an engineer, although not an easy decision, made me be myself.*

ABSTRACT

Akt is a serine/ threonine kinase which phosphorylates a myriad of substrates responsible for cell growth, survival and protein synthesis. Akt is overexpressed in wide varieties of cancers due to several factors including mutations in PI3K/Akt pathway, mutations in growth factor receptors and amplification of Akt kinase activity. Inhibition of Akt is a proven strategy for the treatment of cancer and allosteric inhibition represents a greater specificity towards Akt.

In the present study, a novel scaffold of compounds were identified as an allosteric Akt inhibitor through a combination of e-pharmacophore modelling of allosteric site of Akt and virtual screening of a large dataset chemical library. Akt inhibition was confirmed by biochemical enzymatic reaction and antiproliferative activity was evaluated in various lung cancer cell lines in comparison with normal cells. Further to develop a significant SAR, various derivatives of the identified lead **6** were designed, synthesized and characterized as a lead optimised step.

Among the analogues synthesized, compound **6j** [*N-(3-Acetamidophenyl)-2-((2-methyl-5,6,7,8-tetrahydrobenzo(4,5)thieno(2,3-d)pyrimidin-4-yl)thio)acetamide*] was found to the most active in anti-cancer assays including apoptotic assays. Compound **6j** was found to induce apoptosis through a combination of increased reactive oxygen species and caspase-3 association. At 10 nM and 100 nM concentrations, compound **6j** also abrogated downstream Akt pathway as measured by the amount of pAkt (S^{473}) in lung cancer cell lines. Plasma and metabolic stability studies of compound **6j** indicated that the compound could be administered through parenteral route. Selectivity against a panel of kinases was also performed and at 5 μM concentration compound **6j** was found to be a specific inhibitor to only Akt1, Akt2 and Akt3.

Concomitantly, by incremental exposure to MK2206, a standard allosteric Akt inhibitor, stable Akt inhibitor resistant lung cancer cell lines were developed. MK2206 resistant cell lines were evaluated for changes in biomarkers involved in the oncogenic process by either western blotting or LC-MS analysis. Incremental exposure to MK2206 in H460 and A549 cell lines resulted in stable resistant cell lines (H460R and A549R) with a rightward shift in GI_{50} of MK2206 by 10 and 5-fold respectively. Resistant cells showed down regulation of Akt pathway as evident by the lack of pAkt (S^{473}) and pAkt (T^{308}) levels albeit a comparable total Akt. cMyc levels were found to be elevated in resistant cells along with an increase in glutaminase expression. Addition of specific cMyc and glutaminase inhibitors reversed the resistance of cell lines to MK2206 besides potentiating the effect of MK2206 in both sensitive as well as resistant cell lines. Resistant cell lines were found to be 10-fold more sensitive to a combination of MK2206 and cMyc (10058-F4) or glutaminase (CB-839) inhibitors.

In conclusion, novel allosteric Akt inhibitors were synthesized and characterized for their anti-cancer activity. Mechanism for resistance to Akt inhibitors was identified and novel combination strategies to overcome this resistance were investigated.

TABLE OF CONTENTS

LIST OF TABLES

LIST OF FIGURES

ABBREVATIONS

3D   : 3-Dimensional

4EBP   : Eukaryotic translation initiation factor 4E-binding protein

5'-TOP   : 5' -terminal oligopolypyrimidine

ADME   : Absorption, distribution, metabolism and elimination

Akt   : V-akt murine thymoma viral oncogene homolog 1

Akti   : Akt inhibitor

AML   : Acute myeloid leukaemia

AMP   : Adenosine monophosphate

ANOVA   : Analysis of variance

ATCC   : American type culture collection

ATP   : Adenosine triphosphate

BAD   : Bcl-2-associated death promoter

BEDROC   : Boltzmann-enhanced discrimination of receiver operating characteristic

BRAF   : v-raf murine sarcoma viral oncogene homolog B

BSA   : Bovine serum albumin

CAT   : central kinase catalytic

CEC   : Circulating endothelial cells

CGH   : Comparitive genomic hybridisation

cGMP   : Cyclic guanosine monophosphate

CI   : Combination indices

CLL   : Chromic lymphoid leukaemia

DCFDA   : 2',7'-Dichlorodihydrofluorescein diacetate

DLBCL   : Diffuse large B-cell lymphoma

DLT   : Dose limiting toxicities

DMF   : Dimethyl formamide

DMSO   : Dimethyl sulfoxide

DNA   : Deoxyribose nucleic acid

DNA-PK   : Deoxyribose nucleic acid protein kinase

DTT   : Dithiothreitol

EDCI   : 1-Ethyl-3-(3-dimethylaminopropyl)carbodiimide

EF   : Enrichment factor

EGFR   : Epidermal growth factor receptor

eIF4E   : Eukaryotic translation initiation factor 4E

ER   : Emission ratio

ERBB   : Erythroblastic Leukemia Viral Oncogene

ESI   : Electron spray ionisation

EtOAc   : Ethyl acetate

EtOH   : Ethanol

EXT   : C-terminal extension

F-12K   : Kaighn's modification of Ham's F12 medium

FBS   : Fetal bovine serum

FITC   : Fluorochrome isothiocyanate

FLICA   : Florescent inhibitor of caspases

FOXO   : Forkhead box

FRET   : Fluorescence resonance energy transfer

GAB   : GTPase activating protein

GH   : Groodness of hit

GI_{50} : Growth inhibition 50

GLS   : Glutaminase

GMP   : Guanosine monophosphate

GPCR   : G Protein coupled receptor

GSK 3β : Glycogen synthase kinase 3β

h   : hour

HBA   : Hydrogen bond acceptor

HBD   : Hydrogen bond donor

HER	: Human epidermal growth factor
HM	: Hydrophobic motif
HoBt	: Hydroxybenzotriazole
HPLC	: High performance liquid chromatography
HRP	: Horse radish peroxidase
HTEpiC	: Human Tracheal Epithelial Cells
HTVS	: High throughput virtual screening
HUVEC	: Human Umbilical Vascular Endothelial Cells
IC_{50}	: Inhibitory concentration 50
Ki	: Dissociation constant
KIT	: Tyrosine-protein kinase
KRAS	: Kirsten rat sarcoma viral oncogene homolog
LC/MS	: Liquid chromatography in tandem with mass spectroscopy
LINK	: Linker region
MAPK	: Mitogen activated protein kinase
MDM	: Mouse double minute homologue
MEK	: Mitogen-activated protein kinase kinase
MeOH	: Methanol
MET	: Hepatocyte growth factor receptor
mmol	: Milli moles
mRNA	: Messenger ribose nucleic acid
mTOR	: Mammalian target of rapamycin
mTORC	: Mammalian target of rapamycin complex
MTD	: Maximum tolerated dose
MTT	: 3-(4,5-dimethylthiazol-2-yl)-2,5-diphenyltetrazolium bromide
MYC	: V-myc avian myelocytomatosis viral oncogene homolog
MYCi	: c-Myc inhibitor
N	: Normality
NADH	: Nicotinamide adenine dinucleotide
NADPH	: Nicotinamide adenine dinucleotide phosphate

NF κB	: Nuclear factor κB
NIH	: National institute of health, USA
nM	: Nano molar
NSCLC	: Non-small cell lung cancer
OPLS	: Optimized Potentials for Liquid Simulations
p-Akt	: Phosphorylated Akt
PARP	: Poly ADP ribose polymerase
PDB	: Protein databank
PDGFR	: Platelet derived growth factor receptor
PDK	: Phosphoinositide dependent kinase
PFS	: Progression free survival
PH	: Pleckstrin homology
PI	: Phosphatidylinositol
PI	: Propidium iodide
PI3K	: Phosphoinositide-3-kinase
PIA	: Phosphatidylinositol ether lipid analogues
PIP$_2$	: phosphatidylinositol-4,5- diphosphate
PIP$_3$	: phosphatidylinositol-3,4,5- triphosphate
PK	: Pharmacokinetics
PKA	: Protein kinase A
PKB	: Protein kinase B (Akt)
PKG	: Protein kinase G
PLC	: Protein lipase C
PRAS40	: Proline-rich AKT substrate 40
PS	: Phosphatidylserine
PTEN	: Phosphatase and tensin homologue deleted on chromosome 10
QOD	: Every other day
QW	: Once a week dose
RalGDS	: Ral guanine nucleotide dissociation stimulator
RAS	: Rat sarcoma

Rheb   : Rat homology enhanced in brain

RMSD   : Root mean square division

RNA   : Ribose nucleic acid

ROS   : Reactive oxygen species

RPMI   : Roswell park memorial institute

RSK   : Ribosomal S6 kinase

RTK   : Receptor tyrosine kinase

SAR   : Structure activity relationships

SDS   : Sodium dodecyl sulphate

SEM   : Standard error of mean

SGK   : Serum and glucocorticoid regulated kinase

siRNA   : Small interefering ribose nucleic acid

SP   : Standard precision

STAT   : Signal Transducer and Activator of Transcription

$T_{1/2}$: Half life

TBS   : Tris buffered saline

THF   : Tetrahydro furan

TLC   : Thin layer chromatography

TMS   : Tetramethyl silane

TRAIL   : TNF-related apoptosis-inducing ligand

TSC   : Tuberous sclerosis complez

VEGF   : Vascular endothelial growth factor

WT   : Wild type

XP   : Xtra precision

μM   : Micro molar

CHAPTER 1
INTRODUCTION

CHAPTER 1
INTRODUCTION

The PI3K/Akt/mTOR pathway is one of the most frequently dysregulated signaling cascades in human malignancies and is implicated in a wide variety of neoplasms (Weigelt B *et al.*, 2012). The Akt/PKB (protein kinase B) kinases, which include the isoforms Akt1, Akt2 and Akt3, are serine/ threonine (ser/thr) kinases and are key intermediates of signaling pathways that regulate cellular processes that control cell growth, survival, glucose metabolism, genome stability and neo-vascularisation (Bellacosa A *et al.*, 2005). PTEN (phosphatase and tensin homologue deleted on chromosome 10) is a dual lipid/protein phosphatase. Its primary target is phosphatidylinositol-3,4,5- triphosphate (PIP_3) (Maehama T, *et al.*, 1998), the product of the PI3K. Loss of PTEN function, as well as PI3K activation, results in accumulated PIP_3, triggering the activation of downstream effectors, including PDK1and Akt (**Figure 1.1**).

Activation of PI3K is induced by growth factor and insulin mediated localization of the catalytic subunit to the membrane where it is in close proximity to its substrate, mainly PIP_2. PDK1 contains a C-terminal pleckstrin homology (PH) domain, which binds the membrane-tethered PIP_3, triggering PDK1 activation. Activated PDK1 phosphorylates Akt at T^{308} activating its ser/thr kinase activity. Once phosphorylated on T^{308}, further activation of Akt occurs by phosphorylation of S^{473} by PDK2/ mTORC2 (the complex of rictor/mTOR and DNA-PK).

Akt activation stimulates cell cycle progression, survival and metabolism through phosphorylation of many physiological substrates (Stoke D, 2001; Dahia PL, 2000; Kandel ES *et al.*, 1999, Vivianco I, *et al.*, 2002 and Downward J, 2004). Akt is regulated by PI3K, which

recruits Akt to the cell membrane through PIP$_3$ binding and subsequently activated by PDK1 (Kandel ES, *et al.*, 1999) (**Figure 1.1**). Akt might also be activated by non-canonical pathways. DNA-PK regulates Akt by S^{473} phosphorylation (Surucu B, *et al.*, 2008; Bozulic L, *et al.*, 2008) which is dependent on PDK1 activity. Additionally, Akt may be induced by calcium signalling (Kau TR, *et al.*, 2003; Zanella F, *et al.*, 2008) as evident from the inhibition of phosphorylation of Akt by calmodulin inhibitors and induction by calcium agonists (Zanella F, *et al.*, 2008).
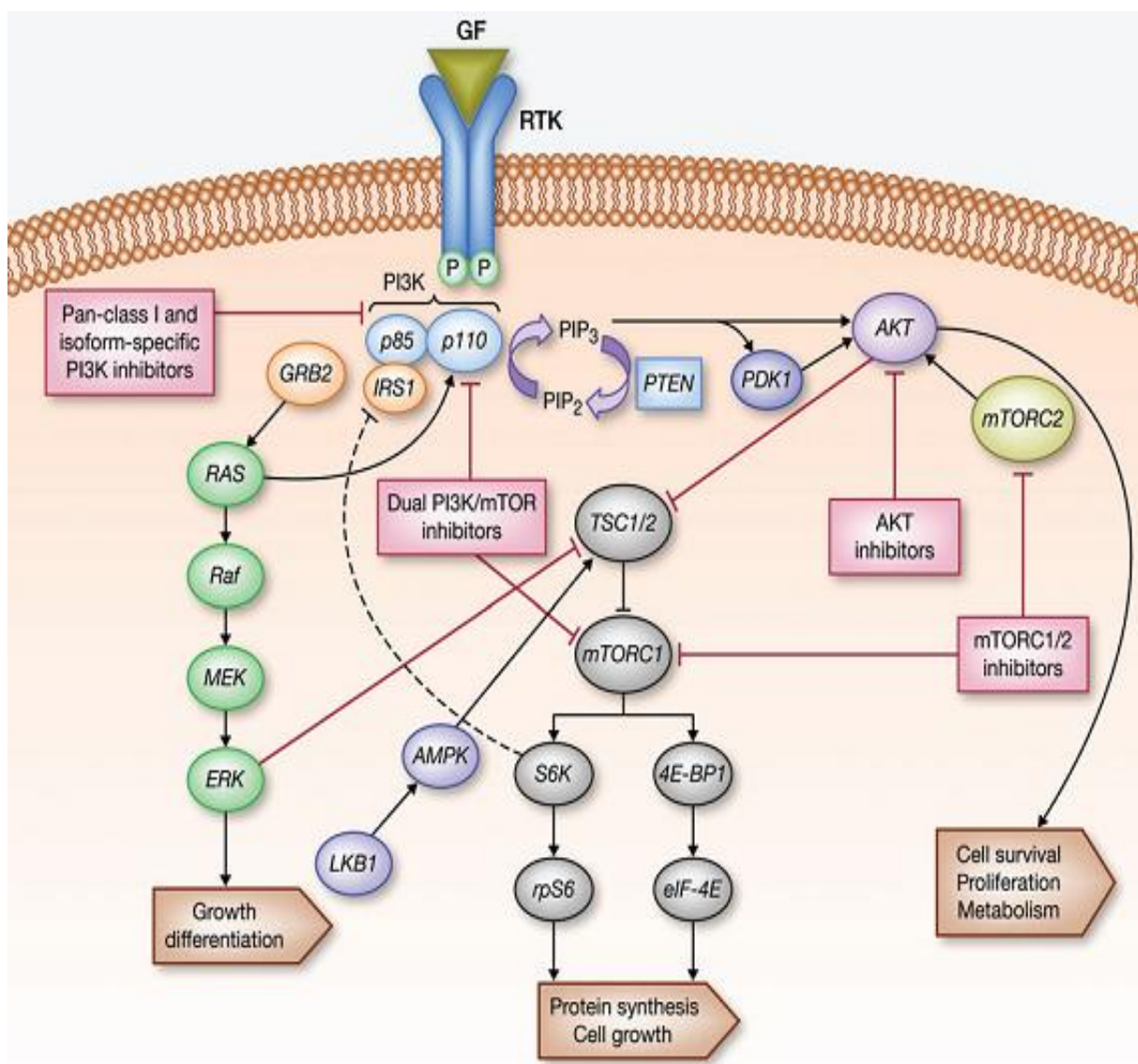
Figure 1.1: Activation of Akt pathway (Carnero A, *et al.*, 2010)

1.1 Role of Akt in cellular processes

Upon activation, Akt phosphorylates a myriad of proteins containing the aminoacid sequence RXRXXS/T-B (Alessi DR, *et al.*, 1996) where X represent any aminoacid, B is any bulky hydrophobic residue, R is arginine and S/T the serine/threonine residue. This diversity of substrates elicit a broad physiological response mediated by multiple downstream effectors (**Figure 1.2**). The three isoforms of Akt are very similar and it is unclear if they have different substrate specificities. However, knockout mice have revealed distinct physiological function for the three Akt isoforms (Manning BD, *et al.*, 2007; Dummler B, *et al.*, 2006; Dummler B, *et al.*, 2007).
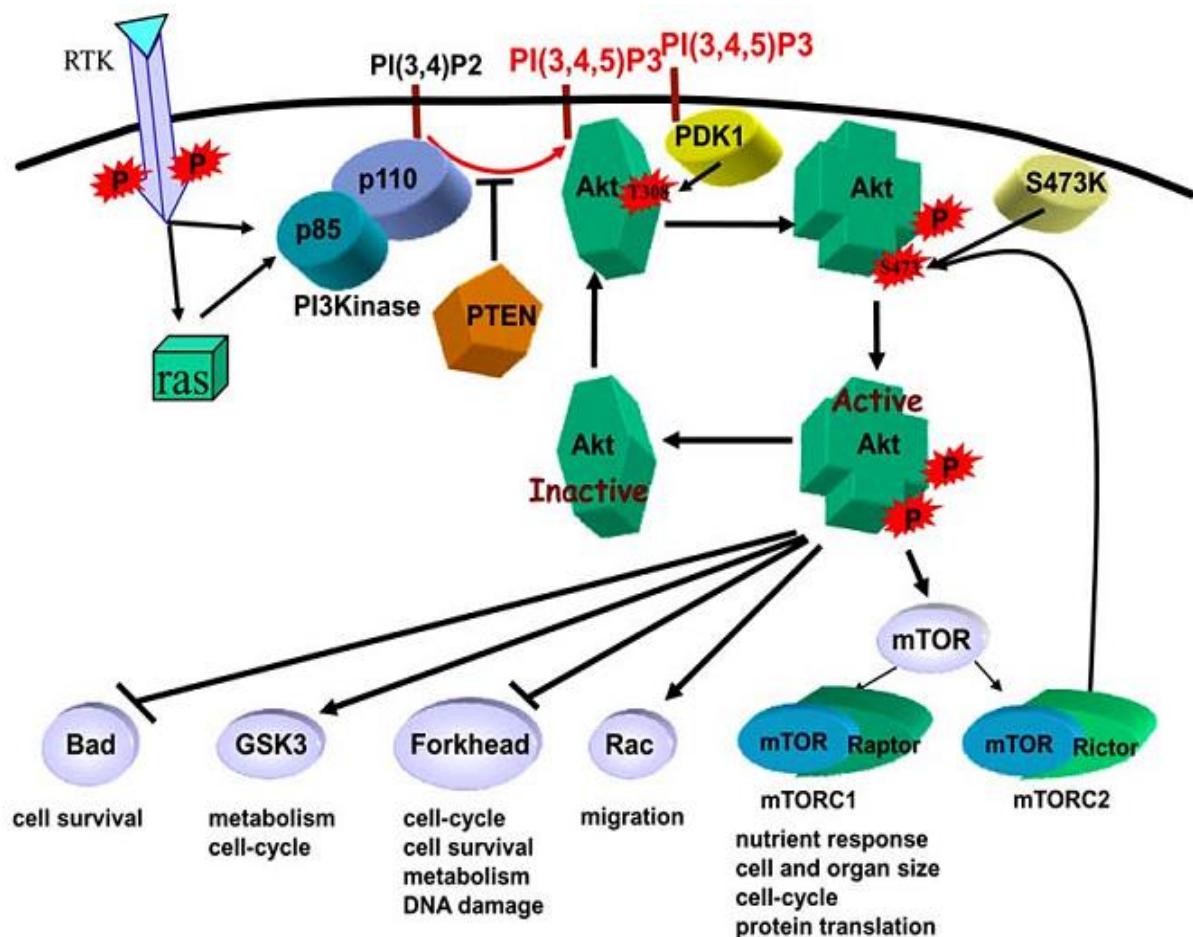
Figure 1.2: Cellular processes controlled by Akt pathway. (Carnero A, *et al.*, 2010)

Akt enhances survival by blocking the function of proapoptotic proteins. Akt phosphorylates and inactivates BAD and procaspase-9 along with the prevention of release of cytochrome-c from mitochondria (Dummler B, *et al.*, 2007; Datta SR, *et al.*, 1997; Cardone MH, *et al.*, 1998). Akt also promotes survival by phosphorylating MDM2, an E3 ubiquitin ligase that accelerates p53 degradation. Akt phosphorylates MDM2, promoting translocation of MDM2 to the nucleus where it negatively regulates p53 function (Mayo LD, *et al.*, 2001; Zhou BP, *et al.*, 2002; Zhou M, *et al.*, 2003). Two transcriptional targets of p53, Puma and Noxa proteins, appear to be essential in p53-induced apoptosis (Villunger A, *et al.*, 2003). Akt also inhibits the expression of BIM through transcription factors such as FOXO and p53 (Dijkers PF, *et al.*, 2002). Akt phosphorylates the FOXO family of proteins (FOXO, FOXO3a and FOXO4) and prevents their nuclear translocation and hence blocks the FOXO mediated transcription of genes that promote apoptosis and cell cycle arrest. Additionally, Akt exerts some of its cell-survival effects through the modification of nutrient uptake and metabolism (Robey RB, *et al.*, 2006).

Akt enhances cell growth by activation of mTORC1 (mTOR and raptor complex 1) pathway which is regulated by growth factors and nutrients (Wullschleger S, *et al.*, 2006). Akt activates mTORC1 by inhibiting TSC2, thereby allowing Rheb-GTP to activate mTORC1 signaling (Kovacina KS, *et al.*, 2003), an important event for 14-3-3 proteins to bind. Akt also phosphorylates PRAS40 that negatively regulates mTORC1 signaling (Sancak Y, *et al.*, 2007). The enhanced sensitivity of mTOR inhibitors in cells overexpressing Akt indicate the importance of mTORC1 signaling in Akt pathway (Sabatini DM, *et al.*, 2006). mTOR stimulates protein synthesis by phosphorylating p70 S6 kinase and eIF4E binding proteins (Plas DR, *et al.,* 2005). In turn, p70 S6 kinase phosphorylates the ribosomal protein S6 to increase translation of mRNAs with 5' -terminal oligopolypyrimidine (5' TOP) tracts, and phosphorylation of 4E-BPs releases the initiation factor eIF4E to promote cap-dependent

translation of messages such as those encoding cyclin D1, Myc, and vascular endothelial growth factor (VEGF) (Ruggero D, *et al.*, 2003; Bjornsti MA, *et al.*, 2004).

Akt activation mediates cell cycle progression by phosphorylation and consequent inhibition of glycogen synthase kinase 3β (GSK 3β) to avert cyclin D1 degradation (Liang J, *et al.*, 2003). Akt also stimulates proliferation through multiple downstream targets impinging on cell-cycle regulation. Akt phosphorylates the cyclin-dependent kinase inhibitors p21Cip1/WAF1 and p27Kip1, promoting their cytosolic localization (Zhou BP, *et al.*, 2002, Liang J, *et al.*, 2002; Shin I, *et al.*, 2002; Viglietto G, *et al.*, 2002) and preventing their cell-cycle inhibitory effects. Akt-dependent phosphorylation of other targets such as GSK3, TSC2, and PRAS40 is likely to drive cell proliferation through regulation of stability and synthesis of proteins involved in cell-cycle entry. Moreover, phosphorylation of Akt/mTOR kinases results in increased translation of cyclin D1, D3 and E transcripts (Helmericks RCM, *et al.*, 1998).

Akt pathway is highly connected with other pathways. Akt signaling activates NF (nuclear factor) -κB transcription factor by direct phosphorylation of IκB kinase α, thereby leading to the activation of kinase upstream to NF-κB (Ozes ON, *et al.*, 1999). Akt also directly phosphorylates c-Raf leading to an inhibitory effect on the MAPK pathway (Zimmermann S, *et al.*, 1999). Akt promotes tumour cell migration (Lefranc F, *et al.*, 2005) along with tumour invasion and metastasis by promoting the secretion of matrix metalloproteinases (Thant AA, *et al.*, 2000) and the induction of epithelial mesenchymal transition (Larue L, *et al.*, 2005). Collectively, these findings implicate upregulation of the Akt pathway in many aspects of tumorigenesis.

1.2 Mechanism of Akt Activation in cancer

Akt pathway is amplified in a wide range of cancers (**Table 1.1**). Overexpression of Akt could be measured by the amount of Akt phosphorylated at both T^{308} and S^{473} sites. Various oncogenes regulate the amplification of Akt pathway, which are further discussed in the following sections. The different mechanisms of Akt activation are depicted in **Figure 1.3**.

Table 1.1: Akt activation in human cancers. (Altomare DA *et al.*, 2005)

Tumour type	% Tumours with active Akt
Glioma	~55
Thyroid carcinoma	80-100
Breast carcinoma	20-55
Small-cell lung carcinoma	~60
Non-small-cell lung carcinoma	30-75
Gastric carcinoma	~80
Gastrointestinal stromal tumour	~30
Pancreatic carcinoma	30-70
Bile duct carcinoma	~85
Ovarian carcinoma	40-70
Endometrial carcinoma	>35
Prostate carcinoma	45-55
Renal cell carcinoma	~40
Anaplastic large-cell lymphoma	~100
Acute myeloid leukaemia	~70
Multiple myeloma	~90
Malignant mesothelioma	~64
Malignant melanoma	43-67
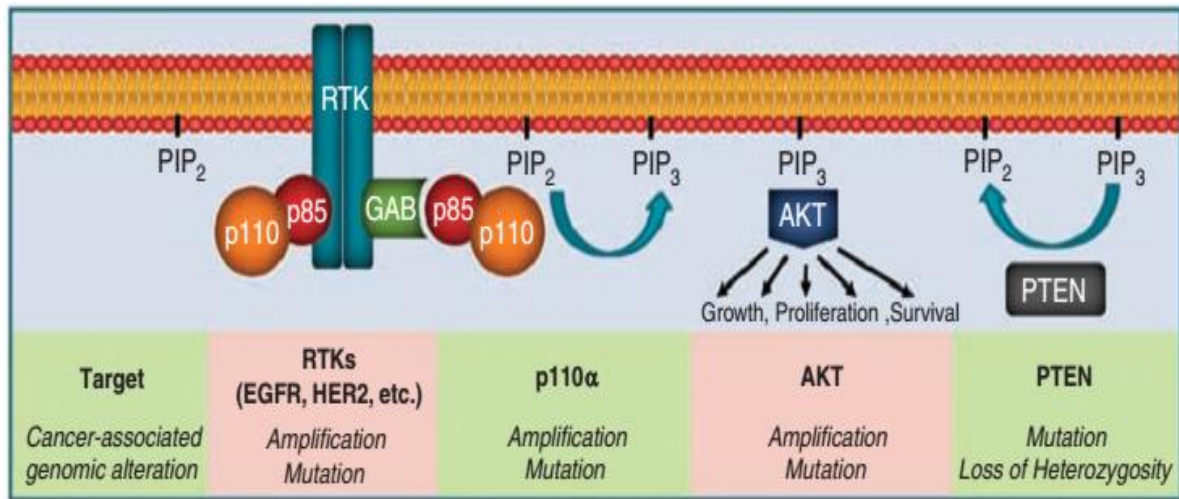
Figure 1.3: The Akt signaling axis. Activation of RTKs recruits PI3K directly or through adaptor proteins such as the GAB proteins. PI3K phosphorylates PIP_2 to generate PIP_3, which leads to AKT activation and activation of numerous effectors that regulate critical cellular functions in cancer cells. PTEN negatively regulates this process through dephosphorylation of PIP_3. All major members of this signaling axis are frequently altered in cancer. PI3K, phosphoinositide 3-kinase; RTKs, receptor tyrosine kinases (Vivianco I, *et al.*, 2002).

1.2.1 Amplification, overexpression and mutation of Akt genes.

The first recurrent alterations in Akt pathway were the amplification and overexpression of Akt2 in 2 out of 15 tumours of ovarian carcinomas (Cheng JQ, *et al.*, 1992). A multicentred trial confirmed these findings in a larger set of tumour specimens, wherein 16 out of 132 (12%) of ovarian carcinoma and 3 out of 106 (3%) of breast cancers had overexpression of Akt2 gene (Bellacosa A, *et al.*, 1995). Akt2 amplification was more frequent in undifferentiated ovarian tumours (4 of 8, $p < 0.02$), suggesting that Akt2 alterations may be associated with tumour aggressiveness. Amplification/overexpression of Akt2 was proposed to influence the malignant phenotype by permitting a tumour cell to become overly responsive to ambient levels of growth factors that normally would not enhance proliferation (Hanahan D, *et al.*, 2000; Testa JR, *et al.*, 2001). Amplification of the chromosome region 19q13.1–q13.2, the native location of the

Akt2 gene, was also reported in other primary ovarian tumours, and amplification and overexpression of Akt2 was demonstrated in several ovarian cancer cell lines (Thompson FH, *et al.*, 1996). In addition, Akt2 amplification has been reported in a non-Hodgkin's lymphoma (Arranz E, *et al.*, 1996). Studies using RNA interference against Akt2 in ovarian cancer cell lines provided evidence that Akt2 was involved in proliferation and chemotherapeutic drug resistance (Noske A, *et al.*, 2007; Xing H, *et al.*, 2008; Weng D, *et al.*, 2009) while overexpression studies revealed the gene's role in invasion and metastasis (Arboleda MJ, *et al.*, 2003).

Amplification and overexpression of Akt2 has been reported in 10–20% of pancreatic tumours and cell lines (Cheng JQ, *et al.*, 1996, Mirwa W, *et al.*, 1996, Ruggeri BA, *et al.*, 1998). The pancreatic cancer cell lines, PANC1 and ASPC1, exhibited amplification of the Akt2 gene in addition to increased mRNA and protein expression (Cheng JQ, *et al.*, 1996). Studies also examined Akt2 activity in primary pancreatic carcinomas versus benign pancreatic tumours and normal pancreas (Altomare DA, *et al.*, 2004). An *in vitro* kinase assay revealed that 12 of 37 pancreatic tumours had greater than three-fold increased Akt2 activity compared to normal pancreas (Altomare DA, *et al.*, 2004). Collectively, these data provided evidence for the role of Akt2 in tumour development in a subset of pancreatic carcinomas.

Unlike Akt2, amplification of Akt3 was rarely reported in cancers. CGH analysis revealed increased copy number of chromosomal region 1q44 (where Akt3is located) in 6 of 19 of hepatitis C virus-associated hepatocellular carcinomas (Hashimoto K, *et al.*, 2004) and in 2–4% of glioblastomas (Ichimura K *et al.*, 2008; Cancer Genome Atlas, 2008). Moreover, 40 to 60% of primary melanomas was reported to have increased total or phosphorylated Akt3 protein compared to normal melanocytes (Stahl JM, *et al.*, 2004). Furthermore, siRNA-mediated knockdown of Akt3 was shown to lower activated phospho-Akt levels in melanoma cell lines, which was not observed when Akt1 or Akt2 were downregulated by siRNA.

Compared to a siRNA control, targeting of Akt3 in the melanoma cell lines resulted in increased apoptosis in cell culture and in xenograft mouse studies (Stahl JM, *et al.*, 2004). In addition, approximately 20% of ovarian tumours of serous, endometrial, and other subtypes exhibited increased Akt3 protein expression (Cristiano BE, *et al.*, 2006).

Recurrent activating mutation in Akt1 were identified in human breast, colorectal, and ovarian cancers (Carpten JD, *et al.*, 2007). The somatic mutation resulted in a lysine substitution for glutamic acid at residue 17 (E17K) of the pleckstrin homology (PH) domain. This mutation was observed in 8% of breast, 6% of colorectal, and 2% of ovarian cancers. Another study uncovered E17K Akt1 mutation in 6% of breast, 1% of colorectal, and less than 1% of lung cancers (Bleeker FE, *et al.*, 2008). In addition, analysis of 137 melanoma clinical specimens identified one sample with the E17K Akt1 mutation and another sample with the E17K Akt3 mutation (Davies MA, *et al.*, 2008). Among the 65 melanoma cell lines analysed, two showed an E17K Akt3 mutation, whereas no E17K mutations were identified in Akt1 or Akt2 (Davies MA, *et al.*, 2008). Subsequent studies by others have identified E17K Akt1 mutation in a similarly small percentage of endometrial (Shoji K, *et al.*, 2009; Cohen Y, *et al.*, 2010), bladder (Askham JM, *et al.*, 2010), and prostate cancers (Boormans JL, *et al.*, 2010). Interestingly, a study found one particular endometrial tumour to have both the E17K Akt1 mutation and an inactivating mutation in PTEN (Cohen Y, *et al.*, 2010), suggesting that full activation of the PI3K pathway required multiple mutations of genes in the same signaling pathway.

1.2.2 Tyrosine kinase receptor mutation

Akt is activated downstream of numerous RTKs and are carefully regulated by the growth factor-receptor interactions.

Epidermal growth factor receptor (EGFR, ERBB1) is an upstream activator of Akt that is frequently altered in cancer. Malignant gliomas often exhibit EGFR amplifications with copy

numbers increased by as much as 20-fold (Sauter *et al.*, 1996). Mutations that confer constitutive kinase activity include the tissue nonspecific EGFRvIII deletion of exons 2–7 (Narita *et al.*, 2002) and non-small cell lung cancer (NSCLC)-specific deletions in exon 19 or L858R substitutions in exon 21 (Arteaga CL, 2006). In addition, exon 20 insertions and T790M mutations have been identified in NSCLC, which confer resistance to the EGFR inhibitors gefitinib and erlotinib (Arteaga CL, 2006).

HER2 (human epidermal growth factor) (EGFR2, ERBB2) is another member of the EGFR family and possesses the strongest catalytic kinase activity of all other family members. HER2 is overexpressed through gene amplification or transcriptional deregulation in 25–30% of invasive breast and ovarian cancers and is associated with poor prognosis (Moasser, 2007). Rare (4% of NSCLC and 10% of lung adenocarcinomas) somatic mutations have been found in the kinase domain of HER2 and occur predominantly in people of Asian descent (Moasser, 2007).

Activating mutations in KIT and PDGFRα can result in the formation of gastrointestinal stromal tumours. Mutations in KIT occur most frequently in exons 9 and 11 and confer constitutive kinase activation through induction of dimerization, whereas mutations in PDGFRα occur most frequently in exon 18, encoding the activation loop (Tornillo and Terracciano, 2006). The PI3K, mitogen-activated protein kinase (MAPK) and STAT pathways are activated downstream of each of these RTKs; however, only inhibition of PI3K results in robust growth arrest and induction of apoptosis in imatinib-resistant tumours (Heinrich *et al.*, 2003). Finally, focal MET amplifications have been found in 22% of acquired gefitnib-resistant lung cancers and have been shown to restore Akt activity via MET-dependent phosphorylation of ERBB3 and consequent activation of PI3K (Engelman *et al.*, 2007).

1.2.3 PIK3CA amplification and activating mutations

Downstream of tyrosine kinase receptors is PI3K; the PIK3CA gene, which encodes the p110α catalytic subunit of PI3K, has been implicated as an oncogene in a number of carcinomas. Amplification of PIK3CA, increased expression of PIK3CA protein and increased PI3K activity has been reported in ovarian carcinomas (Shayesteh L, *et al.*, 1999). PIK3CA amplification has also been reported in a number of other cancers such as head and neck squamous cell carcinomas (Pedrero JM, *et al.*, 2005), primary gastric carcinomas (Byun DS, *et al.*, 2003), and in endometrial carcinomas (Salvesen HB, *et al.*, 2009). Especially noteworthy, PIK3CA amplification in endometrial and gastric cancers has been shown to correlate with poor prognosis (Salvesen HB, *et al.*, 2009; Shi J, *et al.*, 2012). Activating mutations in PIK3CA were discovered as another mechanism by which PI3K can be constitutively activated. Mutations in certain 'hot spots', such as the commonly found E542K, E545K and H1047R, result in mutant proteins that can transform cells with high efficiency (Kang S, *et al.*, 2005). Sequencing of the PIK3CA gene in primary clear cell ovarian carcinoma specimens and cell lines revealed a 33% mutation rate (Kuo KT *et al.*, 2009). Immunohistochemical analysis of clear cell ovarian cancer samples with a PIK3CA mutation revealed intense phospho-Akt staining. Of particular clinical interest, a screening of 54 breast cancer cell lines revealed that those harbouring PIK3CAmutations are more sensitive to the PI3K inhibitor, GDC-0941 and Akt inhibitor, MK-2206 (O'Brien C, *et al.*, 2010).

1.2.4 Mutation or deletions of the p85α regulatory subunit gene, PIK3R1

PIK3R1 gene, which encodes the p85α regulatory subunit of PI3K, is a tumour suppressor. Somatic mutations of this gene were identified in colon, colorectal, and ovarian cancer specimens and cell lines (Philp AJ, *et al.*, 2001). An analysis of online microarray data indicated decreased PIK3R1 mRNA expression in prostate, lung, bladder, ovarian, breast, and

hepatocellular carcinomas (Taniguchi CM, *et al.*, 2010). Another study showed that liver-specific PIK3R1 deletion in mice results in liver carcinomas with metastasis to the lungs.

1.2.5 PTEN deletion and mutations

Working in opposition to PI3K is the PTEN tumour suppressor. As a lipid phosphatase, PTEN dephosphorylates phosphatidylinositol (3,4,5) triphosphate (PIP_3) and phosphatidylinositol (3,4) diphosphate to inhibit Akt activation. PTEN expression can be lost through somatic mutations, deletions, promoter hypermethylation, and defects in protein stability (Chalhoub N, *et al.*, 2009). Cancers commonly exhibiting loss of PTEN include endometrial and prostate carcinomas, high-grade glioblastomas, and melanomas (Chalhoub N, *et al.*, 2009). Studies with knockout mice indicate that PTEN haploinsufficiency contributes to tumorigenesis either alone or by cooperating with other genetic alterations.

1.2.6 Activation of non-overlapping pathways

Growth and survival signaling involves complex networks with redundancies, additive and synergistic effects. Modulation of the various nodes in the Akt network may affect non-linear pathways including negative feedback loops, non-overlapping pathways and autocrine loops. Coexisting mutations can arise if each targeted gene activates non-overlapping pathways that (1) also induce tumorigenesis (growth/proliferation/ motility) or (2) relieve negative feedback on the Akt pathway. These additional pathways, along with redundant activation of Akt signaling, would justify retention of multiple Akt alterations within the same tumour. PIK3CA and PTEN alterations may coexist if PTEN loss results in deregulation of other lipids or proteins that confer a growth advantage or disrupt a negative feedback loop. Similarly, RAS mutations may coexist with PIK3CA mutations/PTEN loss because in addition to the PI3K pathway, RAS activates the RAF and RalGDS pathways, which are also known to be critical for tumour growth (Downward J, 2003). HER2 overexpression and PIK3CA mutations/PTEN

loss may coexist because HER2 overexpression can lead to reshuffling of ERBB family members at the plasma membrane, causing amplification of numerous pathways. HER2–HER3 heterodimers are robust activators of the PI3K pathway, through binding of the p85 subunit to ERBB3/HER3 (Soltoff SP, *et al.*, 1994; Engelman JA, *et al.*, 2005; Hirata A, *et al.*, 2005). However, an increase in HER2–EGFR heterodimers at the membrane activates RAS-MAPK and PLC (Protein lipase C) γ in addition to PI3K. The coexistence of RTK amplifications/mutations and PTEN loss would thus serve to induce Akt activity in conditions of low ligand availability such as the tumour core.

To sum up, Akt signaling drives tumorigenesis in cancers with genetic alterations in p110α, PTEN and ERBBs. However, these genetic lesions should not be treated as a single class of hyper-Akt cancers. Evidence of coexistence between two alterations suggests that individual mutations are not absolutely redundant but bear the capability to also induce Akt-independent signaling, which cooperate to varying degrees with RAS and modulate negative feedback loops (Carracedo A, *et al.*, 2008 and Yuan TL, *et al.*, 2008). This suggests that mutations in the Akt pathway will require and likely be very responsive to Akt inhibitors in combination with other targeted therapies.

CHAPTER 2
LITERATURE REVIEW

CHAPTER 2
LITERATURE REVIEW

Components of the Akt signal transduction pathway are appealing targets for therapeutic intervention, because Akt signaling promotes cell survival, proliferation and invasion, and blocking this pathway could impede the proliferation of tumour cells by either inducing apoptosis or sensitizing tumours to undergo apoptosis in response to other cytotoxic agents. Chemoresistance is a major obstacle to successful cancer therapy. Akt has been shown to play a significant role in the therapeutic resistance of tumour cells, because it works against apoptotic mechanisms to promote cell survival. For example, ovarian cancer cell lines with either constitutive Akt1 activity or Akt2 gene amplification were highly resistant to paclitaxel, in contrast to cells with low Akt levels (Page C, *et al.*, 2000).

In vitro and *in vivo* ovarian cancer models combining the PI3K inhibitor LY294002 with paclitaxel had shown increased efficacy in reducing tumour growth and dissemination compared to single agents alone (Hu L, *et al.*, 2002). Moreover, PI3K inhibition increased apoptosis selectively in tumour cells expressing elevated levels of activated Akt, but not in tumour cells with low levels of activated Akt (Brognard J, *et al.*, 2001; Altomare DA, *et al.*, 2004). Blockage of the Akt/mTOR signaling pathway by rapamycin restored the susceptibility of breast cancer cells to tamoxifen (deGraffenried LA, *et al.*, 2004).

Strategies for targeting the Akt signaling pathway included selective inhibition of upstream receptor tyrosine kinases, as well as PI3K, PDK1, AKT, and mTOR kinases. In particular, mTOR inhibitors, such as RAD001 (Novartis) and CCI-779 (Wyeth Research), are currently being assessed in the treatment of advanced cancer patients. These rapamycin derivatives bind

to the mTOR and thereby prevents phosphorylation of downstream S6K and 4EBP1 (Bjornsti MA, *et al.*, 2004; Sansal I, *et al.*, 2004).

2.1 Sequence and structural analysis of Akt

Akt kinases belong to the AGC kinase family (related to AMP/GMP kinases and protein kinase C) and consist of three conserved domains, an N-terminal pleckstrin homology (PH) domain, a central kinase catalytic (CAT) domain and a C-terminal extension (EXT) containing a regulatory hydrophobic motif (HM) (**Table 2.1**). Among the Akt isoforms, the PH domains are ∼80% identical and ∼30% identical to PH domains in pleckstrin and other proteins. The linker (LINK) region connecting the PH domain to the CAT domain is poorly conserved among the Akt isoforms (17–46% identical) and has no significant homology to any other human protein. The consensus CAT domain is ∼90% identical among the Akt isoforms and is closely related the PKC, PKA, SGK and S6 subfamilies of the AGC kinase family. The C-terminal extension (EXT) is ∼70% identical among the Akt isoforms and is most closely related to the PKC family. The N-terminal 30–40 residues of EXT are homologous in the Akt, S6, SGK, PKA and cGMP kinase families.

Table 2.1: Pairwise % identity in Akt domains (Kumar CC, *et al.*, 2005).
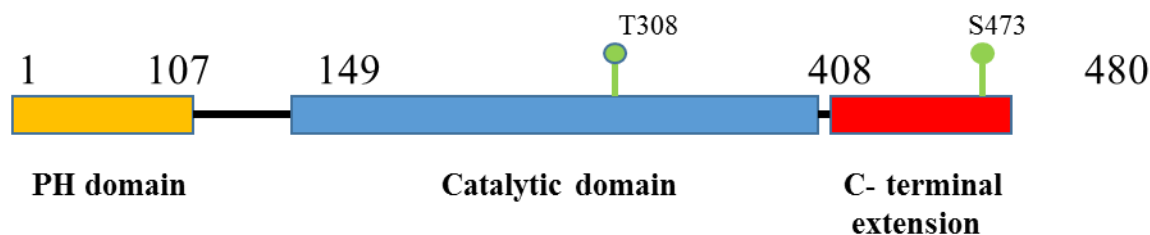
PAIR	PH	LINK	CAT	EXT
Akt1/Akt2	80	46	90	66
Akt1/Akt3	84	40	88	76
Akt2/Akt3	76	17	87	70

Domain definitions using Akt1 residue numbers. PH – Pleckstrin Homology domain, Akt1 (1–107), ~30% identical to pleckstrin and other PH domains. LINK – Linker region, Akt 1(108–148), no significant homology to other proteins. CAT – Kinase Catalytic domain, Akt1 (149–408), homologous to all kinases, ~50% identical to the PKC, PKA, SGK and S6 families. EXT – C-terminal Extension, Akt1 (409–480) is only ~15% identical to the PKA family and ~35–40% identical to the rest of the AGC family members.

2.2 Small molecule inhibitors of Akt

Majority of small molecule Akt inhibitors are classic ATP-competitive inhibitors, which provide little specificity. Phosphatidylinositol (PI) analogs have been reported to inhibit Akt, but these inhibitors may also have specificity problems with respect to other PH domain containing proteins and may have poor bioavailability. Recently, small chemical compounds triciribine/Akt/protein kinase B inhibitor-2 (API-2) and allosteric inhibitors have been reported which were PH domain dependent, and the latter also exhibited Akt isozyme selectivity. In addition, inhibitors toward upstream regulators and downstream targets of Akt have also been tested for their capability of reversing the phenotype of cancer cells expressing altered Akt.

2.2.1 ATP competitive inhibitors

Several small molecule leads that compete with ATP for binding to its pocket were being used as the basis for developing potent and selective inhibitors of Akt. A number of these leads were discovered as inhibitors of PKA or PKC. One PKA inhibitor that has been subjected to optimization for Akt selectivity was H-89 (**Figure 2.1**) which inhibited PKA and Akt with IC_{50} of 35 and 2500 nM, respectively. The crystal structure of the PKA/H-89 complex shows that the isoquinoline nitrogen mimiced N_1 of adenosine in accepting a H-bond from the peptide backbone, while the sulfonamide chain extended in the direction of the triphosphate chain of ATP (**Figure 2.2**). Libraries around the lipophilic amino terminus led to the identification of NL-71–101 (**Figure 2.1**), which inhibited Akt1 2.4-fold better than PKA (IC_{50}s 3.7 and 9 µM respectively) (Reuveni H, *et al.*, 2002). This compound induced apoptosis in OVCAR-3 ovarian carcinoma cells at a high concentrations (>25 µM).
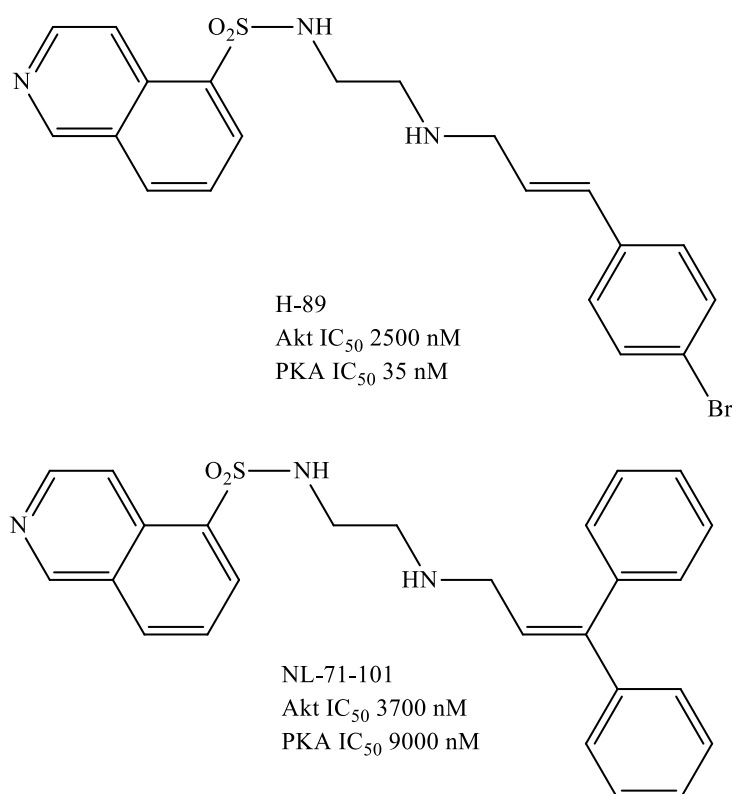
Figure 2.1: Lead molecules for ATP competitive Akt inhbitors
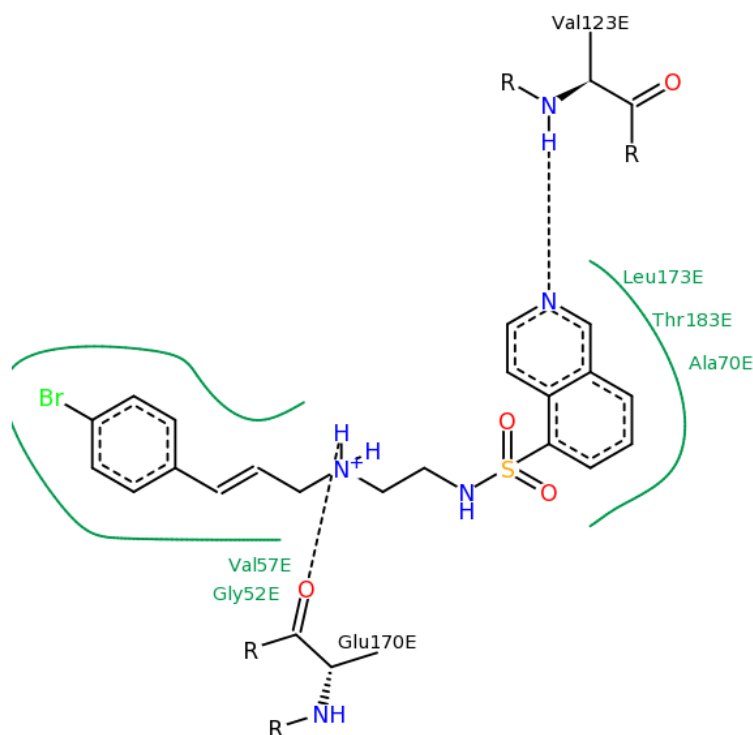
Figure 2.2: Interaction plot for H-89 in ATP binding pocket of PKA.

2.2.1.1 Balanol analogues

Balanol, a non-selective kinase inhibitor with a Ki value of 4 nM for PKA (Protein kinase A), was reported to inhibit Akt with an IC_{50} of 5 nM (Gustafsson AB, *et al.*, 1999). Efforts were made to develop analogues of balanol by replacing ester linkages with metabolically less liable linkers (Narayan N, *et al.*, 1999; Akamine P, *et al.*, 2004; Breitenlechner CB, *et al.,* 2004). However, none of them showed any selectivity towards Akt when compared to PKA. (**Table 2.2**)

Table 2.2: Akt, PKA activities and half-lifes in mouse plasma for balanol analogues.
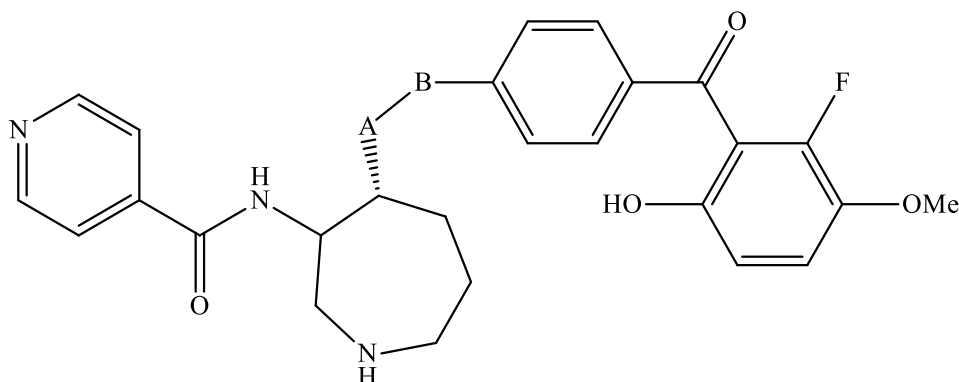
-A-B-	IC$_{50}$ (nM)		T$_{1/2}$ h
	Akt	**PKA**	
-OCO- (Balanol)	5	4	<0.02
-NHCO-	4	2	69
-OCH2	355	39	29
-NHCH2	3000	800	161
-CH2NH-	25	45	NA
-CH=CH-	160	360	NA

2.2.1.2 Pyridine analogues

Novel 3,5-disubstituted pyridines that bind to the ATP binding pocket of Akt, were identified as competitive and reversible Akt inhibitors. A-443654 (**Figure 2.3**), an indazole-pyridine based compound, which inhibited Akt1 with a Ki of 160 pM and blocked the growth of pancreatic and prostate tumour xenografts, but only at concentrations that were two-fold lower than the maximally tolerated dose (Luo Y, *et al.*, 2005). A structural comparison of inhibitor binding to PKA, Akt2 and PKA-Akt chimera revealed that A-443654 adopted a conformation in Akt2 and PKA-Akt chimera that differs from that in PKA (**Figure 2.3**). The methylindazole and the pyridine groups adopted almost identical binding modes in both PKA and Akt. However, the conformation of the indole was very different when bound to Akt, in

which the indole ring was directed towards the front of the ATP-binding cliff in a new hydrophobic pocket formed by the side chains of Met282, Phe439 and Val166.

In its new conformation, the indole ring formed non-polar Van der Waals contacts with the side chain of Met282, which might be the driving force for the new conformation because of the absence of such interaction in PKA due to the presence of Leu173 at the same point. Interestingly, the phenyl ring of Phe163 at the hydrophobic pocket underneath the glycine rich loop was filled by the indole ring of A-443654 bound to PKA. The indole nitrogen was ~3.5Å to the carboxylate oxygen atoms of Glu236, which could explain why N -methylation of the indole was detrimental for Akt activity.

A

B
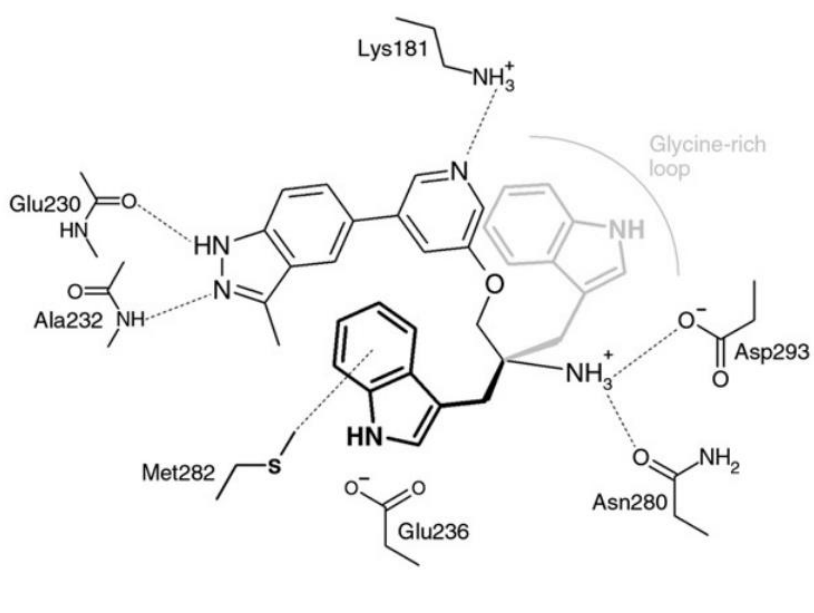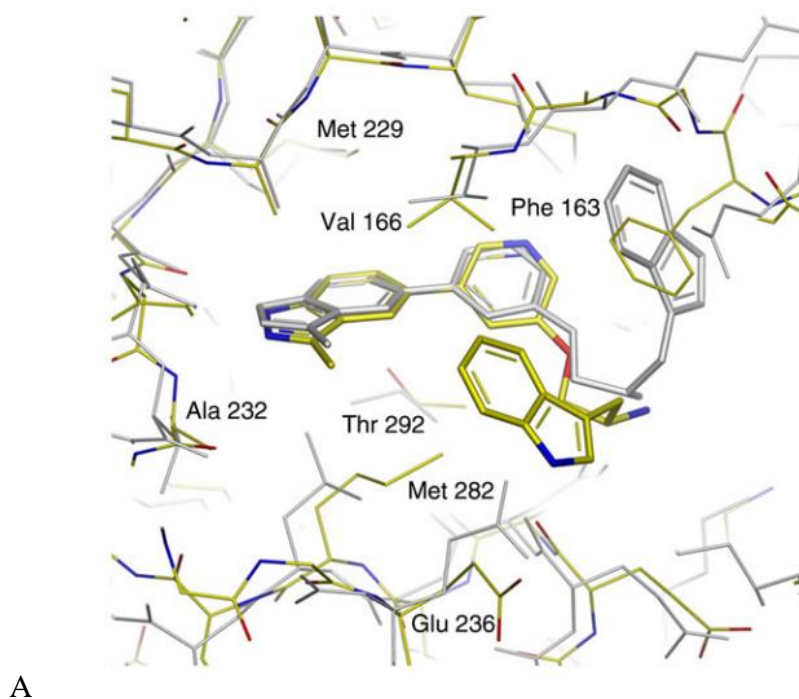
Figure 2.3: Schematic representation of interactions of compound A-443654 in complex PKA and PKB (A). Alternate positions of indole ring with PKA (light grey) and Akt1 (Black) (B) (Davies TG, *et al*., 2007).

Further, a phenyl analogue, A-674563, was identified to have drastically improved PK profile with oral bioavailability of 67% in mouse but was selective towards Akt1 versus Akt2. However, its cellular and xenografts activities were moderate compared to A-443654.

Patents published from GlaxoSmithKline focused on modifications on imadazopyridine group (Heerding DA, et al., 2007a,b,c). The lead compound GSK690693 (**Figure 2.4**) was reported to be in a phase-I clinical trial in patients with solid tumours and lymphomas (Kumar R, *et al.*, 2007, Rhode SN, *et al.*, 2007). GSK690693, a pan-Akt inhibitor exhibited IC_{50} values of 2 nM, 13 nM and 9 nM against Akt1, Akt2 and Akt3 respectively. It revealed dose dependent reduction in phosphorylation of multiple substrates of Akt such as PRAS40, GSK3β and FOXO3a. One of the potential toxic effects of GSK690693 included the acute increase in blood glucose levels which reduced with concentration of the drug in blood.

A-443654

A-674563

GSK690693

AT7867

CCT128930

GSK211083

GSK2141795
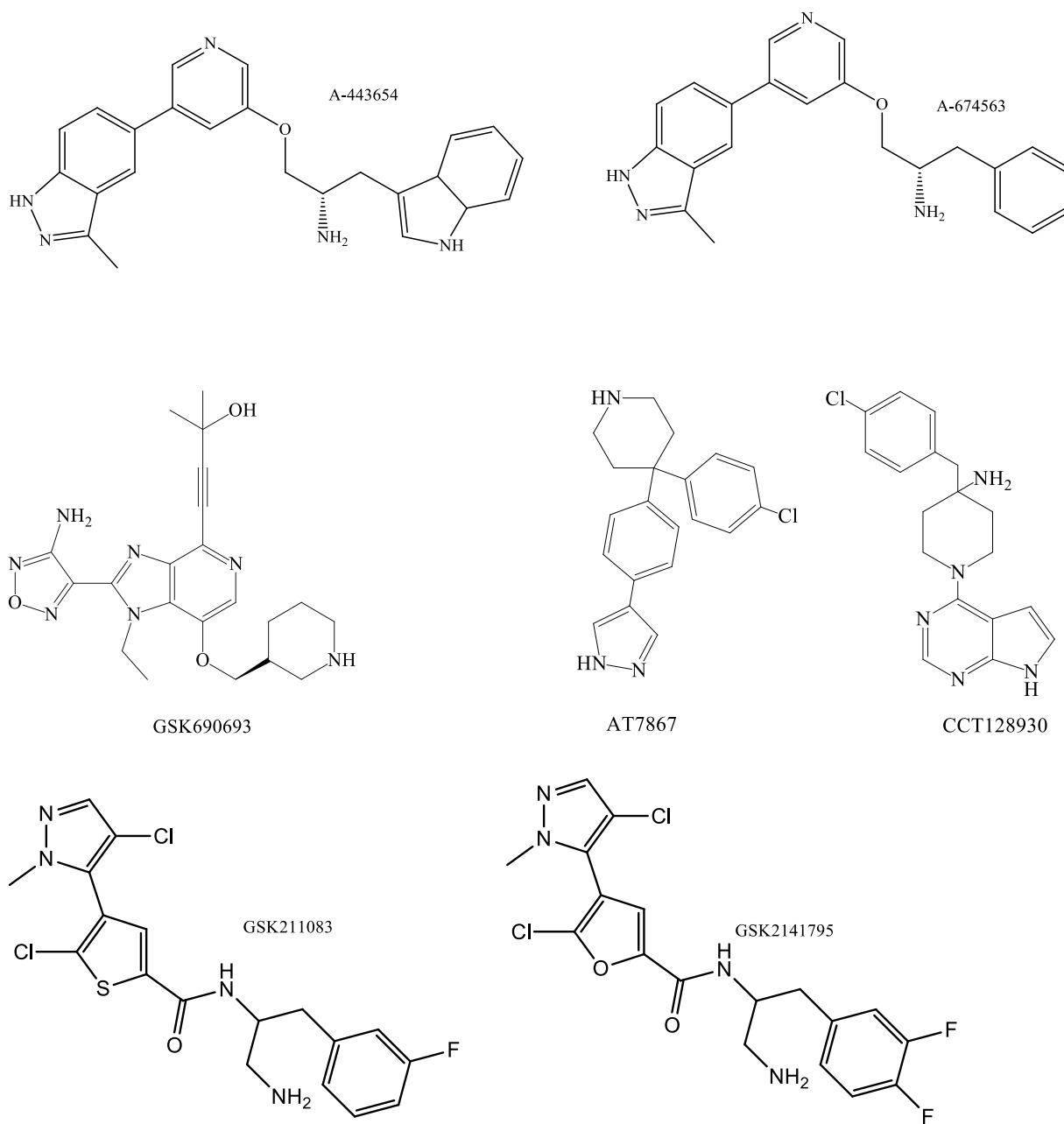
Figure 2.4: Structures of ATP competitive Akt inhibitors

2.2.1.3 Other ATP competitive inhibitors

A fragment based discovery approach led to the identification of AT7867 and CCT128930 (**Figure 2.4**) which were selective towards Akt2 versus Akt1 and PKA. This improved selectivity was due to targeting the single aminoacid difference between Akt1, Akt2 and PKA (Davies TG, *et al.*, 2007; Yap TA, *et al.*, 2011a). Recently, two orally available, potent ATP competitive Akt inhibitors (GSK2110183 and GSK2141795) were identified (Dumble M, *et al.*, 2014). Cells treated with either of these compound showed sustained Akt inhibition along with decreased phosphorylation of several downstream substrates of Akt. In diverse cell line proliferation screen, Akt inhibitors showed increased potency in cell lines with an activated Akt pathway (via PI3K/PTEN mutation or loss) while cell lines with activating mutations in the MAPK pathway (KRAS/BRAF) were less sensitive to Akt inhibition. Further investigation in mouse models of KRAS driven pancreatic cancer confirmed that combining the Akt inhibitor, GSK2141795 with a MEK inhibitor, trametinib, resulted in an enhanced anti-tumour effect accompanied with greater reduction in phospho-S6 levels supporting the clinical evaluation of the Akt inhibitors in cancer, especially in combination with MEK inhibitor.

2.2.2 PH domain inhibitors

Another approach to inhibit Akt kinases was to target the PIP_3 binding site in the PH domain of Akt and to inhibit its membrane translocation. This mode of inhibition would prevent Akt translocation to the plasma membrane and activation. The feasibility of this approach was suggested by the demonstration with D-3-deoxy-myo-inositols inhibiting the growth of transformed cells (Powis G, *et al.*, 1991). It was subsequently found that the inositol derivative DPI had an IC_{50} of 35 μM against H-29 colon cancer cell growth (Kozikowski AP, *et al.*, 1995). A recent study examined 24 modified phosphatidylinositol ether lipid analogues (PIAs) and found that five of them, PIA5, 6, 23, 24, and 25 (**Figure 2.5**), with modifications at two sites

on the inositol ring, inhibited Akt with $IC_{50} < 5$ μM (Castillo SS, *et al.*, 2004). PIAs decreased phosphorylation of many downstream targets of Akt without affecting upstream kinases, such as PI3K or PDK1. Importantly, PIAs selectively induced apoptosis in cancer cell lines with high levels of endogenous Akt activity. These findings identified PIAs as effective Akt inhibitors, and provided proof of principle for targeting the PH domain of Akt. However, the effectiveness of PIAs *in vivo* and their effect on other PH-domain containing proteins are currently unknown. The best compound of this series was PX-316 with an IC_{50} of 1.5 μM and was developed by Prolyx pharmaceuticals (Meuillet EJ, *et al.*, 2004; Williams R, *et al.*, 2006).
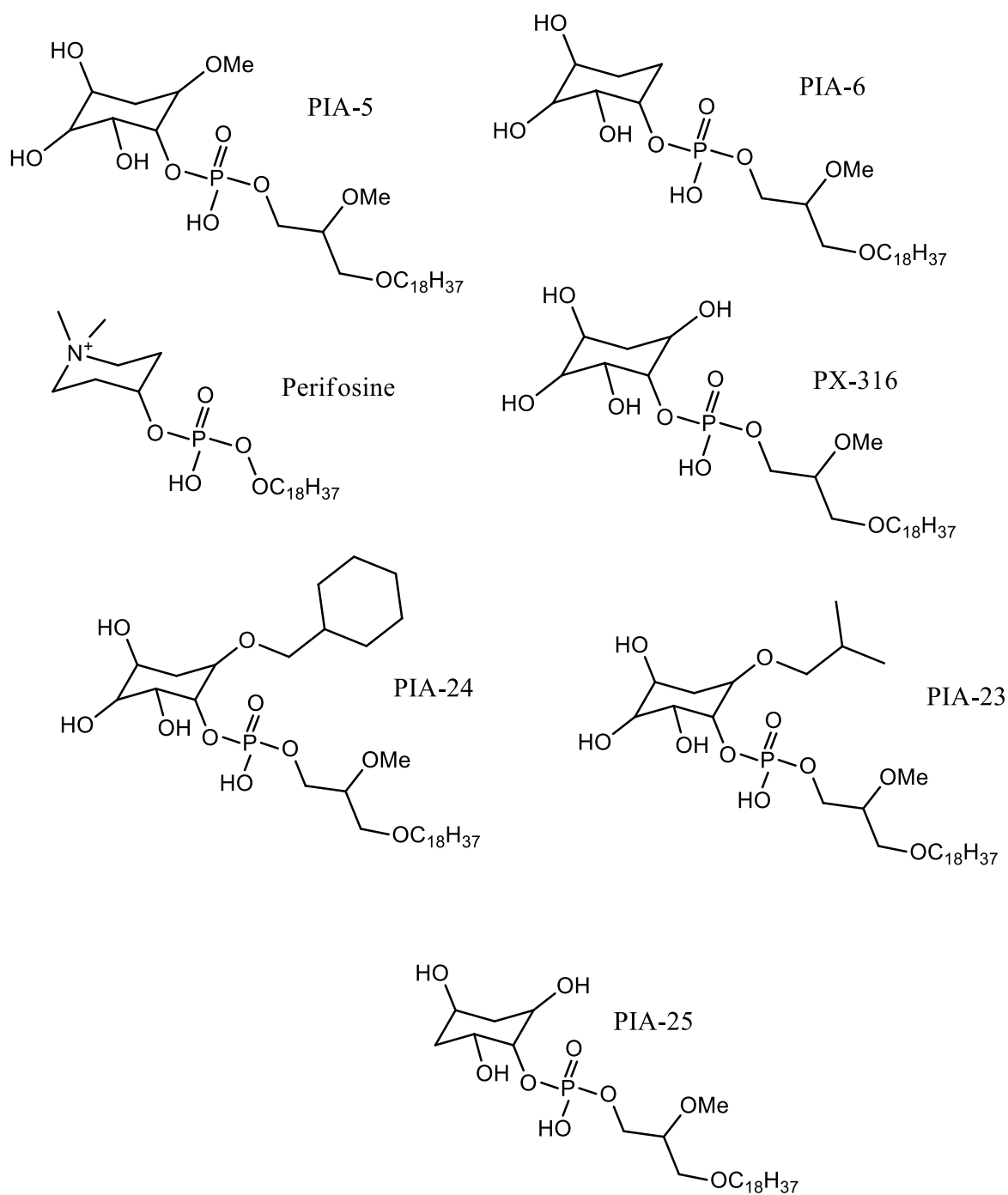
Figure 2.5: Structures of PH domain Akt inhibitors

Perifosine (D-21266, NSC639966, KRX-0401) is an orally active alkylphospholipid presently in phase-III clinical trial for multiple cancers including NSCLC, breast cancer, multiple myeloma and sarcoma. In phase-II study, perifosine showed single agent partial responses or long term disease stabilisation in solid tumours. Several phase II/III trials are currently in

progress for perifosine (NCTIDs: NCT01049841, NCT00590954, NCT00776867 and NCT02238496). However, a phase-III study on the effect of perifosine on combination of dexamethasone and bortezomib was terminated since there was no benefit in progression free survival or overall response rate when perifosine was added to bortezomib and dexamethasone in patients with highly resistant, relapsed and refractory multiple myeloma previously treated with bortezomib (Nagler A, *et al.*, 2013).

2.2.3 Allosteric Akt inhibitors

Preliminary studies have identified novel allosteric Akt kinase inhibitors by screening a collection of approximately 270 000 compounds and application of an iterative analog library synthesis approach (Barnett SF, *et al.*, 2005a, 2005b; DeFeo-Jones D, *et al.*, 2005; Lindsley CW, *et al.*, 2005; Zhao Z, *et al.*, 2005). These inhibitors display an unprecedented level of specificity for Akt against PKA. Not only were they specific with respect to other kinases, but were also isozyme specific, even though no compound specifically targeted Akt3.

These inhibitors all contain a well-known GPCR privileged structure, a piperidinyl benzimidazolone that was crucial for improving potency (Barnett SF *et al.*, 2005; DeFeo-Jones D *et al.*, 2005; Lindsley CW *et al.*, 2005). In addition to inhibiting kinase activity, these inhibitors blocked the phosphorylation and activation of the corresponding Akt isoforms by PDK1. These were reversible inhibitors and had no inhibitory effects on Akt mutants lacking the PH domain, suggesting that they bind to a site formed only in the presence of the PH domain (Zhao Z *et al.*, 2005). Binding of the inhibitor was postulated to promote the formation of an inactive conformation. In support of this model, antibodies to the Akt PH domain or hinge region abrogated the inhibition of Akt by these inhibitors (Wu WI, *et al.*, 2010).

In multiple cell lines, maximal induction of caspase-3 activity was achieved when both Akt1 and Akt2 were inhibited, that is, Akti-1 or Akti-2 alone induced moderate levels of caspase-3

activity (8 units and 10 units after 6 h treatment, respectively). In contrast, simultaneous treatment with both inhibitors resulted in strong synergy of caspase-3 activation (45 units) (DeFeo-Jones D, *et al.*, 2005). Second, as these inhibitors depend on the integrity of the PH domain, constitutively active myr-Akt1 and myr-Akt2 were capable of protecting against caspase activation induced by these compounds. However, the programmed cell death induced by Akti-1 or/and Akti-2 as well as Akti-1/2 could not be reversed by overexpression of functionally active Akt3, suggesting that Akt3 was not able to compensate for the loss of Akt1/2. Third, these inhibitors selectively sensitized tumour cells, but not normal cells, to apoptotic stimuli, suggesting a potential therapeutic window for cancer therapy. Finally, these Akt inhibitors were broadly active chemosensitizers and when used as single agents, Akt1/2 dual inhibitors (Akti-1/Akti-2 or Akti-1,2) showed limited proapoptotic activity in cell culture. Maximal caspase induction is seen only when combining Akt1/2 dual inhibitors with chemotherapeutics such as the topoisomerase inhibitor camptothecin, or biologics, such as the death receptor ligand, TRAIL. Thus, Akt inhibitors combined with conventional chemotherapy or radiation therapy might provide a more effective strategy to improve patient outcome.
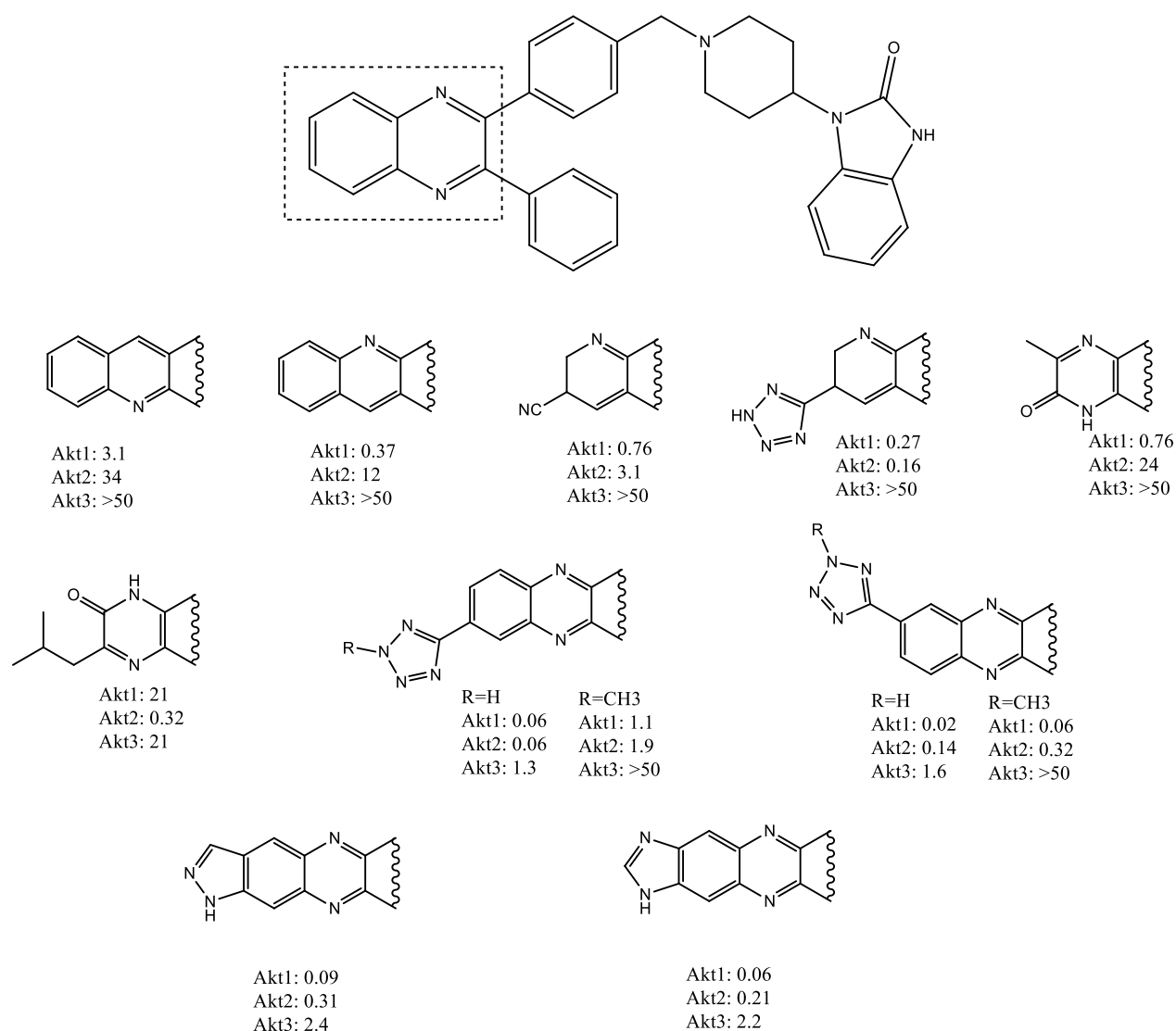
Figure 2.6: Scaffolds of allosteric Akt inhibitors with activities.

The initial compounds identified to be allosteric Akt inhibitors were 2,3-diphenylquinoxaline derivatives (**Figure 2.6**) was further derivatised to compounds that specifically inhibited Akt1 or Akt or Akt1/2, as the compounds did not bind to the PH domain or ATP binding site that was likely to be unique to Akt (Hartnett JC, *et al.*, 2008). Further modifications in the scaffold were carried out to replace quinoxaline ring with pyridopyrimidines (2 and 3), pyridinepyrazine (5), furopyridine (4) and pyrazolopyridine (1) rings (**Figure 2.7**). The benzimidazole ring substitutions were also optimised to produce more potent Akt allosteric inhibitors.
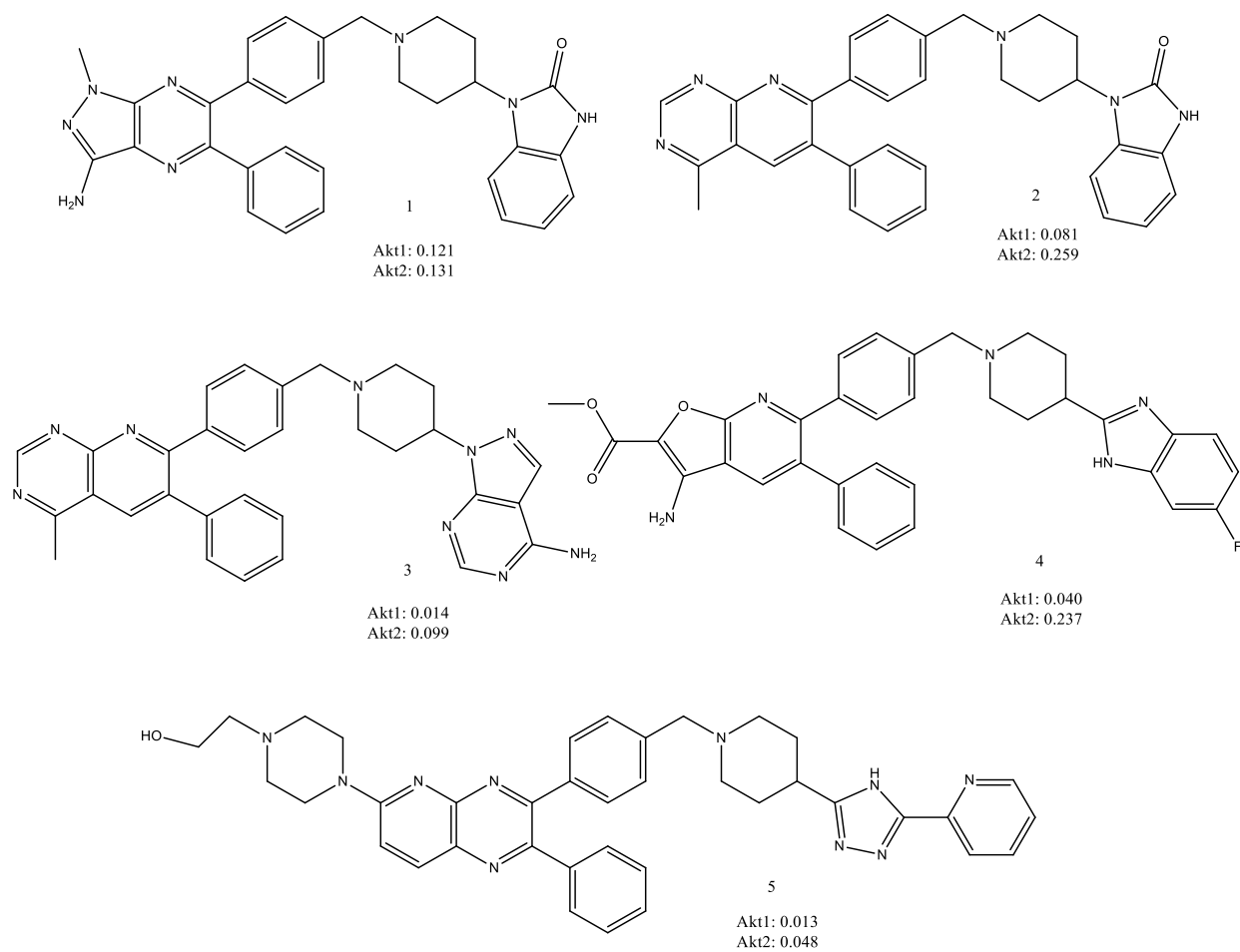
Figure 2.7: Modification of scaffolds of Akt inhibitors.
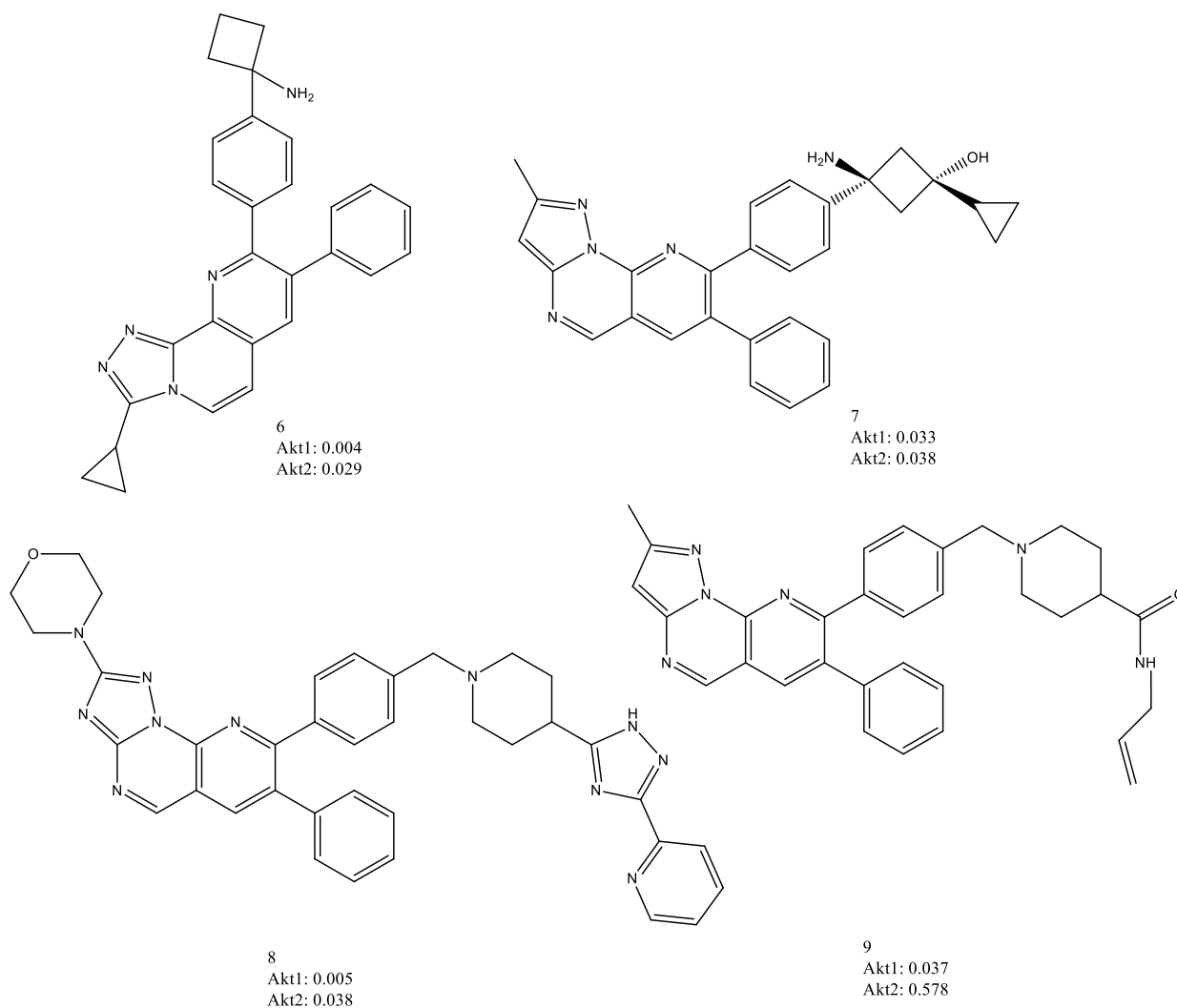
Figure 2.8: Structures of novel allosteric Akt inhibitors from recent patents.

Recent patents on allosteric inhibitors revealed similar structural scaffolds of quinoxaline ring or its isosters (US8614221, 2013; WO2010/104933, 2010). The diphenyl ring system and a cycloalkyl substitution to a phenyl ring however remained unchanged (**Figure 2.8**). The most potent compound of this series was MK2206 (**Figure 2.9**) which is currently in phase-II trials for several solid cancers and lymphomas both as a single treatment and as a combination with several cytotoxic drugs and molecular targeted therapies.
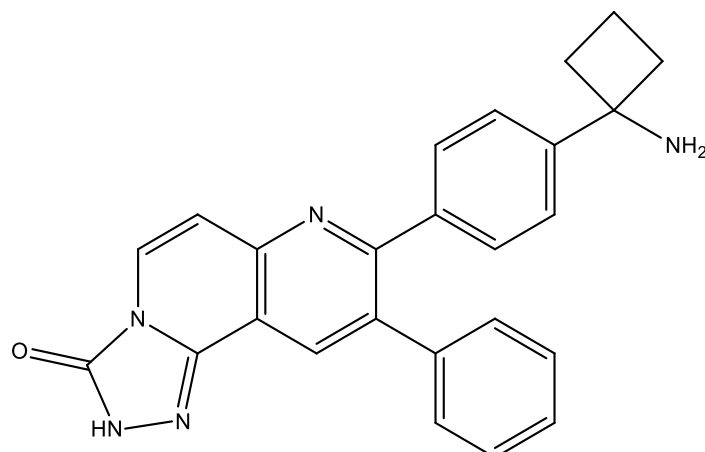
Figure 2.9: Structure of MK2206

MK2206 is a highly potent, selective and an orally active allosteric Akt inhibitor. It is equipotent towards human Akt1 (IC_{50}: 5 nM) and Akt2 (IC_{50}: 12 nM) and approximately 5 times less potent against human Akt3 (IC_{50}: 65 nM). A summary of various clinical trials with MK2206 is presented in **Table 2.3**. MK2206 showed antitumour activity alone or with chemotherapy. This activity is greater in tumours with PTEN loss or PIK3CA mutation, providing a strategy for molecular enrichment of patients in clinical trials (Sangai T, *et al.*, 2012). Combination of MK-2206 with erlotinib in NSCLC cell lines and with lapatinib in breast cancer cell lines led to synergistic growth inhibition (Hirai H, *et al.*, 2009). In xenograft studies utilizing mice bearing the A2780 ovarian cancer cell line, treatment with MK-2206 led to roughly 60% growth inhibition and generated sustained inhibition of all three Akt isoforms (Lu W, *et al.*, 2009). Subsequent *in vitro* data suggested that inhibition of each isoform occurred at nanomolar concentrations.

2.3 Clinical data for MK2206

In a study including 24 healthy male volunteers, doses of MK-2206 ranging between 0.25 to 100 mg oral were well tolerated. Maximal inhibition of Akt occurred roughly 6 hours after an

oral dose and led to Akt inhibition (measured in whole blood) for up to 24 hours. A subsequent phase I study in 19 patients with advanced solid tumours assessed dosing of MK-2206 on an every other day (QOD) schedule (Yap TA, *et al.*, 2011b). With QOD dosing, the MTD was determined to be 60 mg (grade 3/4 mucositis and skin rash were DLTs noted at the next dose level, 90 mg). In this dose-finding study, treatment with MK-2206 was noted to cause central tumour necrosis, a reduction in index lesions and improvement in ascites and peripheral edema. As in the healthy volunteers study, it appeared that the dose of 60 mg led to sustained inhibition of Akt in whole blood. A larger phase I exploration is underway, examining two formulations of MK-2206 – one administered on a weekly schedule (QW) and another on an every other day schedule (QOD) (Capuzzo F, *et al.*, 2011). Preliminary data from this study (with a total of 70 patients accrued thus far) showed DLTs of rash and mucositis at doses of 75 mg and 90 mg QOD, and a DLT of rash at 300 mg QW (Yap TA, *et al.*, 2011b). Correlative studies paired with this analysis showed sustained declines in pAkt with MK-2206 therapy. Furthermore, of 23 patients, 18 (78.3%) had a decline in circulating endothelial cells (CECs).

Table 2.3: MK2206 related clinical trials (as accessed in <u>www.clinicaltrial.gov</u>, 20th October 2014).

S No.	Trial ID	Cancer	Drug Combination	Phase	Status of trial	Notes
1	NCT01071018	Solid tumours	Single agent	1	Completed	Both QOD, QW
2	NCT00670488	Solid tumours	Single agent	1	Completed	Dose escalation study
3	NCT00848718	Solid tumours	Erlotinib/ Paclitaxel	1	Completed	
4	NCT01147211	NSCLC	Erlotinib	1	Active	
5	NCT01783171	Pancreatic	Dinacicilib	1	Active	
6	NCT01283035	Ovarian	Single agent	2	Active	Platinum resistant ovarian cancer
7	NCT01245205	HER[+] Breast cancer	Lapatinib	1	Active	
8	NCT00963547	HER[+] Breast cancer	Trastuzumab/ Lapatinib	1	Completed	
9	NCT01231919	Leukemia	Single agent	1	Completed	
10	NCT01466868	DLBCL	Single agent	1	Completed	
11	NCT01369849	CLL	Rituximab	2	Active	
12	NCT01251861	Prostate	Bicalutamide	2	Active	
13	NCT01294306	NSCLC	Erlotinib	2	Active	
14	NCT01186705	Colorectal Cancer	Single agent	2	Active	PIK3CA mutated, KRAS wild type
15	NCT01258998	Lymphoma	Single agent	2	Active	
16	NCT01239342	Kidney cancer	Everolimus	2	Active	
17	NCT01169649	Pancreatic	Single agent	2	Active	
18	NCT01253447	AML	Single agent	2	Active	
19	NCT01312753	Endometrial	Single agent	2	Active	PIK3CA mutated pool
20	NCT01481129	DLBCL	Single agent	2	Active	
21	NCT01277757	Breast cancer	Single agent	2	Active	
22	NCT01349933	Head and neck cancer	Single agent	2	Completed	
23	NCT01306045	NSCLC	Single agent	2	Active	Targeted therapy
24	NCT01248247	NSCLC	Single agent	2	Active	Biomarker mediated therapy

Given an enlarging portfolio of targeted agents, it could be critical to implement these therapies in selected populations with the greatest likelihood for response. Although Akt inhibitors hold great promise, the challenge that lies ahead is their incorporation into available treatment algorithms across malignancies. Further scaffolds of Akt inhibitors could be made to identify the most potent of compounds with minimal toxicities.

CHAPTER 3
OBJECTIVES AND PLAN OF WORK

CHAPTER 3
OBJECTIVES AND PLAN OF WORK

3.1 Objectives:

Components of the Akt signal transduction pathway are appealing as targets for therapeutic intervention, because Akt signaling promotes cell survival, proliferation and invasion, and blocking this pathway could impede the proliferation of tumour cells by either inducing apoptosis or sensitizing tumours to undergo apoptosis in response to other cytotoxic agents.

After thorough review of literature, design for novel scaffolds of Akt inhibitors was considered as utmost importance. Also, resistance played a crucial role in rendering any chemotherapy. Hence the objectives of these study included

I. To discover novel scaffolds of Akt inhibitors by

   A. Development of e-Pharmacophore models for allosteric Akt inhibitors.

   B. High throughput virtual screening of commercially available database of compounds against the allosteric site of Akt.

II. Synthesis of various analogues of Akt inhibitors based on the hits identified in virtual screening.

III. *In vitro* screening and characterization of the lead molecule among the various analogues synthesized.

IV. Generation of Akt resistant lung cancer cell lines and elucidation of the mechanism for resistance of the same.

V. Identification of novel therapeutic combinations for Akt inhibitors to overcome its resistance.

3.2 Plan of Work:

The plan of work for this project was drafted as follows.

1. Discovery of novel scaffold of Akt allosteric inhibitors.

Development of e- Pharmacophore
⬇
Phase find matches
⬇
Glide Receptor docking HTVS (High Throughput Virtual Screening)
⬇
Glide Receptor docking SP (Standard Precision)
⬇
Glide Receptor docking XP (Extra precision)
⬇
Molecules above -8.00 glide score were analyzed for final hits
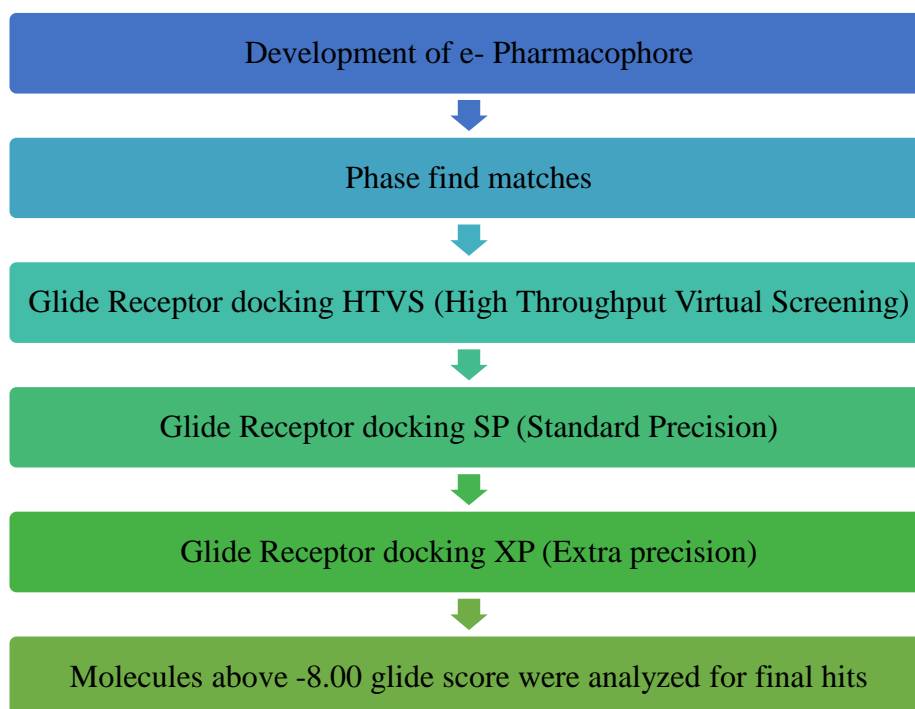
2. Synthesis of analogues based on the hits identified.

3. Identification of a lead molecule for Akt inhibitors by screening the analogues in Akt1 enzyme assay and proliferation assay in NCI-H460 and A549 cell lines.

4. Characterization of the lead molecule:

    a. Apoptosis assay: Estimating the % of cells in apoptosis by labelling with annexin-V/FITC and propidium iodide.

    b. Cell cycle assay: Estimating the % of cells in various phases of cell cycle by labelling with propidium iodide.

    c. Plasma stability: Estimating the % of drug remaining after incubating in rodent, non-rodent and human plasma.

d. Metabolic stability: Estimating the % of drug remaining after incubating in rodent, non-rodent and human liver microsomes.

e. Cellular uptake: Estimating the % of drug permeation after incubating in various cell lines.

f. Biomarker estimation: Quantifying the decrease in p-Akt concentrations in cells treated with the lead molecules.

g. Selectivity of the lead molecule: Estimating the activity of lead molecule in a panel of kinases having at least 50% homology with Akt1 enzyme.

5. Generation of Akt resistant cell lines.

a. Incremental exposure of MK-2206 (a known standard allosteric Akt inhibitor) in H460 and A549 cells to produce respective resistant cell lines.

b. Evaluating the anti-proliferative effect of various Akt inhibitors in both sensitive and resistant cell lines.

6. Mechanism for Akt resistance: Identification of suppression in Akt pathway and over amplification of compensatory pathways.

7. Based on the over expression of compensatory pathways, novel combinations with Akt inhibitors to be tested in both sensitive and resistant cell lines.

CHAPTER 4
MATERIALS AND METHODS

CHAPTER 4
MATERIALS AND METHODS

4.1 Preparation of structure for allosteric domain of Akt1 enzyme:

The structure of Akt1 (3O96 and 4EJN) bound to allosteric inhibitor was retrieved from the protein data bank (PDB). The 3D structure of protein complex was prepared using the protein preparation wizard tool (Schrodinger LLC, 2010); water molecules were deleted other than water molecule in inhibitor bound pocket, bond orders were assigned, hydrogens were added and metals were treated appropriately when present. Next, the orientation of the side chain structures of Gln and Asn was flipped if necessary to provide the maximum degree of H-bond interactions. The charge state of His residues was optimized. Finally, a restrained minimization of the protein structure was performed using the OPLS force field with backbone atoms being fixed (Shivakumar D *et al.*, 2010). The minimized protein was further employed for docking and pharmacophore analysis.

4.2 Grid generation and ligand preparation:

Prepared protein structures were used to generate Glide scoring grids for the subsequent docking calculations. To each of the crystal structures of protein, a grid box of default size (20×20×20A°) was centred on the corresponding active site position. Default parameters were used and no constraints were included during grid generation. The information of binding pocket of a protein for its ligand is very important for revealing true binding mechanism. The crystalized protein structure from PDB already had the sites for IQO and 0R4 bound to 3O96 and 4EJN respectively. The grid was generated for the bound ligand considering it as a reference ligand. The ligand structures of IQO and 0R4 was retrieved from the protein data

bank akin to the Akt1 protein structure. The ligand preparation was then done by ligprep module in Schrodinger (Greenwood JR, *et al.*, 2010).

4.3 Generation of e-pharmacophore models:

Recently developed e-pharmacophore approach of Schrodinger was employed in the construction of these energy – optimized pharmacophores. The e-pharmacophore (Salam NK *et al.*, 2009) conjoins the ligand and receptor-based techniques. Pharmacophoric sites with a default set of six chemical characteristics namely, hydrogen bond donor (HBD), hydrogen bond acceptor (HBA), hydrophobic site, aromatic ring, positive ionisable group and the negative ionisable group are generated using Phase module for each of the best scoring pose in Akt1 complexes obtained from the Glide XP docking calculations. HBD and HBA were represented as vectors along the hydrogen bond axis in accordance with the hybridization of the acceptor or donor atom in the binding site. Projected points allow the possibility of structurally dissimilar active compounds forming hydrogen bonds to the same location, regardless of their point of origin and directionality. The sum of the Glide XP contributions of the atoms is assigned to the respective pharmacophoric features. This mapping of the energy terms to the pharmacophores enables the quantification or the contribution of the ligand sites within the receptor environment (Therese PJ, *et al.*, 2014).

The generated grid files from the prepared receptors of Akt1 were used for the Glide_XP docking calculations. In Glide, the docking module "Write XP descriptor information" option was enabled and rest parameters were kept as default. The XP scoring function was used to order the best ranked compounds and the specific interactions like π-cation and π-π stacking. In brief, the docking models of the IQO and 0R4 were refined using GlideXP, the Glide XP scoring terms were computed, and the energies were mapped into atoms.

4.4 Validation of e-pharmacophore:

In order to verify the reliability of this structure based pharmacophore, decoy set validation was used. Twenty one active compounds collected from literatures were put together with Schrodinger decoy set to build up the test set (Friesner RA, *et al.*, 2004). To determine the performance some important measures were considered i.e., yield of actives, percentage actives and goodness of hit list (GH scoring) were considered. Enrichment factor (EF 1%) was defined as the ratio of the probabilities of searching an active compound in top 1% of dataset given. Boltzmann-enhanced discrimination of receiver operating characteristic (BEDROC) was used to address the "early scoring problem" by Boltzmann weighting of early retrieved hits. The value of α=20.0 and 160.9 were used for comparison. α=20.0 is a reasonable choice for virtual screening evaluations as it corresponds to 80% of the final BEDROC score being accounted in the top 8% of the ranked database.

4.5 Database screening:

4.5.1 E-Pharmacophore mapping:

For the e-pharmacophore approach, explicit matching was required for the most energetically favourable site, provided that it scored better than -1.0 kcal/mol. Multiple sites were included in cases where more than one site had the top score. Screening molecules were required to match a minimum of 3 sites for a hypothesis with 4 sites and a minimum of 4 sites for a hypothesis with 5 or more sites. The distance matching tolerance was set to $2.0A^{0}$ as a balance between stringent and loose fitting alignment. Screening of compounds were performed against Asinex database (www.asinex.com, accessed on 20th May 2012) , were ranked in order of fitness score, a measure of how well the aligned ligand conformer matches the hypothesis based on the RMSD site matching, vector alignments and volume terms. The fitness scoring function was an equally weighted composite of these three terms and ranged from 0 to 3, as implemented

45

in the default database screening of Phase. The ligands with the best fitness scores were docked into the binding sites of 3O96 and 4EJN.

4.5.2 Virtual screening and docking

The starting conformations of ligands were minimized using the OPLS 2005 force field until the energy difference between subsequent structures was 0.001 kJ/mol-A^0. Docking study was performed using Glide. The Glide algorithm estimated a systematic search of positions, orientations and conformations of the ligand in the enzyme-binding pocket *via* a series of hierarchical filters. The shape and properties of the receptor were symbolized on a grid by various dissimilar sets of fields that furnish precise scoring of the ligand pose. The potential hit compounds with good fitness score were considered for docking analysis. All the hits were subjected to high-throughput virtual screen (HTVS) mode. Top 10% of the scoring ligands were kept to move onto the Glide standard precision (SP), where top 5% of the compounds were retained and docked with Glide XP (Xtra Precision). Default values were accepted for van der Waals scaling and input partial charges were used. During the docking process, the G-score was used to select the best conformation for each ligand. G-Score was based on the Chemscore, but included a seric clash term and added buried polar atoms devised by the Schrodinger to penalize electrostatic matches.

4.6 Chemistry

All commercially available chemicals and solvents were used without further purification. TLC experiments were performed on aluminium-backed silica gel 40 F254 plates (Merck, Darmstadt, Germany). Homogeneity of the compounds was monitored by thin layer chromatography (TLC), visualized by UV light and $KMnO_4$ or ninhydrin treatment. Flash chromatography was performed on a Biotage Isolera with prepackaged disposable normal phase silica columns. All ^1H and ^{13}C NMR spectra were recorded on a Bruker AM-400 (400.12

MHz, 75.12 MHz) NMR spectrometer and Bruker BioSpin Corp, Germany respectively. Chemical shifts were reported in ppm (δ) with reference to the internal standard TMS. The signals were designated as follows: s, singlet; d, doublet; dd, doublet of doublets; t, triplet; m, multiplet. Molecular weights of the synthesized compounds were checked by LCMS 6100B series Agilent Technology. Elemental analyses were carried out on an automatic Flash EA 1112 Series, CHN Analyzer (Thermo). Synthesis of target molecules were achieved as depicted in **Figure 4.1** starting from commercially available cyclohexanone.

4.7 Synthetic Scheme

Thiophenopyrimidine analogues were prepared according to the following scheme of reactions.
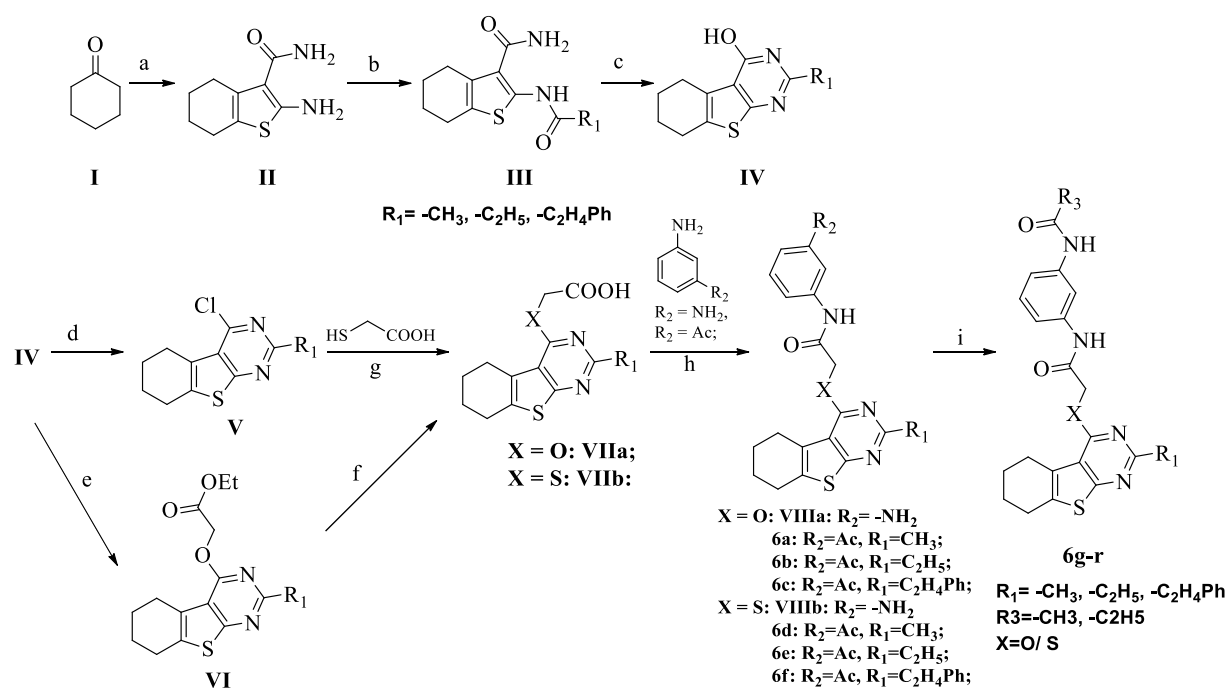
Reagents & Conditions: a: Morpholine, Sulphur powder, EtOH, rt, 7 h; b: R_1COCl, Et_3N, CH_2Cl_2, rt, 4 h; c: NaOH, MeOH, reflux, 12 h; d: $POCl_3$, Toluene, 90 °C, 12 h; e: Ethylbromoacetate, K_2CO_3, DMF, rt, 4 h; f: NaOH, THF/H_2O, rt, 3 h; g: K_2CO_3, DMF, 90 °C, 6 h; h: EDCI, HOBt, Et_3N, CH_2Cl_2, rt, 6 h; i: AcCl or C_2H_5COCl, Et_3N, CH_2Cl_2, rt, 3-6 h;

Figure 4.1: Synthesis procedure for thiophenopyrimide analogues.

4.7.1 Synthesis of compound II

To the stirred solution of compound **I** (3.0 g, 30.56 mmol), 2-cyanoacetamide (2.56 g, 30.56 mmol), sulphur powder (0.97 g, 30.56 mmol) in ethanol (40 mL) was added morpholine (5.31 mL, 61.11 mmol) and stirred the reaction mixture at room temperature for 7 h. the reaction mixture was concentrated, diluted with ethylacetate and washed the organic layer with H_2O (2 × 30 mL). The separated organic layer was dried over anhydrous Na_2SO_4, evaporated and purified by column chromatography to get compound **II** (5.40 g, 90%) as a light yellow solid. ESI-MS found 197 (M+H)$^+$.

4.7.2 General procedure for the synthesis of III

To the stirred solution of compound **II** (1.0 equiv) in CH_2Cl_2 at 0 °C was added Et_3N (2.0 equiv) followed by R_1COCl (1.2 equiv) and allowed to stir at room temperature for 4 h. The reaction mixture was diluted with CH_2Cl_2 and washed with saturated $NaHCO_3$, H_2O and dried over anhy Na_2SO_4 and evaporated under vacuo to get compound **III** as an off-white solid.

2-Acetamido-4,5,6,7-tetrahydrobenzo(b)thiophene-3-carboxamide (IIIa):

To the stirred solution of compound **II** (2.0 g, 10.20 mmol) in CH_2Cl_2 at 0 °C was added Et_3N (2.91 mL, 20.40 mmol) followed by acetyl chloride (0.88 mL, 12.24 mmol) and allowed to stir at room temperature for 4 h. The reaction mixture was diluted with CH_2Cl_2 and washed with saturated $NaHCO_3$ (3 × 30 mL), H_2O (3 × 20 mL) and dried over anhy Na_2SO_4, evaporated under vacuo to get title compound (2.14 g, 87%) as a pale yellow solid. ESI-MS showed desired mass and carried to the next step. Similarly IIIb and IIIc were synthesized using propionoyl chloride and phenyl propyionoyl chloride respectively.

4.7.3 General procedure for the synthesis of IV

To a solution of the respective compound **III** in MeOH (2.0 vol) was added a solution of 1N NaOH (10.0 vol) and the mixture was refluxed for 3 h. then the mixture was poured into water

and neutralised with a concentrated solution of HCl to give a precipitate which was filtered and washed with water and dried to obtain desired compound.

2-Methyl-5,6,7,8-tetrahydrobenzo(4,5)thieno(2,3-d)pyrimidin-4-ol (IVa)

To a solution of 2-acetamido-4,5,6,7-tetrahydrobenzo(b)thiophene-3-carboxamide (2.0 g) in MeOH (4 mL) was added a solution of 1N NaOH (20 mL) and the mixture was refluxed for 3 h and then the mixture was poured into water and neutralised with a concentrated solution of HCl to give a precipitate which was filtered and washed with water, cold ethanol and dried to obtain title compound (1.50 g, 83%) as a white solid. Similarly, IVb and IVc were synthesized from IIIb and IIIc respectively.

4.7.4 General procedure for the synthesis of V

To a suspension of compound **IV** in toluene (10.0 vol) was added dropwise $POCl_3$ (3.0 vol), then the reaction mixture was heated at 90 °C for 12 h and evaporated to dryness. The residue was treated with sat $NaHCO_3$ solution and extracted with CH_2Cl_2. The organic layer was dried over anhy. Na_2SO_4, filtered and evaporated under reduced pressure to get compound **V**.

4-Chloro-2-methyl-5,6,7,8-tetrahydrobenzo(4,5)thieno(2,3-d)pyrimidine (Va)

To the suspension of 2-methyl-5,6,7,8-tetrahydrobenzo(4,5)thieno(2,3-d)pyrimidin-4-ol (3.0 g, 13.63 mmol)in toluene was added $POCl_3$ (9.0 mL, 3V) and the reaction mixture was allowed to stir at 90 °C for 12 h and evaporated to dryness. The residue was treated with sat $NaHCO_3$ (3×30 mL) solution and extracted with CH_2Cl_2. The organic layer was dried over anhy. Na_2SO_4, filtered and evaporated under reduced pressure to get crude residue. The crude was purified by column chromatography using EtOAc/hexanes as eluent to afford title compound (2.70 g, 83%) as a white solid. Similarly, Vb and Vc were synthesized from IVb and IVc respectively.

4.7.5 Synthesis of VI

To a stirred solution of compound **V** in DMF, was added K_2CO_3 (2.5 equiv) followed by ethylbromoacetate (1.2 equiv) and stirred the reaction mixture at room temperature for 4 h. Ice water was added to the reaction mixture and the obtained solids were filtered, washed with water, cold ethanol and hexanes to get compound **VI**.

4.7.6 Synthesis of VIIa

To the stirred solution of compound **VI** in THF/H_2O at 0 °C was added NaOH (3.0 equiv) and stirred at room temperature for 3 h. The reaction mixture was neutralised with 6N HCl and the product was extracted with EtOAc. The combined organic phase was dried over anhy. Na_2SO_4 and concentrated to get solid compound. The solids were triturated with CH_2Cl_2/Hexane to get pure product.

4.7.7 Synthesis of VIIb

To a stirred solution of compound **VI** in DMF, was added K_2CO_3 (2.0 equiv) followed by thioglycolic acid (1.2 equiv) and stirred the reaction mixture at 90 °C for 6 h. Ice water was added to the reaction mixture and the obtained solids were filtered, washed with water, cold ethanol and hexane to get compound **VIIb**.

4.7.8 Synthesis of VIIIa/VIIIb

To the stirred solution of compound **VIIa** (for compound **VIIIa**)/**VIIb** (for compound **VIIIb**) in CH_2Cl_2 at 0 °C was added EDCI, HOBt followed by Et_3N and stirred the reaction mixture for few minutes. A solution of *m*-phenylenediamine in CH_2Cl_2 was added and allowed the reaction mixture to stir at room temperature for 6 h.

4.7.9 General procedure for the synthesis of compounds 6a-f

To the stirred solution of compound **VIIIa** (for compounds **6a-c**)/**VIIIb** (for compounds **6d-f**) in CH_2Cl_2 at 0 °C was added EDCI, HOBt followed by Et_3N and stirred the reaction mixture for few minutes. Then 3-aminoacetophenone was added and allowed the reaction mixture to

stir at room temperature for 6 h. The reaction mixture was diluted with EtOAc, washed with H_2O. The separated organic layer was dried over anhydrous Na_2SO_4 and evaporated to get crude compound. The crude was purified by column chromatography using 30% EtOAc in hexanes as eluent.

4.7.10 General procedure for the synthesis of compounds 6g-r

To the stirred solution of compound **VIIIa** (for compounds **6g-i**)/**VIIIb** (for compounds **6j-l**) in CH_2Cl_2 at 0 °C was added acetyl chloride followed by Et_3N and stirred the reaction mixture at room temperature for 6 h. The reaction mixture was concentrated, obtained solids were washed with H_2O, dried in vacuum oven and triturated with CH_2Cl_2/hexanes to get pure products.

To the stirred solution of compound **VIIIa** (for compounds **6m-o**)/**VIIIb** (for compounds **6p-r**) in CH_2Cl_2 at 0 °C was added propionyl chloride followed by Et_3N and stirred the reaction mixture at room temperature for 6 h. The reaction mixture was concentrated, obtained solids were washed with H_2O, dried in vacuum oven and triturated with CH_2Cl_2/hexanes to get pure products.

4.8 Biological evaluation

Human lung carcinoma cell lines NCI-H460, NCI-H1975, NCI-H2170 and A549 were procured from American Type Culture Collection (Manassas, VA, USA). All cell lines were routinely cultured in RPMI-1640 growth medium supplemented with 10% fetal bovine serum (Sigma, St. Louis, MO, USA) and 1% Penicillin-Streptomycin solution (Sigma, St. Louis, MO, USA) at 37 °C in a humidified 5% CO_2 incubator. Akt inhibitors MK2206, CCT128930 and A674563 were purchased from Selleckchem (Houston, TX, USA). Myc inhibitor 10058-F4 was purchased from Calbiochem (La Jolla, CA, USA). Antibodies against p-Akt (S^{473}), p-Akt (T^{308}), p-Akt (T^{450}), p-p53 (S^{15}), p-p38 (T^{180}), p-Erk (T^{202}), p-STAT5a (T^{694}), Akt, β-Actin, c-Myc and corresponding secondary antibodies were purchased from Cell signalling

technologies (Danvers, MA, USA). Glutaminase antibody was purchased from Abcam (Cambridge, MA, USA). Cobalt chloride and all the other reagents were purchased from Sigma (St. Louis, MO, USA).

Guava cell cycle reagent was purchased from Guava technologies (Hayward, USA). Antibodies were purchased from Cell Signaling (USA). FLICA reagent was purchased from Millipore (USA). Human Umbilical Vascular Endothelial Cells (HUVEC) were also purchased from ATCC and cultured in F-12K medium supplemented with 10% FBS, 0.1 mg/ml heparin and 0.05 mg/ml endothelial cell growth supplement. Human Tracheal Epithelial Cells (HTEpiC) were purchased from ScienCell Research Laboratories (Carlsbad, CA) and maintained in bronchial epithelial cell medium. Cells were maintained at 37 ^{o}C in a 5% CO_2/95% air incubator and were subcultured in 1:5 ratio twice a week.

4.8.1 *In vitro* Akt1 enzyme assay:

Akt1 enzyme inhibition assay was performed according to instructions detailed by the manufacturer (Z'-lyte^{TM} Akt1 assay kit, Invitrogen) and reviewed by Goddard JP, *et al.*, 2004. We used fluorescence resonance energy transfer (FRET) between coumarin and fluorescein for detection. In the primary reaction, the kinase transfered the gamma-phosphate of ATP to a single tyrosine, serine or threonine residue in a synthetic FRET-peptide. In the secondary reaction, a site-specific protease recognized and cleaved non-phosphorylated FRET-peptides. Phosphorylation of FRET-peptides suppressed the cleavage by the development reagent. Cleavage disrupted FRET between the donor (i.e., coumarin) and acceptor (i.e., fluorescein) fluorophores on the FRET-peptide, whereas uncleaved, phosphorylated FRET-peptides maintained FRET. A ratiometric method, which calculated the ratio (the Emission Ratio) of donor emission to acceptor emission after excitation of the donor fluorophore at 400 nm, was used to quantitate reaction progress. Briefly, 2 μM Z'-LYTE^{TM} Ser/Thr peptide 6 was added

to 10 ng/ml Akt1 enzyme at 10 µM concentration of ATP and incubated at room temperature for 1 h along with inhibitors. The reaction was then developed, stopped and fluorescence was measured at 400 nm excitation and 445 and 520 nm emissions and emission ratios (ER) were calculated as shown in the equation below.

Emission ratio (ER) = $\dfrac{\text{Coumarin Emission (445 nm)}}{\text{Fluorescein Emission (520 nm)}}$

The activity of enzyme in presence of compounds were calcualeted based on the equation below.

% Inhibition = 100 - $\dfrac{\text{(Sample ER - Blank ER)*100}}{\text{(Enzyme Control ER - Blank ER)}}$

Blank consisted of all reaction components except enzyme and test compounds, while enzyme control contained all reaction components except test compounds.

4.8.2 Cell proliferation assay

Cell proliferation was assessed using the MTT staining as described by Mossman (Mosmann T, 1983). The MTT assay was based on the reduction of the tetrazolium salt, MTT, by viable cells. The dehydrogenase using NADH or NADPH as coenzyme converted the yellow form of the MTT salt to insoluble, purple formazan crystals (Liu KZ., et al., 1997). Formazan solution was read spectrophotometrically after the crystals were dissolved by organic solvent (DMSO). H460, A549, H1975, H2170, HTEpiC and HUVEC cells ($5*10^3$ cells) were plated per well in a 96 well plate and treated with appropriate concentrations of test compounds and incubated for 72 h at 37 ^{O}C in a 5% CO_2/95% air incubator. Viability of cells was determined by estimating the amount of soluble formazan (in DMSO) formed after addition of 100 µg MTT and a 3.5 h incubation at 37 ^{O}C. Media was removed and the crystals were dissolved in 150 µl DMSO. Absorbance was measured at 450 nm on Fluostar Omega (BMG Labtech, USA). Each concentration was tested in three different experiments, run in

triplicates. Means and standard errors of mean were calculated and reported as the percentage of growth vs. control.

4.8.3 Caspase-3 assay

Caspase-3 activity in cells was measured using CHEMICON®'s CaspaTag™ In Situ Caspase Detection Kit. The methodology was based on fluorochrome inhibitors of caspases (FLICA) based cell permeable and non- cytotoxic dyes which bound covalently to the active caspase (Ekert PG, *et al.*, 1999). This kit employed a carboxyfluorescein-labeled fluoromethyl ketone peptide inhibitor of caspase-3 (FAM-DEVD-FMK), which produced a green fluorescence. When added to a population of cells, the FAM-DEVD-FMK probe entered each cell and was covalently bound to a reactive cysteine residue that resided on the large subunit of the active caspase heterodimer, thereby inhibiting further enzymatic activity. The bound labeled reagent was retained within the cell, while any unbound reagent would diffuse out of the cell and was washed away. The green fluorescent signal was a direct measure of the amount of active caspase-3 or caspase-7 present in the cell at the time the reagent was added. Cells were plated at 100,000 per well in a 6-well plate and incubated with the compound for 72 h at 37 $^{\circ}$C in a 5% CO_2 incubator. Cells were washed and incubated with FLICA reagent for 30 min. After incubation, cells were washed to remove the excess of FLICA and suspended in PBS. Fluorescence was measured at 485 nm excitation and 520 nm emission on Fluostar Omega (BMG Labtech, USA).

4.8.4 Cell cycle analysis

The nuclear DNA content of a cell can be quantitatively measured by flow cytometry using propidium iodide, a fluorescent dye that binds stoichiometrically to the DNA (Krishnan A, 1975). G1 cells would have one copy of DNA and would therefore showed 1X fluorescence intensity. Cells in G2/M phase of the cell cycle would have two copies of DNA and accordingly

would show 2X intensity. Since the cells in S phase would be synthesizing DNA they would have fluorescence values between the 1X and 2X populations. Cells were plated at 100,000 per well in a 6-well plate and incubated with the compound for 72 h at 37 ^{O}C in a 5% CO_2 incubator. After incubation, cells were fixed in 70% ethanol and stored at 4 ^{O}C till analysis. Cells were stained with Guava Cell Cycle reagent (propidium iodide) according to the manufacturer's instructions. Cell cycle data were obtained using the Guava Personal Cell Analysis System (Millipore, USA).

4.8.5 Western blotting

Cells were washed twice with PBS, trypsinized, and washed twice with ice-cold PBS. Cell pellets were lysed in a buffer containing 50 mM Tris-HCl (pH 7.5), 150 mM NaCl, 0.5% sodium deoxycholate, 0.1% Triton X, 0.1% SDS, 25 mM sodium fluoride, 200 μM sodium orthovanadate, 1X protease inhibitor cocktail for 30 min on ice. Cell lysates were clarified by centrifugation for 10 min at 14,000 $\times$ g, and the total protein concentration in the resultant supernatants was determined using a Bradford protein assay kit (Biorad, Hercules, CA). Equal amounts (50 μg) of protein was heated in SDS sample buffer with DTT (final concentration, 10 mM) at 98°C, fractionated by size on 7.5% SDS-polyacrylamide gels, and transferred onto PVDF membranes (Millipore). Membranes were blocked by incubation for 1 h with TBS-T (25 mM Tris-HCl (pH 7.6), 150 mM NaCl, and 0.05% Tween 20) containing 5% BSA (Bovine serum albumin). Membranes were incubated with antibody at 4°C overnight in TBS-T containing 5% BSA followed by the corresponding HRP-linked secondary antibody at room temperature for 1 h in TBS-T containing 5% nonfat milk powder. Chemiluminescence substrate was then added to the membranes followed by the exposure to x-ray films. Band intensity was calculated using ImageJ 1.42 (NIH, USA).

4.8.6 ROS assay:

Reactive oxygen species (ROS) in cells were estimated in cells using a fluorescent dye, DCFDA (2',7'-Dichlorodihydrofluorescein diacetate) (Eruslanov E, *et al*., 2010). The cell permeant DCFDA was chemically reduced to fluorescein in presence of ROS upon cleavage of acetate groups by intracellular esterases and oxidation. Briefly, 100,000 cells were plated in a 6-well plate and incubated with compound for 24 h. Cells were trypsinized and DCFDA was added at 1 μM concentration and incubated at 37 ^{O}C for 15 min followed by a wash with PBS to remove the excess of dye. The fluorescent intensity of cells were obtained using the Guava Personal Cell Analysis System (Millipore, USA).

4.8.7 Annexin V assay

Annexin V-FITC/PI dual labelling identified cells in apoptotic phase. In normal viable cells, phosphatidylserine (PS) was located on the cytoplasmic surface of the cell membrane. However, in apoptotic cells, PS was translocated from the inner to the outer leaflet of the plasma membrane, thus exposing PS to the external cellular environment. The human vascular anticoagulant, annexin V, is a 35–36 kD Ca^{2+}-dependent phospholipid-binding protein that showed high affinity for PS. Annexin V labeled with a fluorophore or biotin could identify apoptotic cells by binding to PS exposed on the outer leaflet (Vermes I, *et al.*, 1995). Briefly, 100,000 cells were plated in a 6-well plate and incubated with compound for 24 h. Cells were trypsinized and Annexin-V-FITC and propidium iodide were added and incubated at 37 ^{O}C for 15 min followed by a wash with PBS and the fluorescent intensity of cells were obtained using the Guava Personal Cell Analysis System (Millipore, USA).

4.8.8 Cellular uptake:

To evaluate the permeability of compound into cells, 100,000 cells were plated in a 6-well plate and incubated with 1 µM of compound for 1 h. Cells were lysed in 1:1 ratio of methanol and water, and the concentration of compound was analysed using LC-MS/MS.

4.8.9 Plasma stability:

To evaluate the stability of compounds in plasma, 1 µM of compound was spiked into 100 µl plasma (human, dog and mouse) and incubated for 1 h followed by extraction with 150 µl methanol and the concentration of compound was analysed using LC-MS/MS.

4.8.10 Metabolic stability:

To evaluate the stability of compound in liver microsomes against metabolic degradation, 1 µM of compound was spiked into 100 µl liver microsomes and incubated for 1 h followed by extraction with 150 µl methanol and the concentration of compound was analysed using LC-MS/MS.

4.8.11 Intracellular glutamine and glutamate concentrations

Intracellular glutamine and glutamate content after a 24 h treatment period was measured by liquid chromatography-tandem mass spectrometry (LC-MS/MS). Samples were prepared as follows: Cells (0.2 million) were treated with compounds for 24 h in a humidified incubator at 37 °C with 5% CO_2. Cells were washed twice in PBS and lysed in 50% methanol: water followed by probe sonication. After centrifugation at 14,000 × g for 10 min, the supernatant was collected and stored at −80°C until analysis by LC-MS/MS. Results were confirmed in two independent experiments.

4.8.12 LC-MS/MS conditions

- Mobile phase buffer : 2 mM Ammonium acetate

- Organic solvent : Methanol

- Flow : Gradient

- Flow rate : 1ml/min

- Run time : 5 min

- Splitter : 1:3

- Column : Varian, C18 250*4.6 mm

- Injection volume : 5 μl

4.9 Statistical analysis

Calculation of growth inhibition GI_{50}s were performed using GraphPad Prism 6.0 (La Jolla, USA) by fitting the data in non-linear regression model with variable slope. Data are expressed as mean ± SEM. Two way analysis of variance (ANOVA) was performed followed by Dunnett's test as a post hoc test for comparison and calculating significant difference. A p value <0.05 was deemed significant. Combination indices were calculated using Compusyn 2.0 (Combysyn, USA).

CHAPTER 5

DESIGN AND LEAD IDENTIFICATION FOR ALLOSTERIC
Akt INHIBITION

CHAPTER 5
DESIGN AND LEAD OPTIMISATION FOR ALLOSTERIC Akt INHIBITION

The potential allosteric inhibitors that were expected to bind the PH-kinase domain and the LINK cavity of Akt1 were identified by using pharmacophore modeling and docking approaches. Pharmacophore models were built based on the information of the binding site of the receptor or based on the previously identified allosteric inhibitors for Akt1. ASINEX drug-like database was filtered based on 3D similarity to the pharmacophore hypotheses. Two-step docking was applied using Glide to predict binding modes and affinities of compounds in the filtered database. The compounds selected were further filtered based on interaction with Trp80, fitness to pharmacophore hypothesis, ADME (absorption, distribution, metabolism and elimination) and drug likeness.

5.1 Development of e-pharmacophore for Akt1 allosteric site

Since the structures of Akt1 enzyme and its allosteric inhibitors were available, energy based pharmacophore (e-pharmacophore) models were derived directly from the complex crystal structures. Template protein-ligand complex as (3O996 and 4EJN) were energetically optimized and the generated energetic terms were computed by the Glide XP scoring function (Glide, version 5.8, Schrödinger, LLC, New York, NY, 2012) to rank the important pharmacophore features. Crystal ligand for 3O96 was taken as reference ligand to generate e-pharmacophore, since it was known to be a non-covalent inhibitor of Akt1 and had a low IC_{50} value of 58 nM. Ligand interaction plots were represented in **Figure 5.1**. All hypotheses were subjected for validation by using decoy set database, which included 21 known active Akt

inhibitors and 1000 decoy compounds. Two e-pharmacophore models were generated using Glide module available in Schrodinger with default parameters from Akt1 complexed with compound **2** (PDB code: 3O96). Five feature pharmacophore model consisted of 3 ring features (R), one acceptor (A) and one donor (D), whereas 4-feature pharmacophore model consisted of 3 ring features and one acceptor. Both pharmacophores were validated using enrichment calculator script available in Schrodinger. Similar pharmacophores were generated from the other crystal structure as well (4EJN). However, enrichment factors (EF) were higher in the pharmacophores developed from 3O96 as shown in **Table 5.1**.

A

B
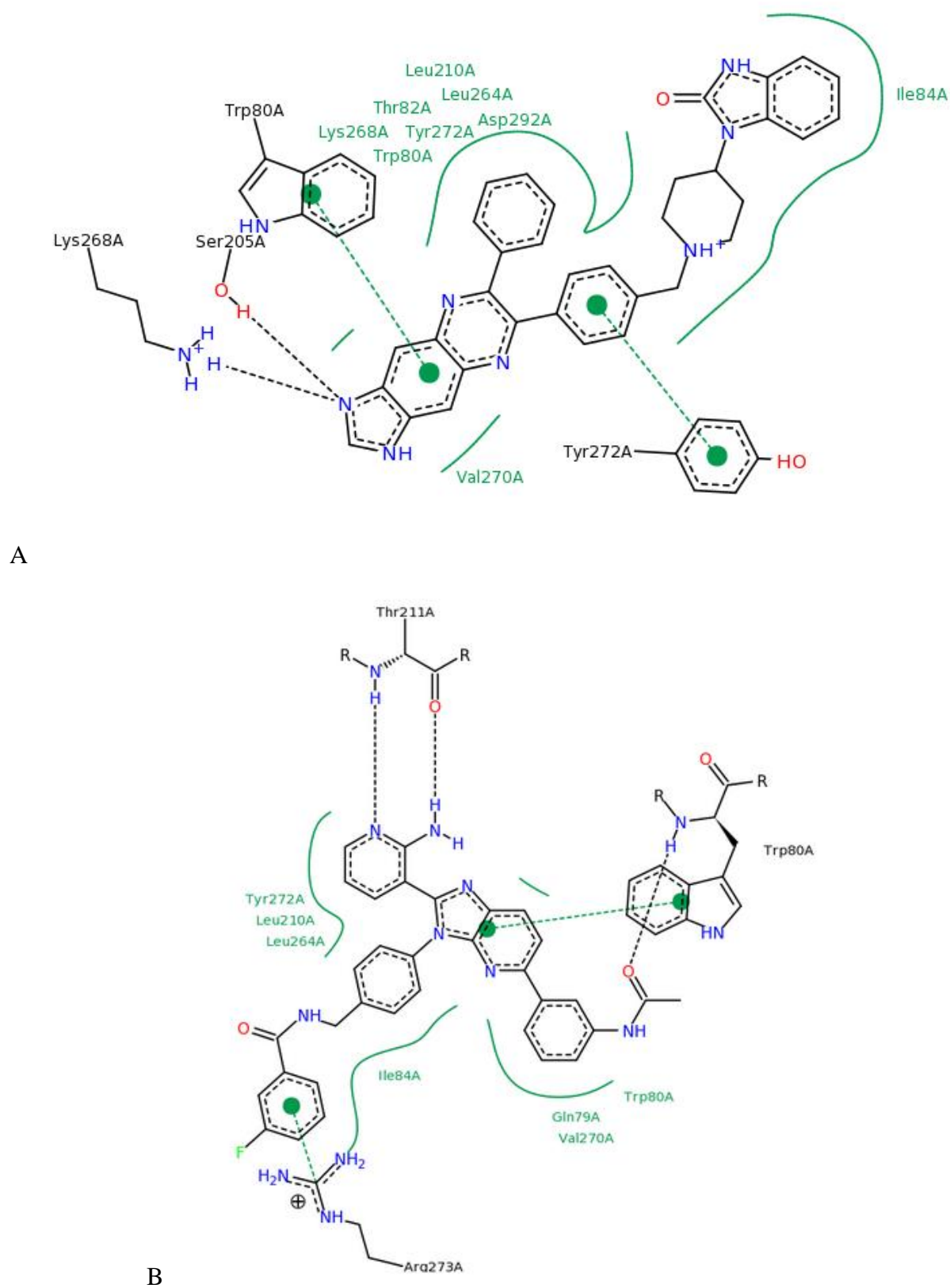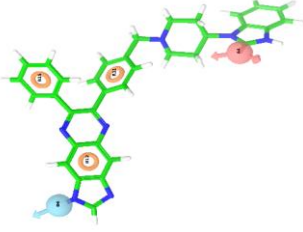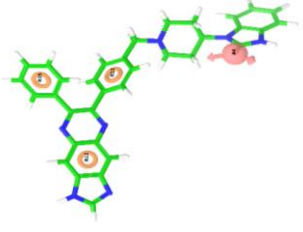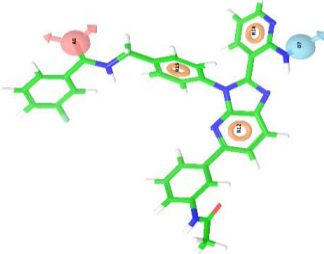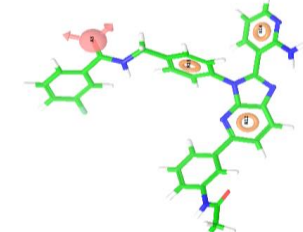
Figure 5.1: Ligand interaction plots for 3O96 (A) and 4EJN (B).

Table 5.1: Pharmacophore models developed for identification of allosteric Akt inhibitors.

Name	3O96_5 Point Hypothesis	3O96_4 Point Hypothesis	4EJN_5 Point Hypothesis	4EJN_4 Point Hypothesis
Pharmacophore				
BEDROC α20.0	0.223	0.316	0.228	0.255
EF1%	19	24	14	4.8
EF2%	9.5	14	7.1	4.8
EF5%	3.8	5.7	4.8	7.6
AUC	1	1	0.99	0.98
GH	0.797	0.239	0.106	0.152

BEDROC: Boltzmann enhanced discrimination of receiver operating characteristic, **EF**: Enrichment factor,

AUC: Area under curve, **GH**: Goodness of hit.

The validated e-pharmcophore was later utilized for the virtual screening workflow, where Glide provided three different levels of docking precision modes, high throughput virtual screening (HTVS), standard precision (SP) and extra precision (XP) and finally with druggability and ADME property filter using QikProp. Commercial database compounds (Asinex) were initially checked for Phase find matches filter, where fitness more than 1.5 were taken as cut-off and further shortlisted based on docking based virtual screening and ADME filter. After visual examination of the docking poses, 16 compounds were found to be good in binding interaction with important amino acid residues including Trp80 within the active pocket of Akt1.

5.2 Virtual screening

Virtual screening studies of the compound database retrieved novel active molecules and filtered out the inactive molecules. The interpretation of the e-pharmacophore provided insights to crucial structural requirements for inhibition of Akt and thus can act as a guide for further modification of the lead molecules. The best validated pharmacophore models were from 3O96 as shown in **Table 5.1,** were used to screen against the database of 5,02,500 compounds (Asinex database). Compound VIII, the crystal ligand for 3O96 with IC$_{50}$ 58 nM (Wu WI *et al.*, 2010) was taken as reference ligand, since it has shown non-covalent interactions with the Akt. MK2206 was also taken as a reference compound for docking as it has highest potency (8 nM) among all the Akt1 allosteric inhibitors. Initially, compounds with fitness more than 1.5 were taken as cut-off and further shortlisted based on predicted activity. While predicted activity more than 5.0 (50246) were taken for HTVS (High throughput virtual screening) as primary docking. 5222 compounds from HTVS with a glide score less than -6.0 were further refined using SP (standard precision) docking module and then 320 ligand molecules were identified with good glide score (< -6.0). Finally, the 320 compounds from standard precision docking was agained docked with XP (Xtra precision) and identified molecules with docking

score of above -9.5. The cut off value was taken as 9.5 as the reference crystal ligand of 3O96 glide score was found to be -9.53. Thus, we acquired 16 compounds from highly precise XP docking study and these ligands were identified based on glide score and visual inspection of the crucial amino acid residue binding and absence of non-peptidic moieties (**Figure 5.2 and Figure 5.3**). The important amino acid residues for good binding were found to be Trp 80 based on the crystal ligand interactions in 3O96. The docking poses of top 16 hit compounds are represented in **Figure 5.2 and 5.3**. Predicted activities, Glide scores, interacting amino acids of the top 10 hits are presented in the **Table 5.2**.
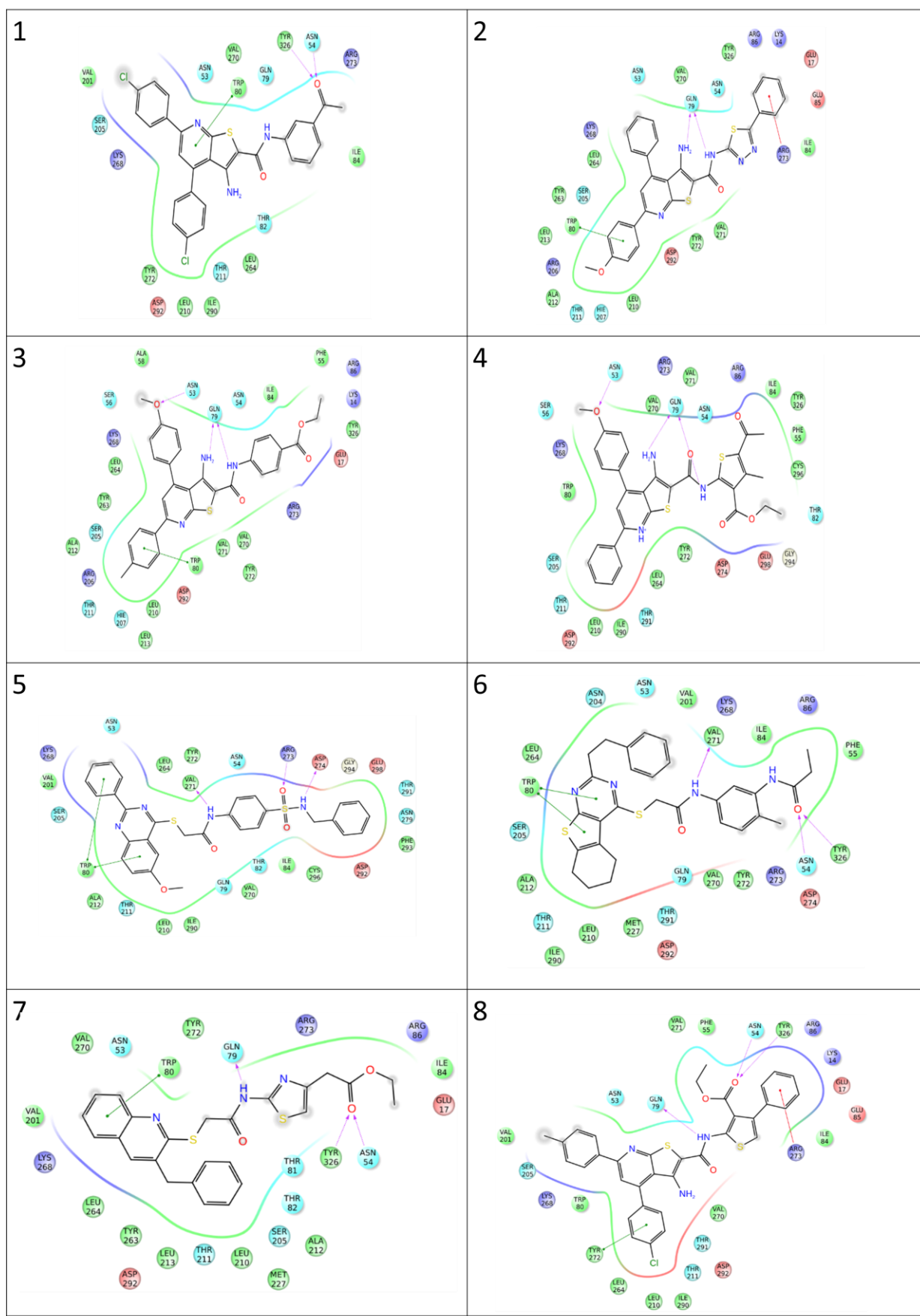
Figure 5.2: Ligand interaction plots for **leads 1-8.**
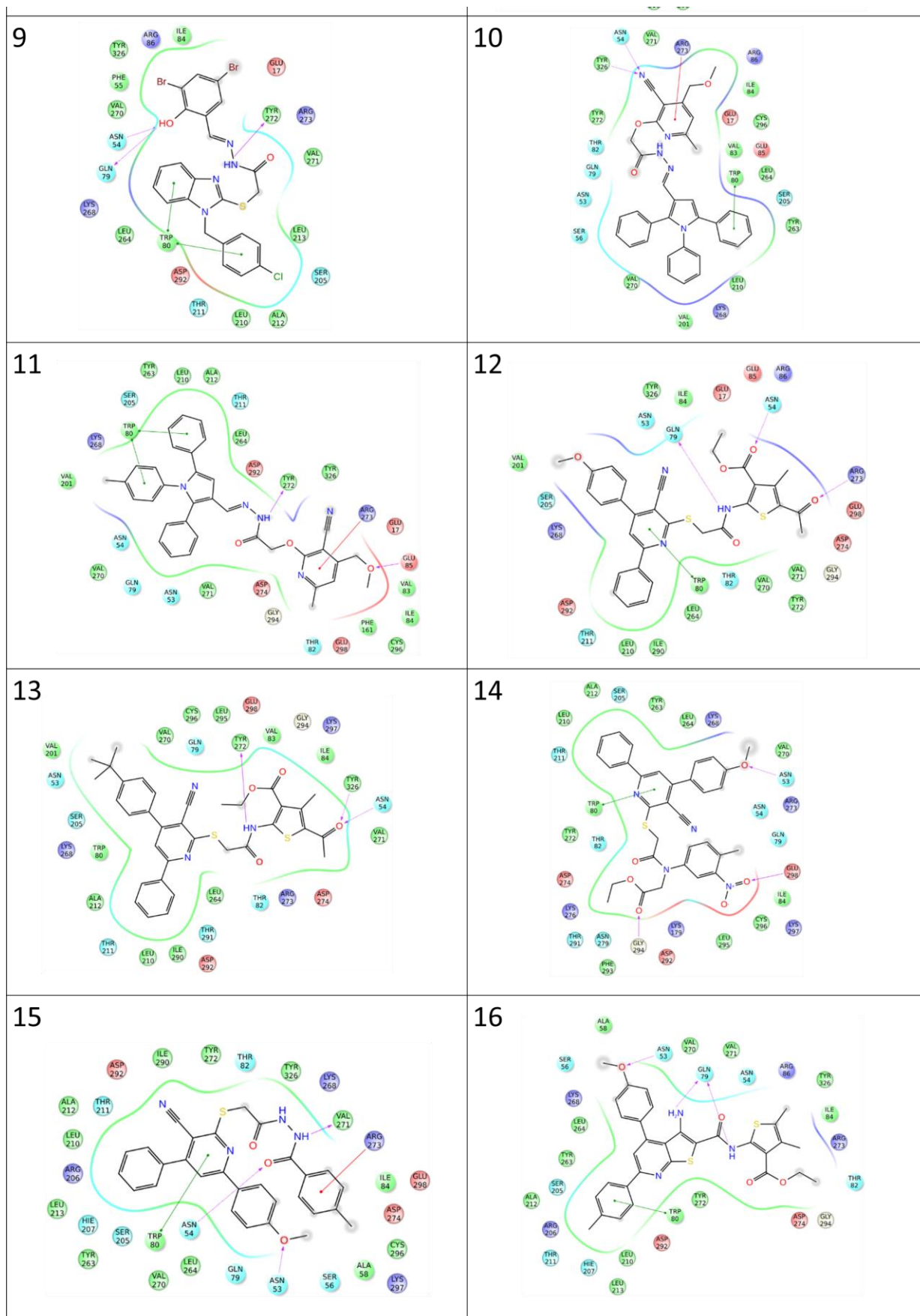
Figure 5.3: Ligand interaction plots for **leads 9-16**.
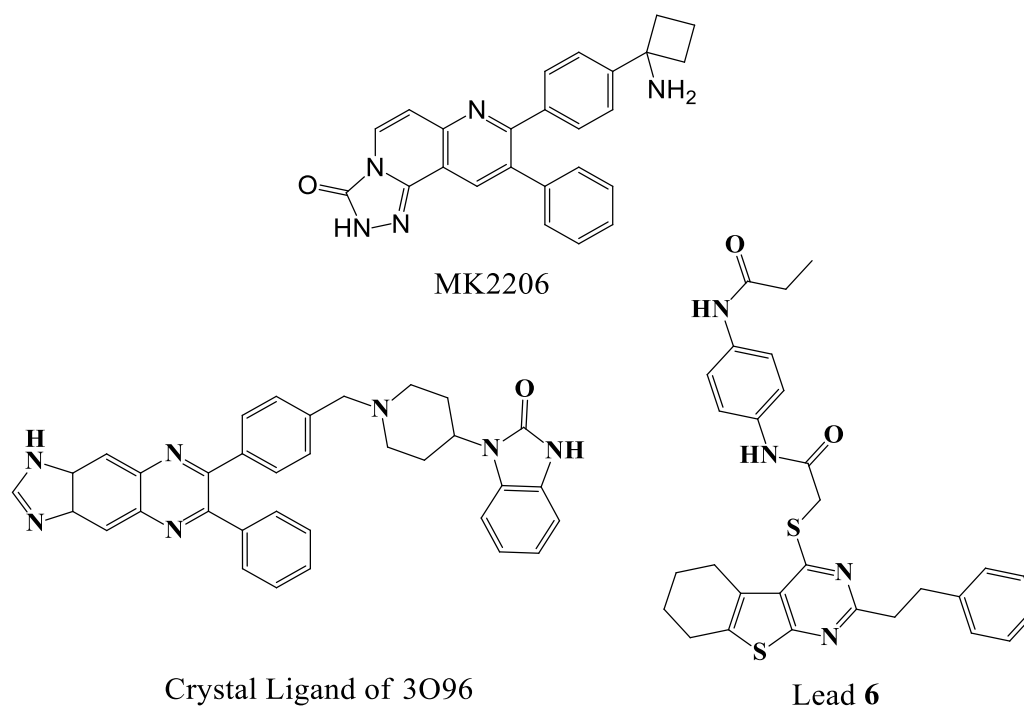
Figure 5.4: Structures of allosteric Akt inhbitiors. MK2206, crystal ligand and lead molecule identified.

5.3 Identification of lead molecules.

Molecules identified by virtual screening were tested *in vitro* for their ability to inhibit Akt activity in Akt1 enzyme assay at a concentration of 1 μM and 10 μM according to the protocol explained under materials and methods section **4.8.1**. Along with Akt inhibition, anti-proliferative activity in H460 and A549 were also tested for these compounds at both 1 μM and 10 μM concentrations. The percentage inhibitions of the compounds are as in **Table 5.2**. Lead **6** showed the best activity in enzyme as well as in cellular proliferation assays and hence was further characterised.

Table 5.2: Akt1 enzyme screening and anti-proliferation activity of selected compounds in H460 and A549 cell lines. % inhibition values were calculated compared to DMSO treated controls and are represented below.

Cells	H460		A549		Akt1 enzyme	
Compound	1 µM	10 µM	1 µM	10 µM	1 µM	10 µM
Lead 1	27.88	46.47	0	54.01	1.52	34.96
Lead 2	4.4	39.86	0	3.2	4.4	31.2
Lead 3	0	37.43	4.43	22.99	0.25	15.75
Lead 4	27.18	24.7	24.55	14.72	15.27	41.21
Lead 5	0	36.58	45.37	46.73	25.36	33.28
Lead 6	29.84	84.44	58.44	82.27	80.12	100
Lead 7	0	42.45	0	4.23	0	0
Lead 8	23.55	32.36	11.41	25.36	15.33	42.59
Lead 9	0	33.1	0	26.74	0	0
Lead 10	0	17.94	7.12	6.2	12.89	26.47
Lead 11	0	0	0	0	24.12	34.76
Lead 12	0	0	24.07	0	0.27	6.21
Lead 13	0	7.31	0	0	1.75	40.25
Lead 14	0	0	0	0	24.39	48.97
Lead 15	0	1.34	25.1	0	7.83	10.09
Lead 16	9.29	48.01	0	3	21.36	41.28
MK2206	30.61	62.39	40.01	73.95	90.24	95.52

5.4 Validation of lead 6 as Akt allosteric inhibitor.

5.4.1 Quantification of Akt1 enzyme activity

Akt1 enzyme inhibition assay was based on a fluorescence resonance energy transfer (FRET) between coumarin and fluorescein for detection. In the primary reaction, the kinase transferred gamma-phosphate of ATP to a single tyrosine, serine or threonine residue in a synthetic FRET-peptide. In the secondary reaction, a site-specific protease recognized and cleaved non-phosphorylated FRET-peptides. Lead **6** was tested for its ability to inhibit Akt1 enzyme *in vitro*. As shown in **Figure 5.5A**, half maximal enzyme inhibition (IC_{50}) for lead **6** was calculated to be 256 nM. IC_{50} for standard Akt inhibitor, MK2206, was found to be 9 nM. To test the allosteric nature of the binding of lead **6**, ATP concentration in the enzymatic reaction was increased from 10 μM to 100 μM and 1000 μM (**Figure 5.5B**). All the three conditions showed similar IC_{50} values for lead **6** with no significant difference indicating that the compound binding to Akt1 enzyme was non-competitive with ATP.
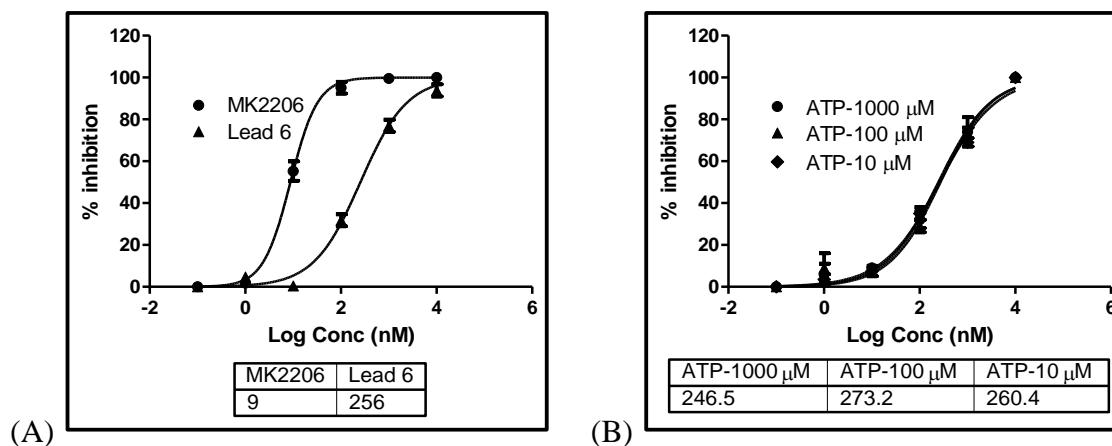
Figure 5.5: Enzymatic activity of lead 6. A. IC_{50} of lead **6** in Akt1 enzyme assay compared to MK2206. B. Allosteric activity of lead **6** in Akt1 enzyme assay. Procedure for Akt1 enzyme assay was detailed in materials and methods chapter **4.8.1**.

5.4.2 *In vitro* cell proliferation assay

To investigate the effect of lead **6** as anticancer agent, it was evaluated for its ability to inhibit growth in various lung cancer cell lines. Expression levels of p-Akt in various cell lines were evaluated prior to using them as tools to test compounds. Rank order of p-Akt expression in the cell lines tested was found to be H460>A549> H2170>H1975 **(Figure 5.6)**. Anti-proliferative activity of lead **6** in the aforementioned cell lines corroborated with the expression levels of p-Akt **(Figure 5.7A).** Half maximal growth inhibition (GI_{50}) values **(Table 5.3)**, indicated a 10-fold difference in sensitivity between H460 and H1975 to lead **6**. In contrast to its effect on H460 and A549, lead **6** did not affect the proliferation of HTEpiC and HUVE cells **(Figure 5.7B)**. A 100-fold change in GI_{50} was observed between the most sensitive of the cell lines (H460) compared to normal HTEpiC cells, indicating a better selectivity of lead **6** towards cancerous cells with inherently high levels of p-Akt.
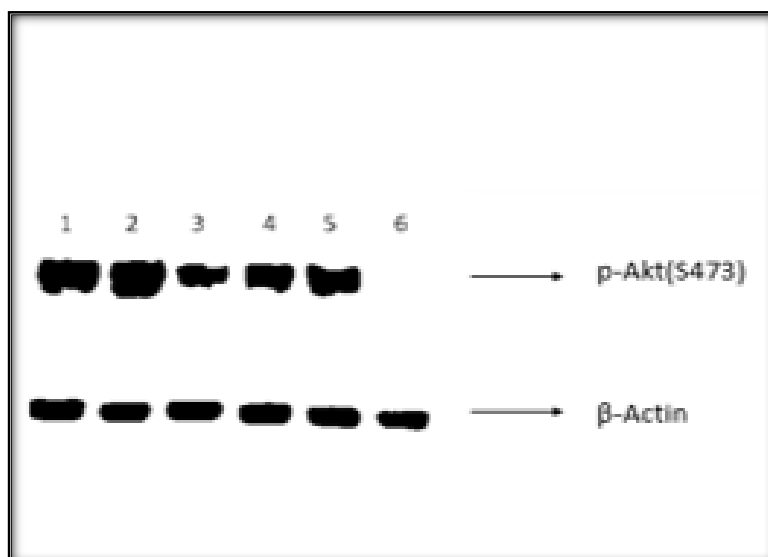
Figure 5.6: Expression of p-Akt in various Lung cancer cell lines. Cells were treated with lead **6** for 4 h, lysed and p-Akt expression was quantified by western blot. Representation of lanes: 1. A549, 2. H460, 3. H1975, 4. H2170, 5. HTEpiC and 6. MDA-MB-231. MDA-MB-231 was taken as a negative control cell line.
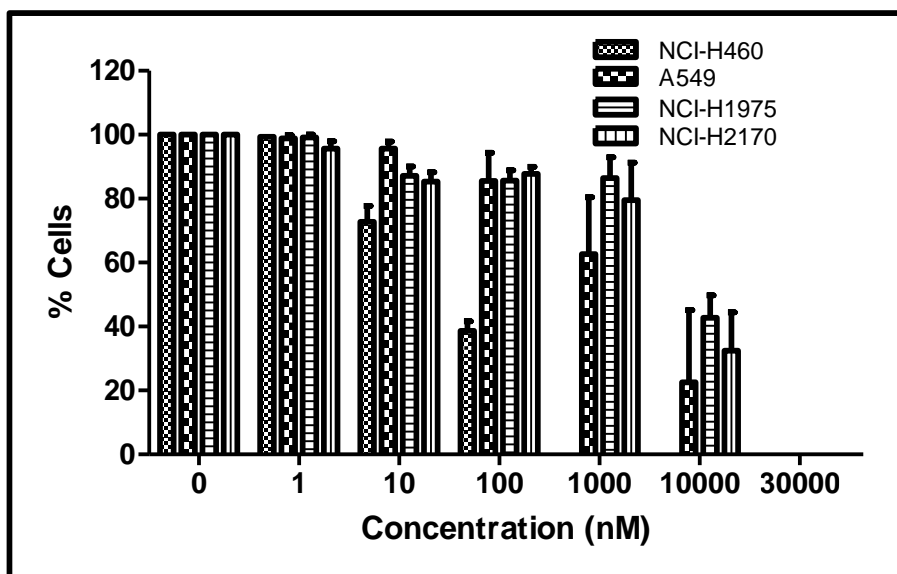
(A)
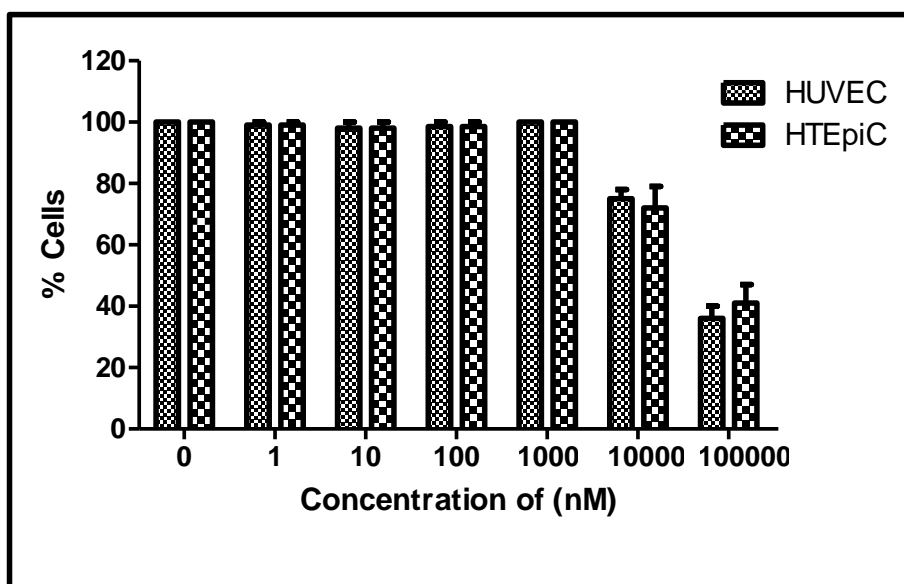
(B)

Figure 5.7: Effect of lead **6** on cellular proliferation in lung cancer cells (A) and normal cells

(B).

Table 5.3: IC$_{50}$ for lead **6** for inhibition of proliferation and p-Akt in lung cancer cells.

S No.	Cell line	Mutation Status (PI3K/KRAS/EGFR)	Proliferation GI$_{50}$ (nM)	p-Akt inhibition IC$_{50}$ (nM)
1	H460	PIK3CA, KRAS	485.5	12.77
2	A549	KRAS	1652	201.7
3	H1975	EGFR 790TM	6589	522.3
4	H2170	WT	3667	217.5
5	HTEpiC	-	53570	-
6	HUVEC	-	46328	-

5.4.3 In-situ caspase-3 assay.

To evaluate the effect of lead **6** on apoptosis, caspase-3 was measured using FLICA reagent as per the protocol mentioned in in the section 4.8.3. **Figure 5.8** indicate the apoptotic activity of lead **6** at 100 nM, 1000 nM and 10000 nM concentrations. There was a significant increase ($p<0.01$) in the levels of caspase-3 when treated with 1000 nM of lead **6** in H460 and A549 indicating its sensitivity. At higher concentrations, there was a 10-fold increase in caspase-3 levels in all the cell lines except H1975. Data correlated with the amount of p-Akt present in the aforementioned cell lines, indicating p-Akt dependent sensitivity towards lead **6**.
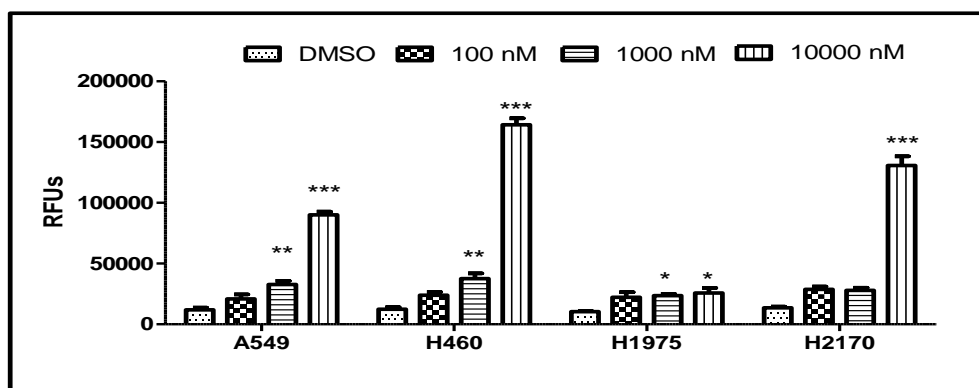
Figure 5.8: Lead **6** induces apoptosis in lung cancer cell lines. ** P<0.01 and *** p<0.001; One-Way ANOVA with Dunnett's as post hoc analysis compared to DMSO control. RFUs were relative fluorescence units.

5.4.4 Cell cycle analysis

The effect of lead **6** on cell cycle in lung cancer cell lines was determined by propidium iodide staining and analyzed by flow cytometry as per the protocol mentioned in the section 4.8.4. **Figure 5.9** indicate that there was a significant increase in cells in the G0/G1 phase (p<0.01) when treated with 100 nM of lead **6** compared to the control. At higher concentrations (1 μM and 10 μM), there was a significant increase in the % cells in sub G0 phase (p<0.001) (data not shown). Results correlate with the levels of caspase-3 after treatment with lead **6** in these cells. Unlike the other cell lines, G0/G1 arrest was not evident in H2170 when treated with 100 nM of lead **6**
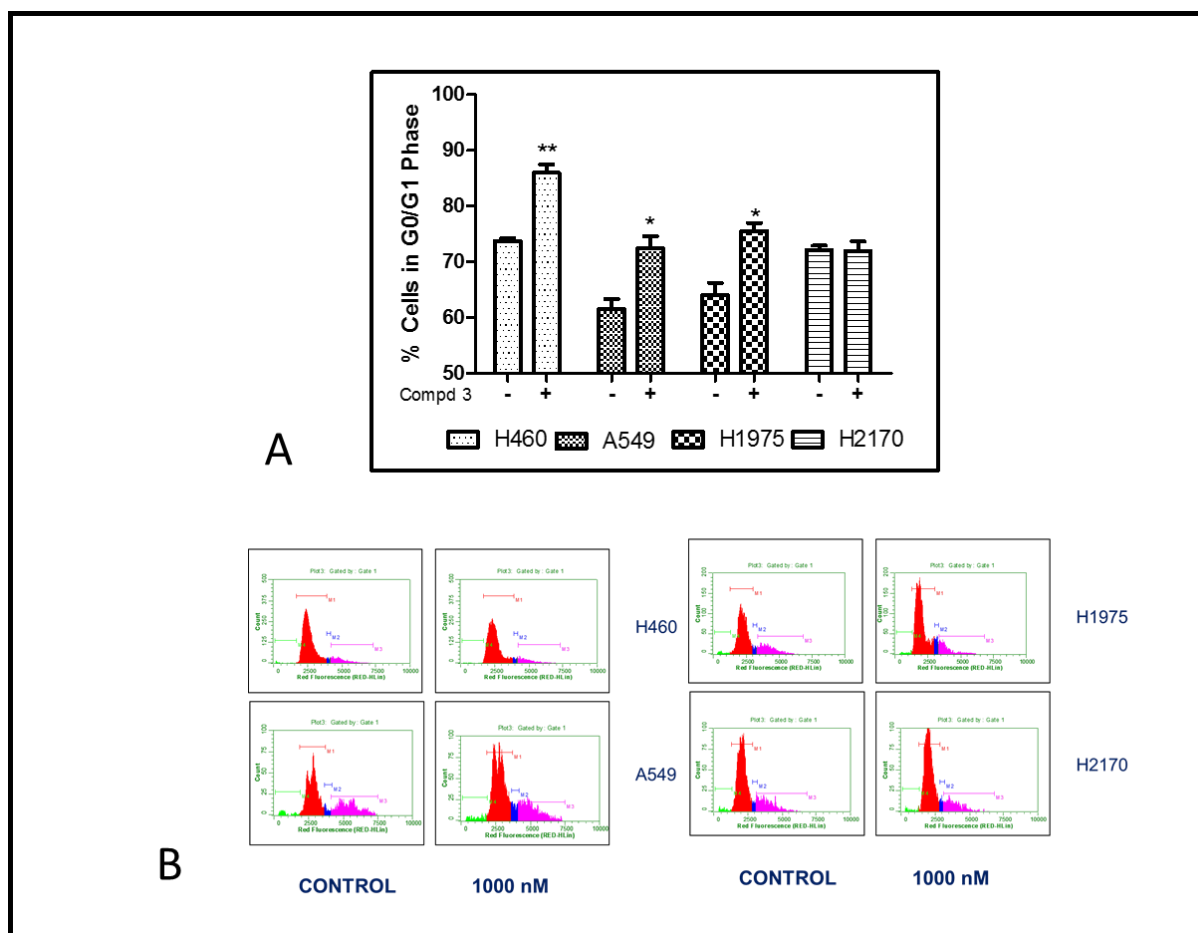
Figure 5.9: Lead **6** arrest the cell cycle in G1 phase in lung cancer cell lines. Cells were incubated with 100 nM lead **6** (+) or DMSO (-) for 72 h before cell cycle analysis (A). Representative histograms for all the cell lines (B) ** $p < 0.01$ and * $p < 0.05$; One-Way ANOVA with Dunnett's as post hoc analysis compared to DMSO control.

5.4.5 Effect of lead 6 on downstream Akt pathway.

To confirm if the activity of lead **6** was due to inhibition of Akt phosphorylation, the lung cancer cell lines were treated with lead **6** and the levels of p-Akt (Ser[473]) were determined. Lead **6** was found to downregulate p-Akt in a dose dependent manner **(Figure 5.10).** IC_{50} for lead **6** in different cell lines are presented in **Table 5.3**. The order of sensitivity towards lead **6** was found to be H460>A549>H2170>H1975. A 40-fold difference in activity between

sensitive (H460) and resistant cell lines (H1975) was noticed upon treatment with lead **6**.
Inhibition of p-Akt expression correlated with the anti-proliferative activity of lead **6** in lung
cancer cell lines thereby elucidating its mode of action.
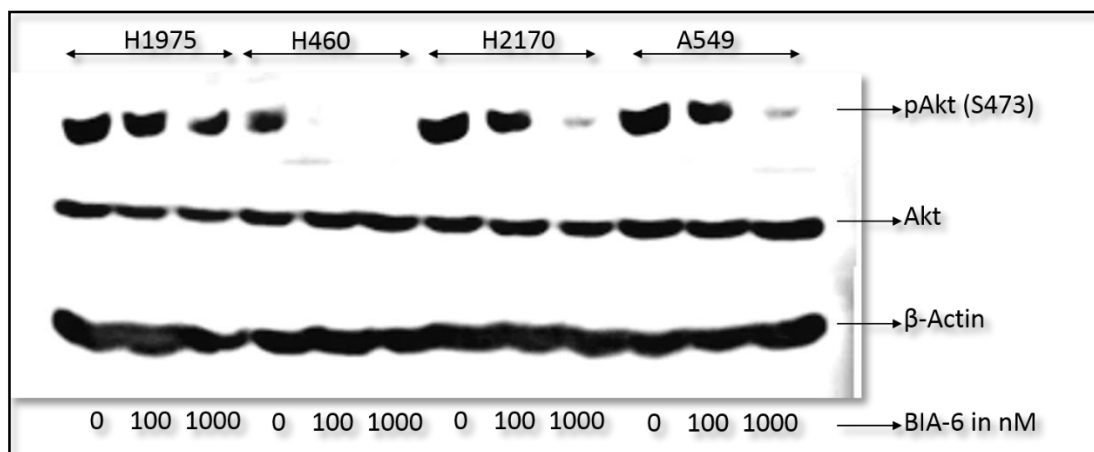
Figure 5.10: Cellular efficacy is due to the inhibition of Akt pathway. Cells were treated with
lead **6** for 4 h, lysed and p-Akt was estimated by western blot. The levels of p-Akt were
quantified at 100 nM and 1000 nM concentration in lung cancer cell lines.

5.4.6 Lead 6 exhibits synergism with standard chemotherapy of lung cancer

Standard chemotherapy for lung cancer include various antimetabolites and taxanes along with
platinum based compounds. Lung cancer cell lines (H460, A549, H1975 and H2170) were
treated with a combination of lead **6** (**B**) and gemcitabine, an antimetabolite (G) or lead **6** (**B**)
and docetaxel, a taxol derivative (D) to test for anti-proliferative activity **(Figure 5.11)**. Cells
were treated at a fixed ratio of 1:10 of G/D: B and the combination indices (CI) were calculated
according to Chou and Talalay method using CompuSyn (Chou TC *et al*., 2010).

CI values were calculated based on the formula

$$CI = \frac{D_1}{(D_1)_m} + \frac{D_2}{(D_2)_m}$$

where D1 and D2 were concentrations of two different drugs and (D1)m, (D2)m represented the corresponding median effect concentrations respectively

CI values were calculated on the basis of parameters derived from median effect plots of lead **6** alone, G/D alone, and the combination of two agents at fixed ratios. A CI <1 was evident for synergy, whereas a CI >1 indicated antagonism. A CI value approaching 1 indicated an additive effect. As represented in **Figure 5.11**, a strong synergism was identified between lead **6** and G/D across all the cell lines.
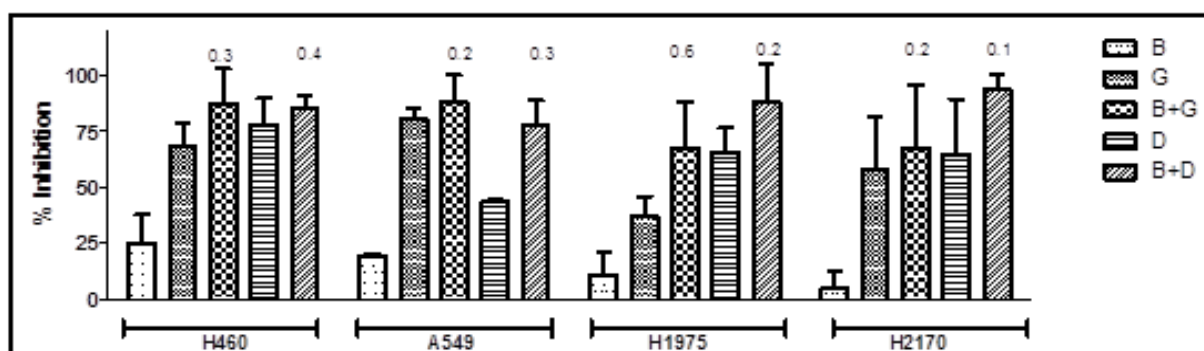
Figure 5.11: Combination of lead **6** with Gemcitabine/Docetaxel in lung cancer cell lines. The concentrations of the drugs are as follows: Lead **6** (B) 1000 nM; Gemcitabine (G) 100nM; Docetaxel (D) 100 nM. Values in the graph indicate the Combination Indices at the respective concentrations. CI<1 indicates synergism.

5.5 Summary and conclusion.

The PI3K/Akt/mTOR signaling cascade, a pivotal pathway that was reported to be dysregulated in a wide variety of human cancers and strongly contribute to both tumorigenesis and therapy resistance. Considering the crucial role of aberrantly activated Akt in the pathogenesis of lung cancer, we designed a pharmacophore for Akt inhibitor, identified and studied the efficacy of lead **6**, a novel allosteric Akt inhibitor, as a potential therapeutic lead.

In the current study, lead **6** was found to be efficacious in lung cancer cell lines that harboured mutations of PIK3CA (H460). The finding was consistent with the powerful role of this mutation in the activation of PI3K/Akt pathway. Significant preferentiality of the effects of lead **6** was observed in cells harboring RAS mutations (A549). The effect of lead **6** was minimal in cells that did not harbor PI3K/Akt mutations or RAS mutations (H1975, H2170). The genetic dependence of lead **6** activity in lung cancer cells was reflected by its lower IC_{50} values as well as higher levels of capsase-3 in H460 followed by A549.

Lead **6** dephosphorylated Akt on Ser 473, indicating an indirect targeting of mTORC2, through the Akt/mTOR cascade. As Akt is upstream to TSC1/TSC2 complex, lead **6** indirectly downregulated mTORC2 activity. The efficacy of lead **6** in inhibiting H460, A549 cell proliferation was due to its ability to arrest the cell cycle as well as induction of apoptosis. This was evident with the increase in caspase-3 levels in cells at lower concentrations followed by increase in % cells in G_0/G_1 phase.

Lead **6** demonstrated synergism with standard chemotherapeutic agents for lung cancer (G and D). Results indicated a CI value <1 irrespective of the genetic dependence of the lead **6** activity. Although GEM and DOC inhibited Akt phosphorylation in cancer cell lines, they were associated with severe adverse events such as anemia, neutropenia, thrombocytopenia, infection, hair loss, nausea and diarrhea, thereby limiting their efficacy potential.

Our finding could potentially have a clinical relevance for lung cancer patients, as a combination of lead **6** with low doses of G/D. Lead **6** was generally well tolerated at doses required for *in vitro* activity and the drug only slightly affected the proliferation of normal tracheal epithelial cells (HTEpiC) and endothelial cells (HUVEC). Addition of lead **6** to G/D could potentially help overcome the limitation related to the therapeutic index and possibility of acquired resistance of the chemotherapeutic agents.

CHAPTER 6

LEAD OPTIMISATION OF ALLOSTERIC Akt INHIBITOR

CHAPTER 6
LEAD OPTIMISATION OF ALLOSTERIC Akt INHIBITOR

Lead **6** was identified as a promising hit compound with a novel scaffold for Akt1 allosteric inhibitors. Lead **6** could be used as a single agent or as a combination therapy with standard chemotherapeutic agents for the treatment of lung cancer. To obtain more potent compounds from this scaffold, substructure modification of lead **6** was performed. By retaining the important interactions required for activity, several analogues were identified. Thus the objectives of this study included

1. Synthesis of various analogues of lead **6**

2. Establish structure-activity relationship among the analogues synthesized.

3. Characterisation of lead molecule identified among the various analogues synthesized.

6.1 Synthesis of analogues of lead 6

To synthesize analogues of lead **6**, a substructure analysis was done as shown in **Figure 6.1**. The tricyclic ring system was considered as ring **A**, phenyl ring attached to the tricyclic ring *via* an ethyl bond linkage was termed ring **B** and the ethyl linkage was termed linker **L2**. Mercaptoacetamide group was labelled linker **L1**. The phenyl ring attached to **L1** was assigned ring **C** and the m-substitution on ring **C** was termed linker **L3**.

Ligand interaction plot (**Figure 6.2**) for lead **6** indicated that the most important interactions include a π-π stacking interaction of ring **A** with Trp80 and the hydrogen bonding of Asn54 with linker **L3**.
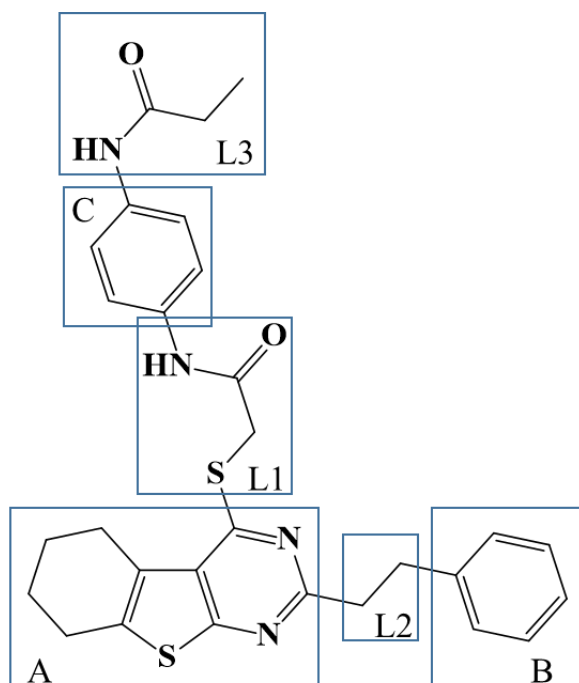
Figure 6.1: Substructure analysis of lead **6** into three ring structures **A**, **B**, **C** and three linkers **L1**, **L2** and **L3**.
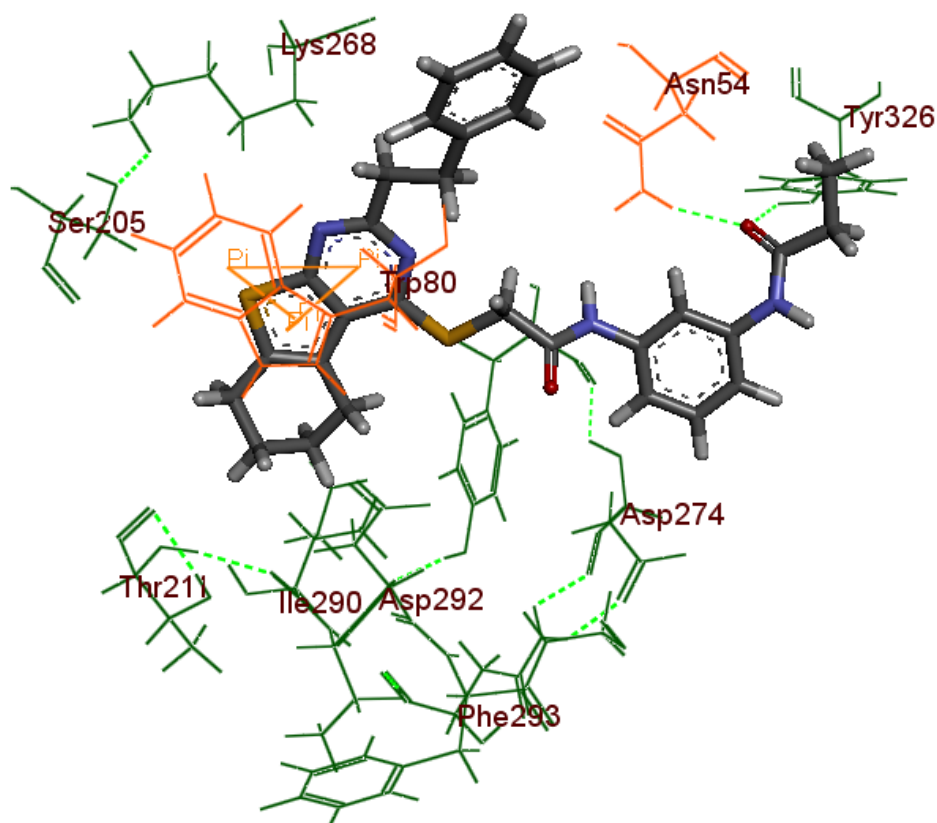
Figure 6.2: Interaction plot of lead **6**. Interactions indicate the importance of Trp80 and Asn54 residues binding to the compound

Considering the interaction pattern, following changes were made for the synthesis of further analogues as a step towards lead optimisation.

1. Ring B was removed and linker L2 was shortened to one carbon length

2. Sulphur atom in linker L1 was replaced with oxygen.

3. Carbon length in linker L3 was reduced or amide group was replaced by a ketone group.

Analogues of lead **6** were synthesised as discussed in the section **4.6** wherein the general procedure for the synthesis of compounds are mentioned. The scheme of reactions was depicted in **Figure 4.1.** Specific procedures for each compound and its corresponding chemical characterisation are described below.

*N-(3-Acetylphenyl)-2-((2-methyl-5,6,7,8-tetrahydrobenzo(4,5)thieno(2,3-d)pyrimidin-4-yl)oxy)acetamide (**6a**)*

MS(ESI) *m/z* 396 (M+H)$^+$. ^{1}H NMR (400 MHz, DMSO-d_6): δ 10.24 (s, 1H, NH), 8.05 (s, 1H), 7.33–7.15 (m, 3H), 4.91 (s, 2H), 2.83 (t, *J* = 7.2 Hz, 2H), 2.72 (t, *J* = 7.2 Hz, 2H), 2.49 (s, 3H), 2.18 (s, 3H), 1.88-1.79 (m, 4H); ^{13}C NMR (100 MHz, DMSO-d_6) δ 188.9, 169.4, 168.1, 161.1, 146.4, 138.3, 134.3, 133.2, 129.3, 127.4, 126.4, 123.5, 120.5, 119.4, 60.9, 29.6, 25.2, 24.3, 24.1, 22.7, 22.5. Anal. calcd for $C_{21}H_{21}N_3O_3S$: C, 63.78; H, 5.35; N, 10.63 % Found C, 63.88; H, 5.39; N, 10.76%.

*N-(3-Acetylphenyl)-2-((2-ethyl-5,6,7,8-tetrahydrobenzo(4,5)thieno(2,3-d)pyrimidin-4-yl)oxy)acetamide (**6b**)*

MS(ESI) *m/z* 410 (M+H)$^+$. ^{1}H NMR (400 MHz, DMSO-d_6): δ 10.32 (s, 1H, NH), 8.02 (s, 1H), 7.36–7.19 (m, 3H), 4.88 (s, 2H), 2.94–2.85 (m, 6H), 2.52 (s, 3H), 1.84-1.79 (m, 4H), 1.16 (t, *J* = 7.6 Hz, 3H); ^{13}C NMR (100 MHz, DMSO-d_6) δ 188.2, 167.4, 164.9, 163.6, 143.2, 140.4, 139.2, 133.9, 132.4, 130.9, 128.6, 124.4, 122.5, 118.8, 61.6, 32.4, 25.2, 24.6, 23.9, 22.9, 22.5, 12.6. Anal. calcd for $C_{22}H_{23}N_3O_3S$: C, 64.53; H, 5.66; N, 10.26 % Found C, 64.58; H, 5.69; N, 10.34%.

*N-(3-Acetylphenyl)-2-((2-phenethyl-5,6,7,8-tetrahydrobenzo(4,5)thieno(2,3-d)pyrimidin-4-yl)oxy)acetamide (**6c**)*

MS(ESI) *m/z* 486 (M+H)$^+$. ^{1}H NMR (400 MHz, DMSO-d_6): δ 10.27 (s, 1H), 7.45 (d, *J* = 7.6 Hz, 1H), 7.33–7.18 (m, 8H), 4.90 (s, 2H), 2.99–2.85 (m, 8H), 2.34 (s, 3H), 1.84-1.78 (m, 4H); ^{13}C NMR (100 MHz, DMSO-d_6) δ 190.8, 172.8, 169.3, 167.9, 143.6, 142.9, 141.7, 137.6, 135.9, 135.0, 134.6, 133.2, 130.7, 128.7(2C), 126.8(2C), 125.3, 124.5, 120.6, 68.4, 40.3, 26.2, 24.9, 24.5, 24.1, 23.4, 23.2. Anal. calcd for $C_{28}H_{27}N_3O_3S$: C, 69.25; H, 5.60; N, 8.65 % Found C, 69.32; H, 5.71; N, 8.72%.

*N-(3-Acetylphenyl)-2-((2-methyl-5,6,7,8-tetrahydrobenzo(4,5)thieno(2,3-d)pyrimidin-4-yl)thio)acetamide (**6d**)*

MS(ESI) *m/z* 412 (M+H)$^+$. ^{1}H NMR (400 MHz, DMSO-d_6): δ 9.97 (s, 1H, NH), 8.01 (s, 1H), 7.38–7.19 (m, 3H), 4.21 (s, 2H), 2.94 (t, *J* = 7.2 Hz, 2H), 2.89 (t, *J* = 7.2 Hz, 2H), 2.52 (s, 3H), 2.14 (s, 3H), 1.82-1.76 (m, 4H); ^{13}C NMR (100 MHz, DMSO-d_6) δ 171.9, 168.5, 165.4, 159.2, 147.5, 142.8, 134.6, 133.9, 133.0, 128.8, 128.2, 127.2, 120.3, 118.2, 40.9, 25.6, 23.8, 23.1, 22.9, 22.3, 21.4. Anal. calcd for $C_{21}H_{21}N_3O_2S_2$: C, 61.29; H, 5.14; N, 10.21 % Found C, 61.38; H, 5.19; N, 10.26%.

*N-(3-Acetylphenyl)-2-((2-ethyl-5,6,7,8-tetrahydrobenzo(4,5)thieno(2,3-d)pyrimidin-4-yl)thio)acetamide (**6e**)*

MS(ESI) *m/z* 426 (M+H)$^+$. ^{1}H NMR (400 MHz, DMSO-d_6): δ 10.17 (s, 1H, NH), 7.99 (s, 1H), 7.37–7.18 (m, 3H), 4.18 (s, 2H), 2.92–2.81 (m, 6H), 2.50 (s, 3H), 1.83-1.78 (m, 4H), 1.19 (t, *J* = 7.2 Hz, 3H); ^{13}C NMR (100 MHz, DMSO-d_6) δ 186.9, 166.5, 163.2, 162.4, 144.4, 141.5, 138.4, 136.3, 134.6, 129.4, 127.5, 124.7, 121.5, 117.9, 42.4, 31.5, 24.4, 23.4, 22.5(2C), 21.6, 13.5. Anal. calcd for $C_{22}H_{23}N_3O_2S_2$: C, 62.09; H, 5.45; N, 9.87 % Found C, 62.18; H, 5.49; N, 9.96%.

*N-(3-Acetylphenyl)-2-((2-phenethyl-5,6,7,8-tetrahydrobenzo(4,5)thieno(2,3-d)pyrimidin-4-yl)thio)acetamide (**6f**)*

MS(ESI) *m/z* 502 (M+H)$^+$. ^{1}H NMR (400 MHz, DMSO-d_6): δ 10.11 (s, 1H, NH), 8.02 (s, 1H), 7.48–7.22 (m, 8H), 4.23 (s, 2H), 3.01–2.86 (m, 8H), 2.36 (s, 3H), 1.86-1.77 (m, 4H); ^{13}C NMR (100 MHz, DMSO-d_6) δ 189.9, 169.4, 167.5, 165.8, 144.3, 143.2, 140.4, 138.4, 136.3, 135.4, 130.2, 128.2(2C), 127.2, 126.0(2C), 123.2, 122.4, 119.2, 117.9, 42.1, 35.5, 27.4, 26.1, 25.2(2C), 24.6, 21.7. Anal. calcd for $C_{28}H_{27}N_3O_2S_2$: C, 67.04; H, 5.42; N, 8.38 % Found C, 67.12; H, 5.51; N, 8.42%.

*N-(3-Acetamidophenyl)-2-((2-methyl-5,6,7,8-tetrahydrobenzo(4,5)thieno(2,3-d)pyrimidin-4-yl)oxy)acetamide (**6g**)*

MS(ESI) *m/z* 411 (M+H)$^+$. ^{1}H NMR (400 MHz, DMSO-d_6): δ 10.34 (s, 1H, NH), 9. 94 (s, 1H, NH), 7.98 (s, 1H), 7.38–7.17 (m, 3H), 4.88 (s, 2H), 2.94 (t, *J* = 7.6 Hz, 2H), 2.86 (t, *J* = 7.6 Hz, 2H), 2.52 (s, 3H), 2.16 (s, 3H), 1.84-1.79 (m, 4H); ^{13}C NMR (100 MHz, DMSO-d_6) δ 168.4, 166.8, 165.6, 161.4, 160.6, 140.4, 140.1, 135.4, 133.9, 128.9, 128.2, 114.9, 113.5, 109.2, 63.6, 24.8, 24.2, 23.5, 22.9, 22.3, 21.4. Anal. calcd for $C_{21}H_{22}N_4O_3S$: C, 61.44; H, 5.40; N, 13.65 % Found C, 61.48; H, 5.49; N, 13.71%.

*N-(3-Acetamidophenyl)-2-((2-ethyl-5,6,7,8-tetrahydrobenzo(4,5)thieno(2,3-d)pyrimidin-4-yl)oxy)acetamide (**6h**)*

MS(ESI) *m/z* 425 (M+H)$^+$. ^{1}H NMR (400 MHz, DMSO-d_6): δ 10.30 (s, 1H, NH), 9.98 (s, 1H, NH), 8.04 (s, 1H), 7.41–7.28 (m, 3H), 4.82 (s, 2H), 2.92–2.83 (m, 6H), 2.19 (s, 3H), 1.87–1.80 (m, 4H), 1.14 (t, *J* = 7.6 Hz, 3H); ^{13}C NMR (100 MHz, DMSO-d_6) δ 169.6, 167.2, 165.4, 162.1, 159.3, 139.4, 137.6, 136.4, 132.9, 130.7, 128.2, 121.4, 118.4, 114.6, 63.4, 30.6, 25.4, 24.3, 23.8, 23.3, 22.5, 13.5. Anal. calcd for $C_{22}H_{24}N_4O_3S$: C, 62.24; H, 5.70; N, 13.20 % Found C, 62.28; H, 5.76; N, 13.31%.

*N-(3-Acetamidophenyl)-2-((2-phenethyl-5,6,7,8-tetrahydrobenzo(4,5)thieno(2,3-d)pyrimidin-4-yl)oxy)acetamide (**6i**)*

MS(ESI) *m/z* 501 (M+H)$^+$. ^{1}H NMR (400 MHz, DMSO-d_6): δ 10.21 (s, 1H, NH), 9.87 (s, 1H, NH), 8.02 (s, 1H), 7.60–7.36 (m, 8H), 4.89 (s, 2H), 2.99–2.86 (m, 6H), 2.83 (t, *J* = 7.6 Hz, 2H), 2.13 (s, 3H), 1.87-1.78 (m, 4H); ^{13}C NMR (100 MHz, DMSO-d_6) δ 173.4, 170.1, 167.2, 163.4, 160.5, 149.2, 148.3, 138.2, 136.1, 134.8, 133.0(2C), 132.4(2C), 130.8, 127.4, 126.3, 124.6, 117.8, 112.2, 63.9, 39.6, 26.1, 25.4, 24.7, 24.2, 23.4, 22.4. Anal. calcd for $C_{28}H_{28}N_4O_3S$: C, 67.18; H, 5.64; N, 11.19 % Found C, 67.28; H, 5.69; N, 11.32%.

*N-(3-Acetamidophenyl)-2-((2-methyl-5,6,7,8-tetrahydrobenzo(4,5)thieno(2,3-d)pyrimidin-4-yl)thio)acetamide (**6j**)*

MS(ESI) *m/z* 427 (M+H)$^+$. ^{1}H NMR (400 MHz, DMSO-d_6): δ 10.31 (s, 1H, NH), 9.92 (s, 1H, NH), 7.90 (s, 1H), 7.33–7.15 (m, 3H), 4.20 (s, 2H), 3.01 (t, *J* = 7.2 Hz, 2H), 2.82 (t, *J* = 7.2 Hz, 2H), 2.52 (s, 3H), 2.04 (s, 3H), 1.90-1.79 (m, 4H); ^{13}C NMR (100 MHz, DMSO-d_6) δ 168.3, 166.0, 165.3, 161.3, 160.2, 139.6, 139.2, 135.2, 128.8, 126.7, 125.0, 114.1, 114.0, 110.0, 39.5, 34.3, 26.0, 25.1, 25.0, 24.0, 21.9. Anal. calcd for $C_{21}H_{22}N_4O_2S_2$: C, 59.13; H, 5.20; N, 13.13 % Found C, 59.18; H, 5.29; N, 13.21%.

*N-(3-Acetamidophenyl)-2-((2-ethyl-5,6,7,8-tetrahydrobenzo(4,5)thieno(2,3-d)pyrimidin-4-yl)thio)acetamide (**6k**)*

MS(ESI) *m/z* 441 (M+H)$^+$. ^{1}H NMR (400 MHz, DMSO-d_6): δ 10.33 (s, 1H, NH), 9.98 (s, 1H, NH), 7.96 (s, 1H), 7.40–7.29 (m, 3H), 4.22 (s, 2H), 2.94 (t, *J* = 7.6 Hz, 2H), 2.89 (t, *J* = 7.6 Hz, 2H), 2.51 (q, *J* = 7.6 Hz, 2H), 2.16 (s, 3H), 1.86-1.79 (m, 4H), 1.18 (t, *J* = 7.2 Hz, 3H); ^{13}C NMR (100 MHz, DMSO-d_6) δ 168.5, 166.3, 164.8, 160.2, 139.9, 139.0, 136.4, 134.8, 133.9, 127.3, 125.6, 119.9, 117.0, 115.3, 41.4, 29.2, 25.2, 24.9, 24.3, 22.4, 21.2, 13.9. Anal. calcd for $C_{22}H_{24}N_4O_2S_2$: C, 59.97; H, 5.49; N, 12.72 % Found C, 60.08; H, 5.55; N, 12.91%.

*N-(3-Acetamidophenyl)-2-((2-phenethyl-5,6,7,8-tetrahydrobenzo(4,5)thieno(2,3-d)pyrimidin-4-yl)thio)acetamide (**6l**)*

MS(ESI) *m/z* 517 (M+H)$^+$. ^{1}H NMR (400 MHz, DMSO-d_6): δ 10.39 (s, 1H, NH), 9.89 (s, 1H, NH), 8.02 (s, 1H), 7.49–7.27 (m, 8H), 4.24 (s, 2H), 2.97–2.83 (m, 6H), 2.81 (t, *J* = 7.6 Hz, 2H), 2.19 (s, 3H), 1.84-1.74 (m, 4H); ^{13}C NMR (100 MHz, DMSO-d_6) δ 172.5, 169.3, 166.4, 164.4, 143.2, 142.4, 139.2, 136.4, 135.4, 130.4, 128.2, 127.4, 125.4(2C), 124.6(2C), 123.4, 118.3(2C), 116.1, 40.9, 36.7, 28.0, 25.6, 24.1(2C), 23.2, 20.7. Anal. calcd for $C_{28}H_{28}N_4O_2S_2$: C, 65.09; H, 5.46; N, 10.84 % Found C, 65.18; H, 5.51; N, 10.92%.

*N-(3-(2-((2-Methyl-5,6,7,8-tetrahydrobenzo(4,5)thieno(2,3-d)pyrimidin-4-yl)oxy)acetamido)phenyl)propionamide (**6m**)*

MS(ESI) *m/z* 425 (M+H)$^+$. ^{1}H NMR (400 MHz, DMSO-d_6): δ 10.45 (s, 1H, NH), 9.85 (s, 1H, NH), 7.96 (s, 1H), 7.31–7.19 (m, 3H), 4.90 (s, 2H), 2.85 (t, *J* = 7.6 Hz, 2H), 2.76 (t, *J* = 7.6 Hz, 2H), 2.51 (s, 3H), 2.31 (q, *J* = 7.6 Hz, 2H), 1.89-1.71 (m, 4H), 1.05 (t, *J* = 7.6 Hz, 3H); ^{13}C NMR (100 MHz, DMSO-d_6) δ 170.6, 169.4, 166.9, 162.6, 160.4, 142.7, 140.2, 139.4, 133.3, 131.4, 130.2, 124.5, 121.2, 118.2, 69.3, 29.8, 24.9(2C), 24.2, 22.6, 22.2, 12.4. Anal. calcd for $C_{22}H_{24}N_4O_3S$: C, 62.24; H, 5.70; N, 13.20 % Found C, 62.33; H, 5.80; N, 13.31%.

*N-(3-(2-((2-Ethyl-5,6,7,8-tetrahydrobenzo(4,5)thieno(2,3-d)pyrimidin-4-yl)oxy)acetamido)phenyl)propionamide (**6n**)*

MS(ESI) *m/z* 439 (M+H)$^+$. ^{1}H NMR (400 MHz, DMSO-d_6): δ 10.33 (s, 1H, NH), 9.81 (s, 1H, NH), 8.01 (s, 1H), 7.54–7.39 (m, 3H), 4.96 (s, 2H), 2.96–2.82 (m, 6H), 2.50 (q, *J* = 7.6 Hz, 2H), 1.89-1.82 (m, 4H), 1.16 (t, *J* = 7.6 Hz, 3H), 1.08 (t, *J* = 7.6 Hz, 3H); ^{13}C NMR (100 MHz, DMSO-d_6) δ 178.3, 170.6, 166.4, 162.6, 143.8, 142.6, 139.5, 134.8, 132.6, 128.6, 127.3, 122.4, 120.6, 118.4, 68.3, 27.4, 26.8, 24.8, 24.2, 23.6, 22.9, 12.6, 11.5. Anal. calcd for $C_{23}H_{26}N_4O_3S$: C, 62.99; H, 5.98; N, 12.78 % Found C, 63.03; H, 6.09; N, 12.81%.

*N-(3-(2-((2-Phenethyl-5,6,7,8-tetrahydrobenzo(4,5)thieno(2,3-d)pyrimidin-4-yl)oxy)acetamido)phenyl)propionamide (**6o**)*

MS(ESI) *m/z* 515 (M+H)$^+$. ^{1}H NMR (400 MHz, DMSO-d_6): δ 10.47 (s, 1H, NH), 9.97 (s, 1H, NH), 8.01 (s, 1H), 7.39–7.12 (m, 8H), 4.92 (s, 2H), 2.97–2.82 (m, 8H), 2.47 (q, *J* = 7.6 Hz, 2H), 1.87–1.81 (m, 4H), 1.08 (t, *J* = 7.6 Hz, 3H); ^{13}C NMR (100 MHz, DMSO-d_6) δ 174.6, 169.2, 163.8, 162.9, 144.8, 142.4, 139.3, 136.2, 135.4, 134.2, 133.4(2C), 133.0(2C), 130.5, 128.6, 125.9, 124.3, 121.8, 118.9, 67.3, 39.6, 30.4, 26.9, 25.3, 24.9, 24.6, 24.1, 11.7. Anal. calcd for $C_{29}H_{30}N_4O_3S$: C, 67.68; H, 5.88; N, 10.89 % Found C, 67.72; H, 5.93; N, 10.91%.

N-(3-(2-((2-Methyl-5,6,7,8-tetrahydrobenzo(4,5)thieno(2,3-d)pyrimidin-4-yl)thio)acetamido)phenyl)propionamide (6p)

MS(ESI) m/z 441 (M+H)$^+$. ^{1}H NMR (400 MHz, DMSO-d_6): δ 10.38 (s, 1H, NH), 9.87 (s, 1H, NH), 8.08 (s, 1H), 7.45–7.31 (m, 3H), 4.24 (s, 2H), 2.96 (t, J = 7.6 Hz, 2H), 2.89 (t, J = 7.6 Hz, 2H), 2.48 (s, 3H), 2. 36 (q, J = 7.6 Hz, 2H), 1.86–1.79 (m, 4H), 1.08 (t, J = 7.6 Hz, 3H); ^{13}C NMR (100 MHz, DMSO-d_6) δ 171.9, 168.8, 167.2, 159.4, 146.2, 140.4(2C), 133.4, 132.6, 130.4, 129.3, 120.1(2C), 117.2, 41.3, 29.4, 25.0(2C), 24.1, 22.9, 22.3, 13.2. Anal. calcd for $C_{22}H_{24}N_4O_2S_2$: C, 59.97; H, 5.49; N, 12.72 % Found C, 60.03; H, 5.59; N, 12.81%.

N-(3-(2-((2-Ethyl-5,6,7,8-tetrahydrobenzo(4,5)thieno(2,3-d)pyrimidin-4-yl)thio)acetamido)phenyl)propionamide (6q)

MS(ESI) m/z 455 (M+H)$^+$. ^{1}H NMR (400 MHz, DMSO-d_6): δ 10.47 (s, 1H, NH), 9.91 (s, 1H, NH), 7.99 (s, 1H), 7.44–7.28 (m, 3H), 4.22 (s, 2H), 2.97 (t, J = 7.6 Hz, 2H), 2.86–2.46 (m, 6H), 1.88–1.80 (m, 4H), 1.17 (t, J = 7.6 Hz, 3H), 1.11 (t, J = 7.6 Hz, 3H); ^{13}C NMR (100 MHz, DMSO-d_6) δ 170.1, 167.4, 165.3, 160.2, 144.9, 142.4, 137.3, 133.0, 127.3, 124.5, 119.0, 118.7, 117.1, 116.2, 42.3, 32.2, 30.6, 25.9, 25.0(2C), 22.3, 13.4, 12.6. Anal. calcd for $C_{23}H_{26}N_4O_2S_2$: C, 60.77; H, 5.76; N, 12.32 % Found C, 60.83; H, 5.79; N, 12.41%.

N-(3-(2-((2-Phenethyl-5,6,7,8-tetrahydrobenzo(4,5)thieno(2,3-d)pyrimidin-4-yl)thio)acetamido)phenyl)propionamide (6r)

MS(ESI) m/z 531 (M+H)$^+$. ^{1}H NMR (400 MHz, DMSO-d_6): δ 10.35 (s, 1H), 9.82 (s, 1H), 7.99 (s, 1H), 7.35–7.03 (m, 8H), 4.21 (s, 2H), 3.15–2.96 (m, 6H), 2.84 (t, J = 7.6 Hz, 2H), 2.34 (q, J = 7.6 Hz, 2H), 1.88–1.73 (t, J = 7.6 Hz, 4H), 1.09 (t, J = 7.6 Hz, 3H); ^{13}C NMR (100 MHz, DMSO-d_6) δ 170.4, 168.9, 166.3, 163.6, 143.2, 141.6, 138.6, 137.9, 134.6, 131.6, 129.4, 126.6, 124.9(2C), 124.2(2C), 123.8, 119.1(2C), 116.5, 41.2, 36.4, 28.4, 24.9, 24.3(2C), 23.6, 21.6, 12.4. Anal. calcd for $C_{29}H_{30}N_4O_2S_2$: C, 65.63; H, 5.70; N, 10.56 % Found C, 65.72; H, 5.83; N, 10.71%.

Representative ^{1}H and ^{13}C NMR spectra were shown in **Figures 6.3, 6.4.**
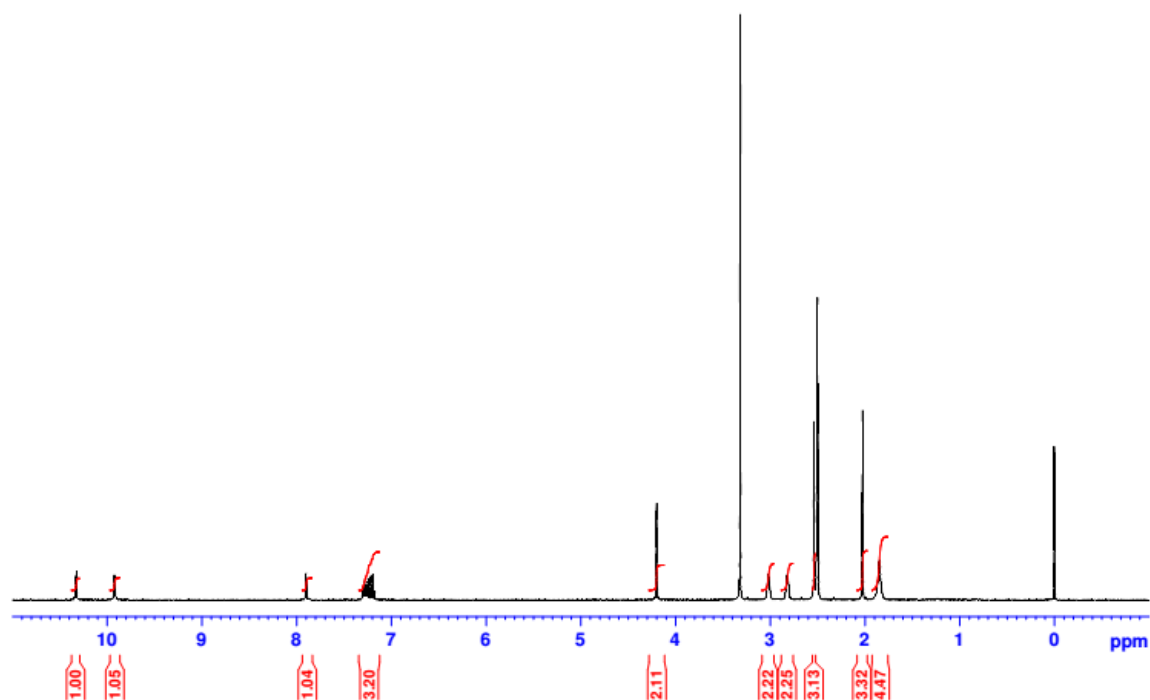
Figure 6.3: ^{1}H NMR spectrum for compound **6j.**
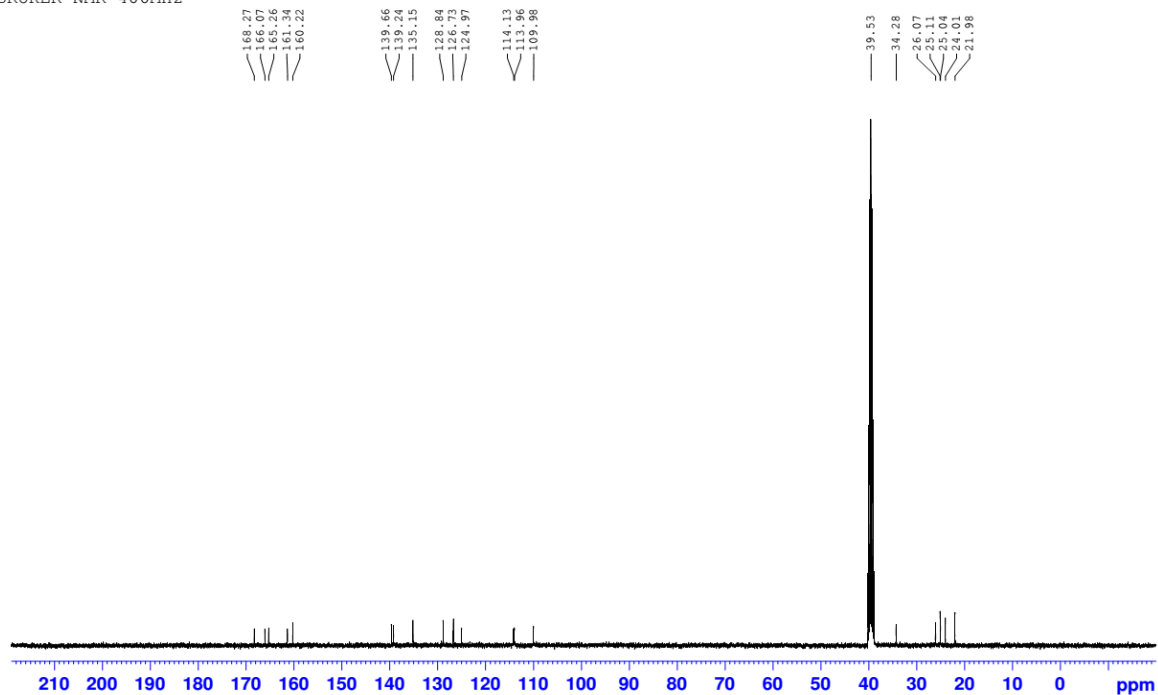
Figure 6.4: ^{13}C NMR spectrum for compound **6j.**

The structure and yields of the compounds are tabulated in **Table 6.1**.

Table 6.1: Structures of analogues synthesized.

6a-f   6g-l   6m-r
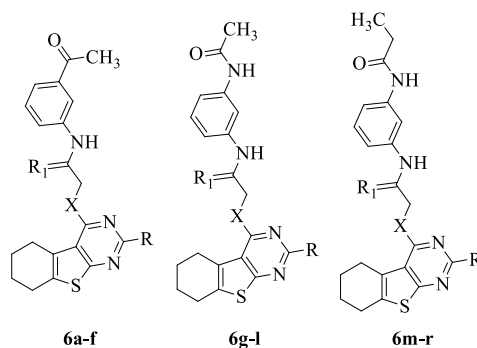
Compd No.	R	R1	%Yield	Melting Point
6a	-CH$_3$	-O-	79	203
6b	-C$_2$H$_5$	-O-	81	216
6c	-C$_2$H$_4$-C$_6$H$_5$	-O-	72	233
6d	-CH$_3$	-S-	94	223
6e	-C$_2$H$_5$	-S-	84	187
6f	-C$_2$H$_4$-C$_6$H$_5$	-S-	69	233
6g	-CH$_3$	-O-	74	212
6h	-C$_2$H$_5$	-O-	79	189
6i	-C$_2$H$_4$-C$_6$H$_5$	-O-	82	185
6j	-CH$_3$	-S-	87	197
6k	-C$_2$H$_5$	-S-	70	187
6l	-C$_2$H$_4$-C$_6$H$_5$	-S-	66	220
6m	-CH$_3$	-O-	76	181
6n	-C$_2$H$_5$	-O-	82	199
6o	-C$_2$H$_4$-C$_6$H$_5$	-O-	88	207
6p	-CH$_3$	-S-	90	191
6q	-C$_2$H$_5$	-S-	66	215
6r	-C$_2$H$_4$-C$_6$H$_5$	-S-	72	234

6.2 Biological evaluation of the synthesized compounds

The synthesised compounds were tested for *in vitro* Akt1 enzyme activity along with anti-proliferative activity in H460 and A549 cells as per the protocol discussed in sections **4.8.1** and **4.8.2**. Half maximal responses (IC$_{50}$s) were calculated and are presented in **Table 6.2**.

Table 6.2 Biological activity and docking scores of compounds synthesised.

Compd No.	% Inhibition 1μM	IC$_{50}$ (nM)	GI$_{50}$ (μM)	GI$_{50}$ (μM)	Docking score
Cell line			H460	A549	
6a	72.56	179.2	18.7	26.4	-10.575
6b	79.39	201.5	7.9	27.4	-10.847
6c	100	117.9	7.5	5.2	-11.001
6d	86.11	379.4	2.9	4.5	-10.78
6e	68.35	367.2	2.8	5.4	-10.624
6f	100	224.9	5.5	5.6	-10.59
6g	100	176.7	16.5	15.1	-11.269
6h	100	155.4	10.3	6.5	-11.49
6i	97.47	137.4	6.4	6.3	-10.476
6j	85.23	327.4	0.9	1.6	-11.203
6k	61.73	573.5	2	4.4	-10.739
6l	70.65	237.1	7.4	7.3	-11.248
6m	74.97	159.4	16.5	11.6	-10.637
6n	82.76	194.3	17.4	8.4	-10.695
6o	100	139.4	5.4	5.5	-10.734
6p	70.17	387.3	2.5	4	-10.828
6q	75.99	359.4	5	3	-11.183
6r	84.05	256.6	2.8	5.5	-11.407
MK2206	100	8.8	6.9	4.5	-10.206

Crystal structure analysis revealed that there were 2 hydrogen bonds with Asn54 and one π-π stacking interaction with Trp80 essential for the binding of lead **6** to Akt1. Most importantly, hydrogen bonding of lead **6** to the PH domain anchored this inhibitor in the hydrophobic pocket where it showed π-π stacking interactions with the Trp80 in PH domain and phenyl ring aligned towards the hydrophobic cleft surrounded by Val83, Phe161, Leu210, Leu264, Val270, Val271, Tyr272 and Ile290. Therefore, these hydrogen bonds and π-π stacking interactions to the PH domain should play a vital role in the inhibitory activities. To explore the possible structural change of lead **6**, eighteen structurally modified analogues were docked into Akt1 grid using Glide in its XP mode. The compounds to be synthesized were processed by LigPrep, for each compound at most three docking conformations were used for further analysis.

Keeping the important interactions into consideration, a subset of analogues were designed and synthesized (**Figure 4.1**) as a step to lead optimization and derivation of structure activity relationships (SAR). Intermediates **I-VIIIa/b** were tested in enzyme activity assay and found to be inactive in Akt1 indicating the importance of interaction HBA (hydrogen bond acceptor) in linker **L3**. Among the 18 analogues synthesized, all the compounds were active in the Akt1 enzyme activity with an IC_{50} of less than 0.5 μM. Compound **6c** was the most potent molecule with an IC_{50} of 117.9 nM. This was well supported by a very good interaction profile in docking studies with a Glide docking score of -9.28 kcal mol^{-1} orienting in a similar manner to the lead **6** retaining the crucial π-π stacking interactions with Trp80 and two hydrogen bond interactions with Asn54. Further the cyclohexyl ring was oriented towards the hydrophobic cleft with stabilizing hydrophobic interactions leading to a better potency than the lead **6** (**Figure 6.6**).

Hydrogen bond donor (HBD, -NH group) was hypothesized not to be crucial for compound binding. So, HBD was removed along with decreasing chain lengths in linker L3 (compounds **6a-f**) i.e., amide group was reduced to a ketone group along with a decrease in carbon chain length by one carbon. There was no significant difference in the activity of these compounds

compared to their respective longer linker L3 compounds (Compounds **6m-r**). Also, since the chain length reduction had no significant effect on the activity, the chain length in the amide group was also decreased. As predicted, activity of compounds **6g-l** was not dependent on chain length of linker L3 as indicated by comparative IC_{50}s with compounds **6m-r**.

Since phenyl-ethyl group (ring **B**) showed no interactions with Akt1, ring **B** was removed along with reduction of the chain length of linker **L2** to methyl and ethyl with no significant change in the enzyme activity (Compounds **6a,b,d,e,g,h,j,k,m,n,p,q**). Also there was no significant difference between methyl (Compounds **6a,d,g,j,m,p)** and ethyl (Compounds **6b,e,h,k,n,q**) substitutions in linker **L2**. Although insignificant, phenyl-ethyl group was more potent than methyl and ethyl substitutions which was also supported by higher docking scores.

Next, sulphur in linker **L1** was replaced by oxygen to test if it had any effect on enzyme activity. Surprisingly, the compounds with oxygen as a linker **L1** (Compounds **6a-c, g-i, m-o**) are more potent than the molecules with S as linker **L1** (Compounds **6d-f, j-l, p-r)** in inhibiting the Akt1 enzyme activity. The potency of molecules with oxygen in **L1** could be attributed to the smaller hydrogen bond length interactions with the Asn54 and subsequent stronger bonding. However, in contrary to the enzyme activities, sulphur containing molecules had better growth inhibition properties than the molecules with oxygen in **L1**. To identify the cause for the increased cellular activity of S-linked compounds, cellular permeability of a representative compounds with both S-linkage and O-linkage was determined. It was found that the cellular uptake was significantly higher in S-linked compounds when compared to their identical O-linked compounds. Also ROS concentration in cells when treated with S-linked molecules was higher than that of O-linked molecules. Thus the S-linker contributed to the overall permeability of the compounds and cytotoxicity whereas O-linker increased the enzyme activity.

Interaction plots for the compounds are represented in **Figure 6.5-6.7** and ADME predictions are represented in **Table 6.3**. According to **Table 6.2**, compound **6j** was found to be the most active in cellular screening and hence, it was further characterised.

Table 6.3: ADME properties for the compounds synthesized.

Compound No.	Mol wt	Qplog Po/w	Qplog HERG	QPPCaco	QPlogBB	QPP MDCK	Percent Human Oral Absorption
6a	395.5	4.0	-6.0	757.3	-0.9	653.5	100.0
6b	409.5	4.5	-6.0	995.4	-0.9	874.3	100.0
6c	485.6	5.8	-6.7	866.1	-1.0	755.8	100.0
6d	411.5	4.2	-5.7	743.1	-0.8	842.3	100.0
6e	425.6	4.6	-5.7	840.7	-0.8	963.3	100.0
6f	501.7	6.5	-7.5	848.0	-1.1	894.6	91.4
6g	410.5	3.9	-6.2	669.4	-1.0	571.5	100.0
6h	424.5	4.3	-6.3	900.0	-1.0	782.4	100.0
6i	500.6	6.1	-7.8	902.0	-1.2	794.8	89.5
6j	426.6	4.1	-6.1	591.8	-1.0	680.3	100.0
6k	440.6	4.5	-6.4	632.8	-1.1	652.3	100.0
6l	516.7	5.6	-7.1	741.8	-1.4	621.4	85.3
6m	424.5	3.6	-5.2	543.7	-1.2	483.7	97.0
6n	438.5	4.8	-6.3	1077.0	-0.9	955.8	100.0
6o	514.6	6.3	-7.2	989.6	-1.1	872.8	91.5
6p	440.6	4.6	-6.5	745.5	-1.1	796.0	100.0
6q	454.6	5.0	-6.6	849.9	-1.1	934.3	100.0
6r	530.7	6.6	-7.8	757.5	-1.3	811.5	91.1
MK2206	407.5	3.4	-7.2	54.9	-1.1	23.7	78.1

QPlogPo/w Predicted octanol/water partition co-efficient log p (acceptable range from −2.0 to 6.5).

QplogHERG Predicted IC_{50} value for blockage of HERG K+ channels (concern below −5.0).

QPPCaco Predicted Caco-2 cell permeability in nm/s (acceptable range: <25 is poor and >500 is great).

QPlogBB Predicted brain/blood partition coefficient (acceptable range from −3.0 to1.2)

QPPMDCK Predicted MDCK cell permeability in nm/s (acceptable range: <25 is poor and >500 is great).

% human oral absorption Percentage of human oral absorption (<25% is poor and >80% is high).
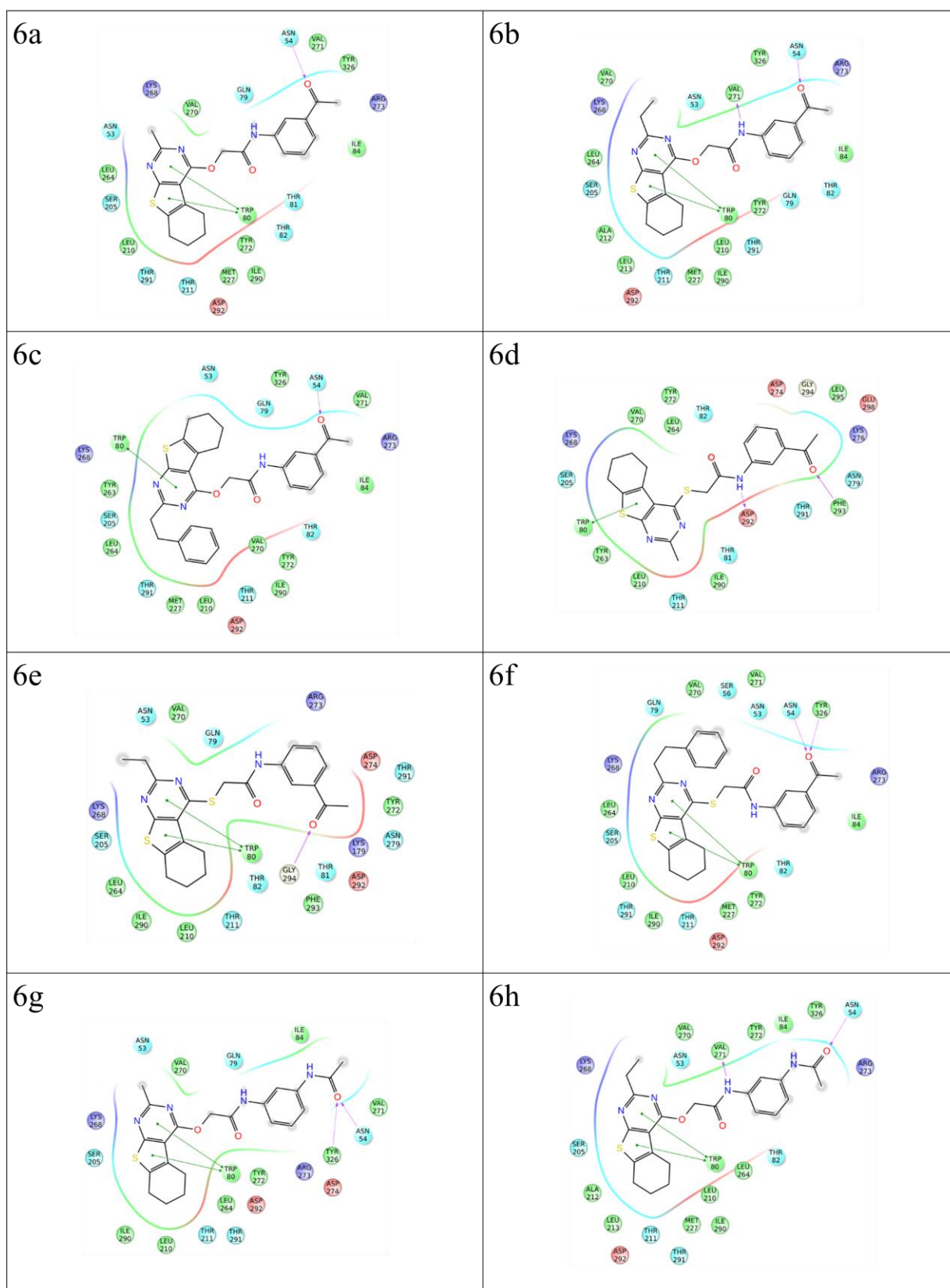
Figure 6.5: Ligand interaction plots for compounds **6a-h.**
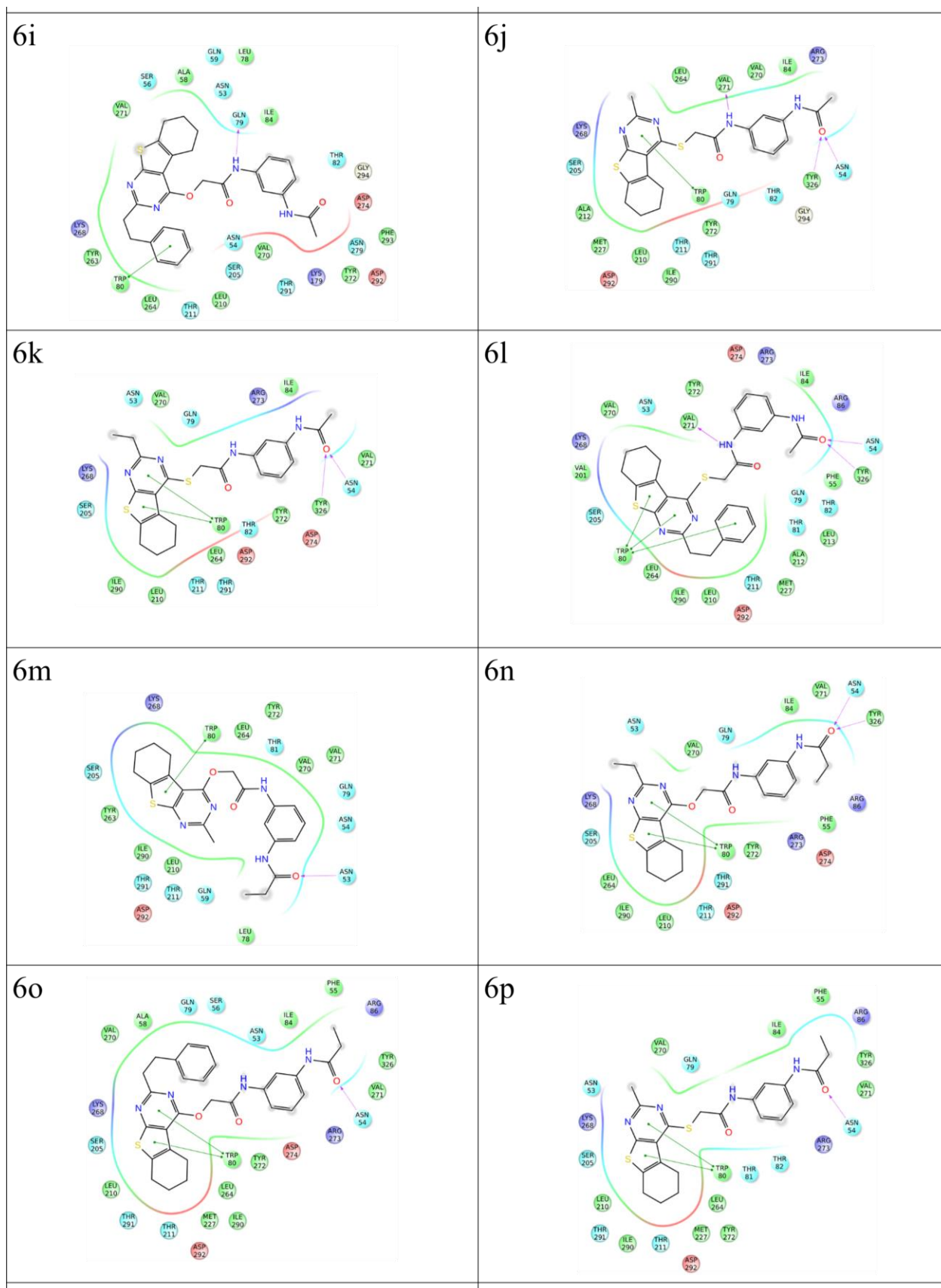
Figure 6.6: Ligand interaction plots for compounds **6i-p.**
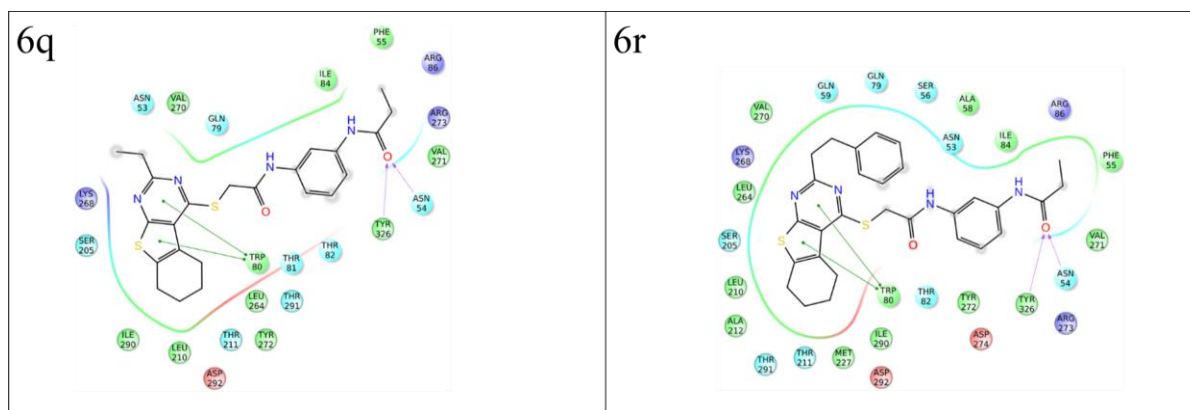
Figure 6.7: Ligand interaction plots for compounds **6q-r.**

6.3 Biological Characterisation of optimised lead molecule: Compound 6j.

6.3.1 Apoptosis and in-situ Capase-3 assay

Based on the promising anti-proliferative activity, compound **6j** was tested for its ability to cause apoptosis based on the binding of annexin-V to phosphatidylserine (PS) translocated to outer leaflet of plasma membrane according to the protocol mentioned in section **4.8.7**. In H460 cells when treated at 1 μM concentration, compound **6j** caused an early apoptosis as indicated by an increase in cells falling in $FITC^+/PI^-$ region (early apoptosis) consistently similar with MK2206 as well as the parent molecule, lead **6** (**Figure 6.8A**). Cells in $FITC^+/PI^-$ were 3.7%, 54.2%, 56.2% and 35.7% respectively for control and compounds **6j**, lead **6** and **MK2206** whereas cells in $FITC^-/PI^-$ (healthy cells) were 93.1%, 36.2%, 37.1% and 55.1% respectively indicating the superior apoptotic activity of compounds **6j** and lead **6** when compared to the standard compound, MK2206. Data from apoptosis assay corroborated with the anti-proliferative activity wherein $GI_{50}s$ for lead **6** and compound **6j** were higher than that of MK2206 in both H460 and A549 cells. Consequently, amount of activated caspase-3 in cells was estimated when treated with compounds MK2206, lead **6** and compound **6j**. As shown in **Figure 6.8B**, lead **6** and **6j** showed better activity in inducing caspase-3 compared to MK2206.

ROS (Reactive oxygen species) concentration was also measured in H460 cells according to the protocol discussed in section **4.8.6**. As shown in **Figure 6.8C**, percentage of ROS$^+$ cells were 80.8%, 70.6% and 30.5% respectively for compounds **MK2206,** lead **6** and compound **6j**.
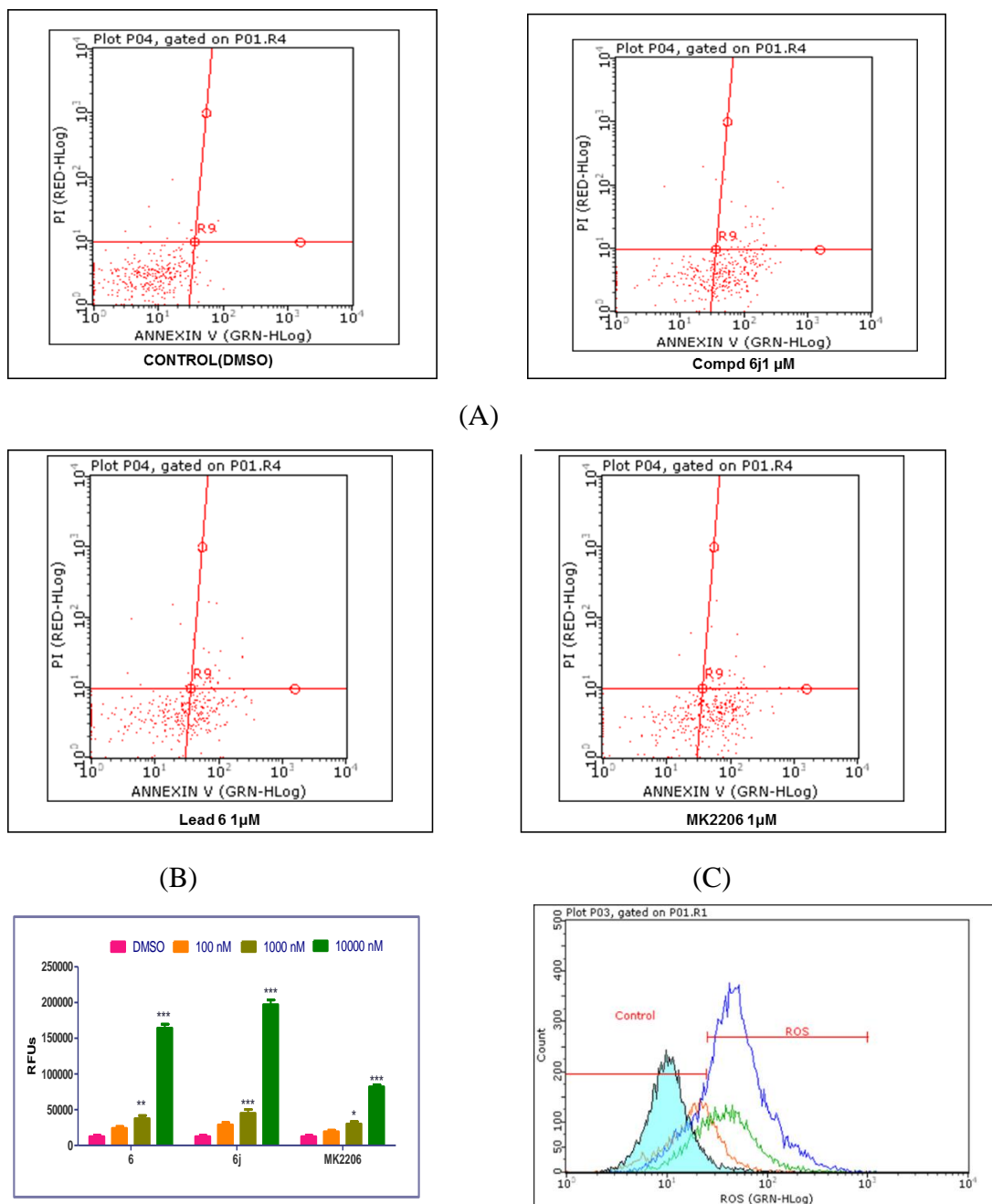
Figure 6.8: Compound **6j** induces early apoptosis by activating caspase-3 and increasing ROS in H460 cells. Effect of compound **6j** on apoptosis (A), caspase-3 (B) and ROS (C) in H460 cells were measured.

6.3.2 Cell cycle assay

The effect of compound **6j** on cell cycle in lung cancer cell lines was determined by propidium iodide staining and analyzed by flow cytometry as per the protocol mentioned in the section **4.8.4. Figure 6.9** indicated that there was a significant increase in cells in the G0/G1 phase ($p<0.01$) when treated with 100 nM of compound **6j** compared to the control. At higher concentrations (1 µM and 10 µM), there was a significant increase in the % cells in sub G0 phase ($p<0.001$). Results correlated with the levels of caspase-3 after treatment with compound **6j** in these cells.

H460	G0/G1%	S%	G2/M%	Sub G0%
Control	70.4	4.5	23.8	0.5
10,000 nM	40.9	7.9	42.1	7.9
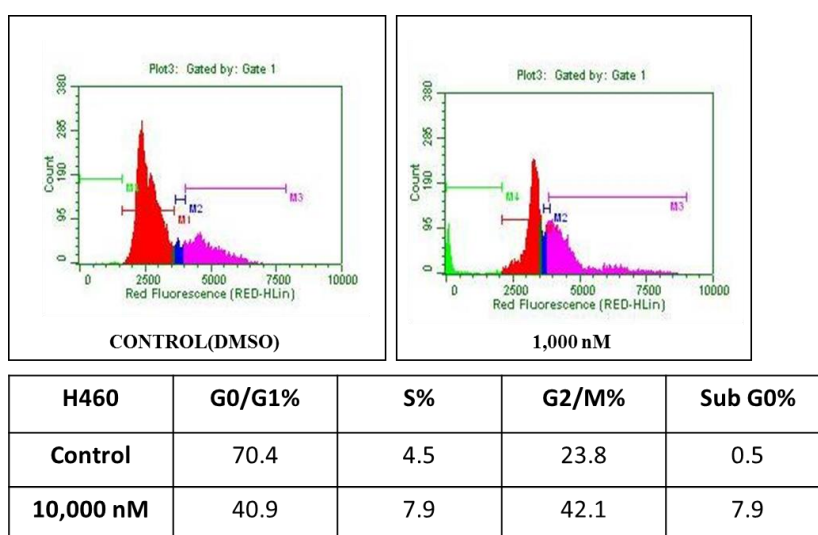
Figure 6.9: Compound **6j** induces cell cycle arrest in lung cancer cell lines.

6.3.3 Effect of compound 6j on downstream Akt pathway

To confirm if the activity of compound **6j** was due to inhibition of Akt phosphorylation, the lung cancer cell lines were treated with compound **6j** and the levels of p-Akt (Ser^{473}) were determined. Compound **6j** downregulated p-Akt in a dose dependent manner **(Figure 6.10)**. The order of sensitivity towards compound **6j** was H460>A549>H2170>H1975. The order of sensitivity was the same as seen for lead **6** in section **5.4.5**. A 40-fold difference in activity between sensitive (H460) and resistant cell lines (H1975) was noticed upon treatment with

compound **6j**. Inhibition of p-Akt expression correlated with the anti-proliferative activity of compound **6j** in lung cancer cell lines thereby elucidating its mode of action.
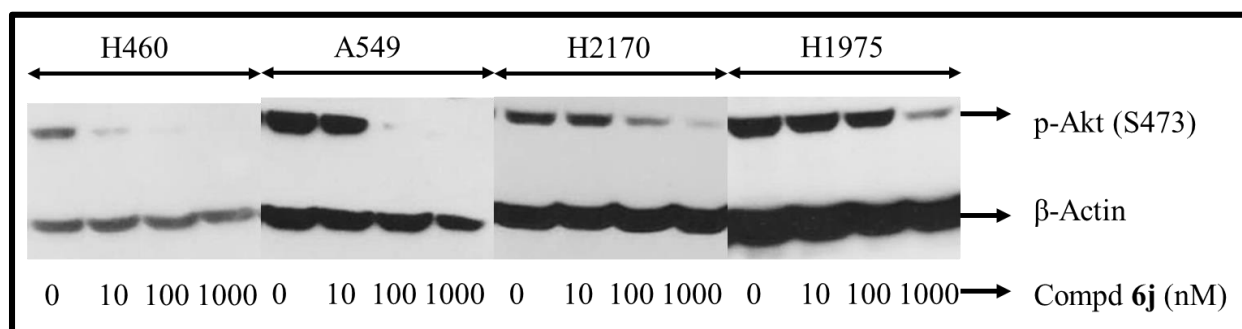
Figure 6.10: Cellular efficacy of compound **6j** is due to the inhibition of Akt pathway. Cells were treated with compound **6j** for 4 h, lysed and p-Akt was estimated by western blot. The levels of p-Akt were quantified at 10 nM, 100 nM and 1000 nM concentration in lung cancer cell lines.

6.3.4 Cellular uptake, plasma and metabolic stability:

To determine the biopharmaceutical properties of compound **6j**, cellular uptake in H460 cells and its stability in liver microsomes and plasma was determined. As shown in **Table 6.4**, compound **6j** revealed a high permeability in H460 cells. When cells were treated with 1 μM of compound **6j**, cellular concentrations reached to 252 nM in H460 cells and 372 nM in A549. Lead **6** also showed a high cellular uptake compared to the standard compound, MK2206, in both H460 and A549 cells. This enhanced permeability explain the higher cellular activities of compounds **6j** and lead **6** when compared to MK2206 although the enzyme activity was higher for MK2206. However, the plasma and metabolic stabilities of compounds **6j** and lead **6** were lower compared to MK2206 indicating that the compounds could be used only through parenteral route rather than oral route as in the case with MK2206.

Table 6.4: Cellular uptake and stability of compound **6j**.

Compd No.	Cellular uptake (nM)	Cellular uptake (nM)	Metabolic stability (%Drug remaining)			Plasma stability (%Drug remaining)		
	H460	**A549**	**Mouse**	**Dog**	**Human**	**Mouse**	**Dog**	**Human**
6g	116	121	1.1	1.1	2.1	5.2	96.7	95.4
6j	252	372	1.2	1.3	2.8	4.2	100	100
6k	247	301	2.3	1.2	2.2	9.6	100	86.1
6p	241	261	1.1	1.5	3.3	23.8	96.6	91.3
6	216	241	12.8	8.4	5.7	2.3	98.1	89.5
MK2206	169	152	94.8	74.8	84.7	97.4	98.3	99.4

6.3.5 Selectivity of compound 6j.

To determine if the molecule could selectively bind to Akt, compound **6j** was tested for enzyme inhibition in a panel of 14 kinases. The kinases were selected based on the homology with Akt1 enzyme. Enzyme assay was done using Z'-Lyte^{TM} kinase assay kits at K_m values of ATP concentration according to the protocol discussed in the section **4.8.1**. As shown in the **Table 6.5**, at 5 μM concentration, compound **6j** selectively inhibited only the three isoforms of Akt (Akt1, Akt2 and Akt3) and not other kinases of PKA, PKC and PKG family thereby limiting the chances of off target toxicities.

Table 6.5: Kinase selectivity for compound **6j**. Selectivity was done at 5 μM concentration of compound **6j** and at k_m value of ATP concentration for various kinases using Z'-Lyte™ assay kits.

Kinase Tested	% Inhibition at 5 μM
AKT1 (PKB alpha)	95
AKT2 (PKB beta)	92
AKT3 (PKB gamma)	98
PDK1 Direct	-10
PRKACA (PKA)	13
PRKCA (PKC alpha)	14
PRKCB1 (PKC beta I)	-14
PRKCD (PKC delta)	10
PRKCG (PKC gamma)	2
PRKG1	-9
PRKG2 (PKG2)	-12
RPS6KA1 (RSK1)	14
RPS6KB1 (p70S6K)	2
SGK (SGK1)	23

6.4 Summary and conclusion

Aberrant regulation of PI3K/Akt/mTOR pathway is implicated in pathogenesis of several cancers. Akt has a critical role as a regulator in cell apoptotic machinery. It is a critical downstream mediator for several growth factor receptors involved in tumorigenesis. On the basis of the strong rationale for targeting Akt in cancer, many efforts have been made to develop small molecule inhibitors of Akt.

Majority of the kinase inhibitors developed till date target the ATP binding site. However, there are several limitations to this strategy since the ATP binding pocket is fairly conserved in most of the kinases. Also, the inhibitors thus designed have to compete with a very high levels of intracellular ATP (~2-10 mM) to be effective. Allosteric inhibitors, however, bind to sites which are mostly conserved only in a specific subfamilies of kinases and hence have greater specificity. Several Akt allosteric inhibitors have been reported till date. These inhibitors include MK2206 which is in Phase III clinical trials for its ability to increase the PFS in lung cancer patients, especially in combination with erlotinib, paclitaxel, premetrexed and gemcetabine.

In the present study, a scaffold of novel molecules for lead **6**, a promising hit for Akt inhibitor, was developed by performing its substructure modification. To sum up the structure activity relationship, (1) Ring **A** was important for π-π stacking with Trp80. However, more isosteric tricyclic ring structures could be tested to optimise its activity. (2) Ring **B** was not essential for activity and hence could be substituted with any alkyl chain to fit in the hydrophobic cleft in the kinase domain of Akt1. The length of the alkyl chain in linker **L2** and substitutions within the chain could still be optimised. 3. Ring **C** was not modified in the SAR as there was no interaction by phenyl ring with any aminoacid residue in Akt1 and isosteric ring could replace the phenyl ring along with modifications in linker **L3** where a was important for interaction

with Asn54. (4) Sulphur containing linker **L3** showed better solubility and permeability compared to the corresponding oxygen containing linker **L3** but with a less potent Akt1 enzyme inhibition.

In comparison to known allosteric inhibitors, compound **6j** was less potent than MK2206 but exhibited better cellular activity. This could be attributed to either the high cellular permeability of compound **6j** (which was atleast 3 times higher than MK2206) or due to inhibition of off-target cellular enzymes that were yet to be identified. Selectivity of compound **6j** was tested in a panel of kinases that shared at least 50% homology with Akt1 and was found to be selective towards Akt 1/2/3 only. Further, the potency and pharmacokinetic properties could be enhanced to make an ideal druggable candidate.

The structure based e-pharmacophore development and subsequent identification of specific inhibitors thus presents a successful strategy to identify novel scaffolds of inhibitors to druggable kinases. Increased understanding of the active site pockets and strengthened chemistry of specific kinases for the presentation of potential new clinical candidates were demonstrated.

CHAPTER 7

MECHANISM OF ACQUIRED RESISTANCE TO Akt INHIBITORS AND METHODS TO OVERCOME THE SAME

CHAPTER 7
MECHANISM OF ACQUIRED RESISTANCE TO Akt

Acquired resistance due to mutations in target kinase render cancer cells insensitive to kinase inhibitor upon prolonged therapy, thereby remaining an important clinical concern. Although the clinical experience with PI3k/Akt inhibitors was limited, one might anticipate complementary resistance mechanisms as observed with other targeted therapies such as imatinib (Bransford S, *et al.*, 2002) and erlotinib (Pao W, *et al.*, 2005; Nguyen KS, *et al.*, 2009). Proposed mechanisms for resistance to PI3K/Akt pathway inhibitors include the IRS-mediated feedback due to inhibition of mTORC1, FOXO3a mediated upregulation of growth factor receptors, and β-catenin mediated nuclear transcription of FOXO3a (Klempner S *et al.*, 2013). However, the exact mechanisms for resistance and their incidences upon long term exposures to Akt inhibitors was unknown.

To understand the mechanism by which lung cancer cells acquired resistance to Akt inhibitors, we developed MK2206 resistant NCI-H460 and A549 cells (hereby referred to as H460, A549 for sensitive and H460R, A549R for resistant cell lines) by incremental exposure to MK2206 for approximately 6 months. Unlike the parental cell lines, phosphorylation of Akt (p-Akt) was minimal in H460R and A549R cells upon addition of MK2206. The objective of this study was to evaluate the compensatory feedback mechanisms involved in resistance to Akt inhibitors and clinically relevant strategies to overcome the same under *in vitro* experimental conditions.

7.1 Establishment of MK2206 resistant cell lines.

As depicted in **Figure 7.1**, the GI_{50} of Akt inhibitors were higher in resistant cells compared to the sensitive cell lines. Half maximal inhibition for MK2206 was increased by 10- fold in H460R and 5- fold in A549R cell lines. Similar results were observed with both lead **6** and **6j**. To determine if the resistance was specific to an isoform of Akt, we tested Akt1 (A674563) and Akt2 (CCT128930) selective inhibitors in proliferation assay. The GI_{50} for A674563 were 5- fold and 7- fold higher in H460R and A549R respectively when compared to their sensitive counterparts (**Figure. 7.1c, 7.1d**). The GI_{50} for CCT128930 was also similar to A674563 indicating that the resistance caused was not due to any specific isoform of Akt. Also, A674563 and CCT128930 were ATP competitive inhibitors of Akt unlike MK2206 and lead **6**. Resistance to Akt inhibitors in H460R and A549R therefore did not appear to be selective based on the mode of binding of the inhibitors.
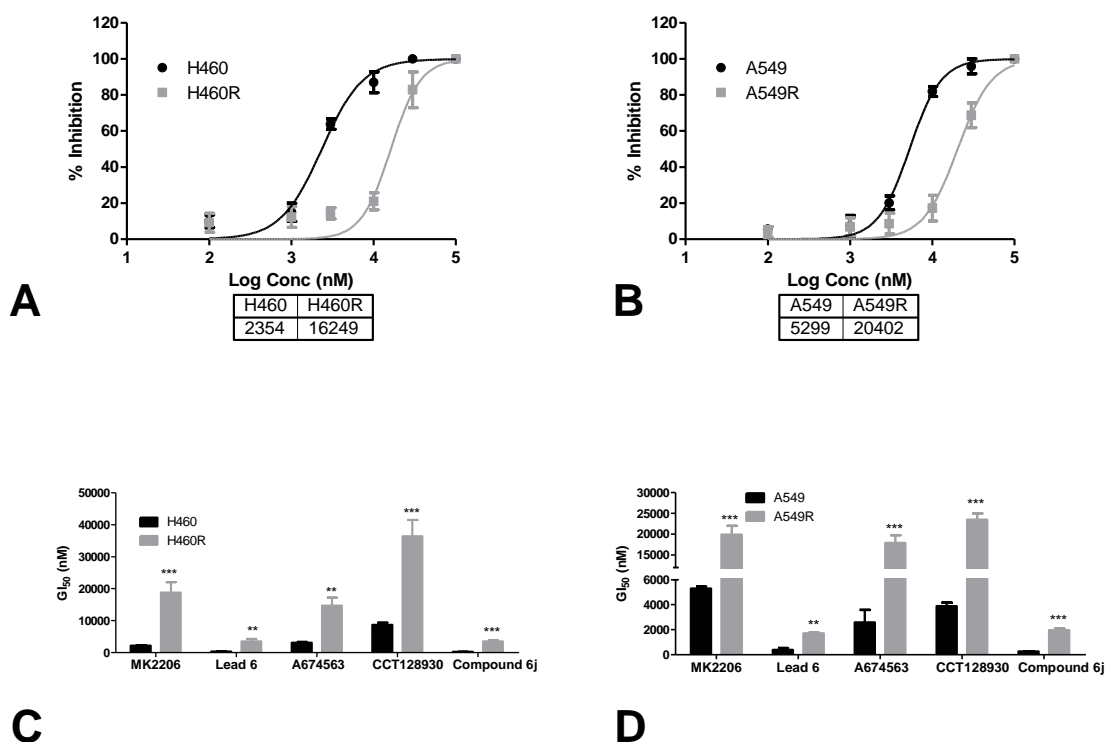
Figure 7.1: Establishment of resistant cell lines. Cells were treated with various concentrations of Akt inhibitors and incubated for 72 h followed by MTT assay. Dose response curves for MK2206 in H460 (A), A549 (B) along with their corresponding resistant cell lines followed by comparison in H460 (C) and A549 (D) for various Akt inhibitors were done. Lead 6, compound 6j are allosteric Akt inhibitor whereas A674563 and CCT128930 are competitive Akt1 and Akt2 selective inhibitors respectively. Data (Mean ±SEM) are from wells plated in triplicate and are representative of three independent experiments. *$p<0.05$, ** $p<0.01$, ***$p<0.001$.

7.2 Amplification of cMyc pathway

Expression of p-Akt (both T^{308} and S^{473}) was diminished in resistant cells compared to the sensitive cells (**Figure 2**). Levels of pErk, p-p38, p-p53, pSTAT5a and pAkt (T^{450}) remained unchanged indicating that these proteins were not affected in resistant cells (**Figure 7.2**). However, cMyc expression was increased in both H460R and A549R cells compared to the sensitive cell lines (**Figure 7.3A**). GI_{50} of a standard Myc inhibitor, 10058-F4 (herewith referred as MYCi) was reduced by 10- fold in both H460R and A549R (**Figure 7.3B, 7.3C**). Hypoxic conditions antagonized the effect of cMyc on survival and apoptosis pathways. To check if MK2206 had any effect under hypoxic conditions, cobalt chloride (a hypoxia mimetic agent) was added to cells at different concentrations and GI_{50} were calculated. As shown in **Figure 7.3F**, there was a dose dependent reduction in GI_{50} of MK2206 as the concentration of $CoCl_2$ increased in H460 cells, indicating sensitivity towards Akt inhibitors with decreasing concentration of cMyc. However, a similar effect was seen only at 200 μM concentration of $CoCl_2$ in H460R indicating cMyc amplification in these cells rendered them less responsive to hypoxic conditions.
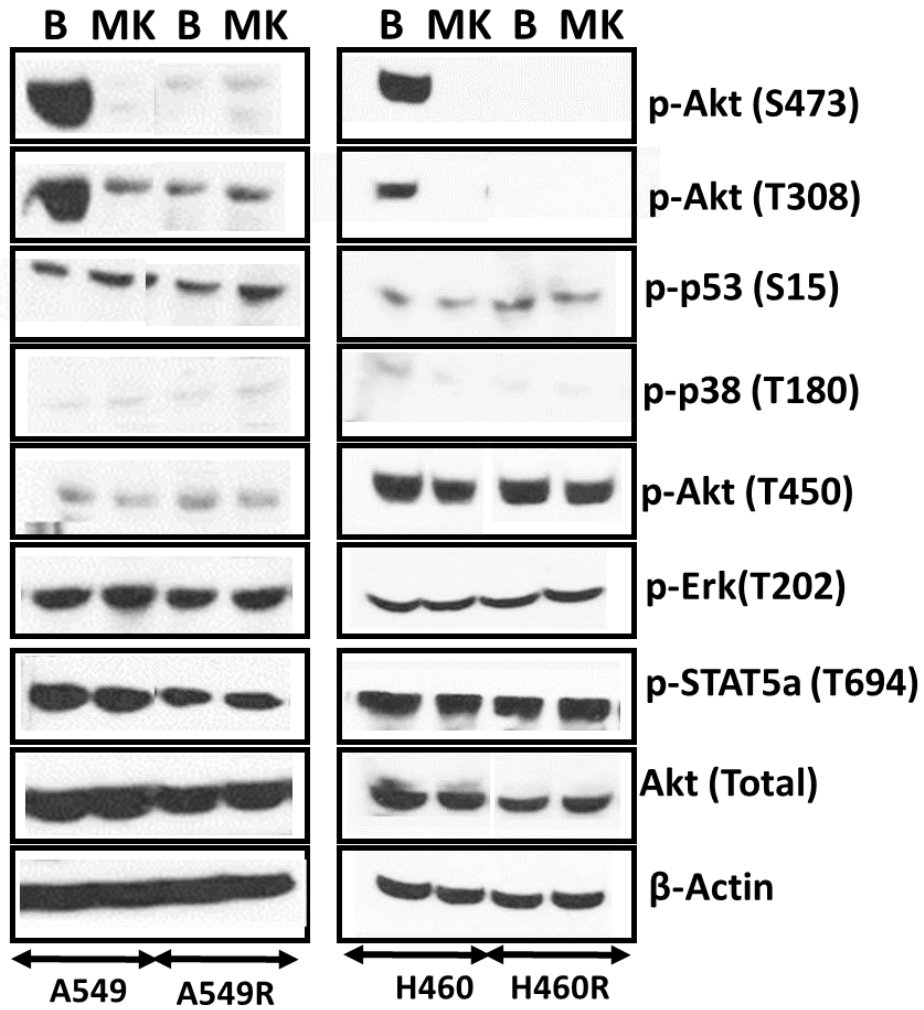
Figure 7.2: Identification of a compensatory mechanism for Akt resistance. Cells were incubated with compound for 24 h, lysed and using specific antibodies, p-Akt and Akt (Total) were estimated along with p-p53, p-p38, p-Erk and p-STAT5a in H460 and A549 cell lines. β-Actin was used as loading control. Lane indications: B. DMSO blank, M. MK2206 at 1 μM

7.3 Combination of Akti and MYCi produced a synergistic effect

To check if the combination of Myc and Akt inhibitors was synergistic in resistant cells, 1 μM of MK2206 or compound **6j** was added to different concentrations of MYCi and combination GI_{50} were calculated. In both H460 and H460R, significant decrease in GI_{50} of MYCi were observed in presence of MK2206 (**Figure 7.3D, 7.3E**). The effect of a time-lag between the addition of MK2206 and MYCi was also determined in both H460 and H460R cells. As evident in **Figure 7.4A**, potency of the combination was greater when MYCi was added after a 4 h incubation with MK2206 in both the cell lines. To arrive at the optimal dosing interval between the two compounds, the combination was tested for different incubation periods in proliferation assays for H460 and H460R cells. While a 72 h incubation was needed for maximal effect in H460, the same was observed at 48 h in H460R, indicating a translational change in the resistant cells (**Figure 7.4B**).
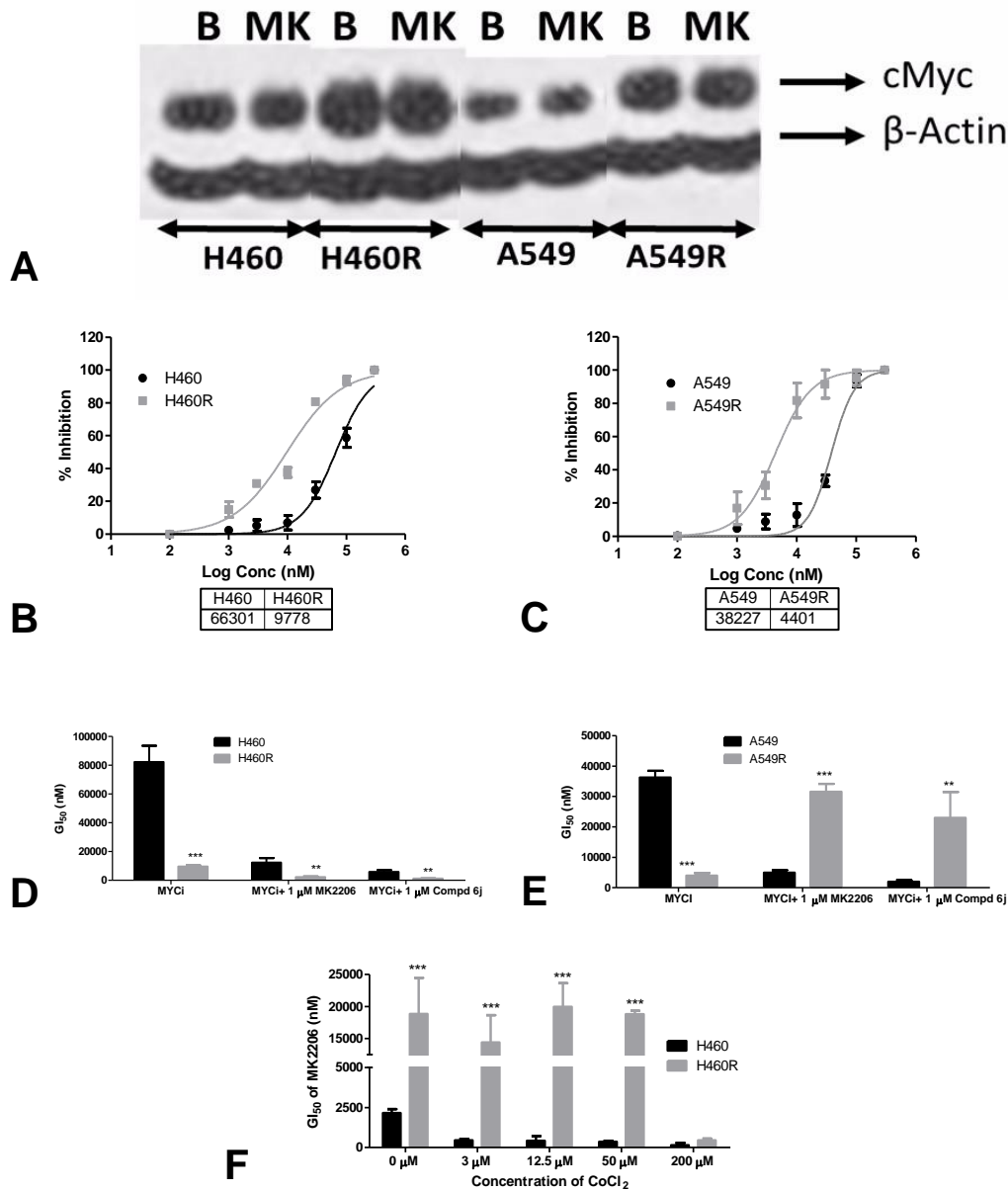
Figure 7.3: cMyc pathway is amplified in Akt resistant cell lines. Expression of cMyc in H460 and A549 cell lines (A) with β-Actin used as loading control. Dose response of cMyc inhibitor (MYCi) were calculated in H460 (B) and A549 (C) followed by a combination of 1 μM MK2206 or compound **6j** and GI_{50}s for MYCi in H460 (D) and A549 (E). Later, effect of MK2206 was estimated in presence of various concentrations of a hypoxia mimetic agent, $CoCl_2$ (F). Data (Mean ±SEM) were from wells plated in triplicate and were representative of three independent experiments. *$p<0.05$, ** $p<0.01$, ***$p<0.001$.
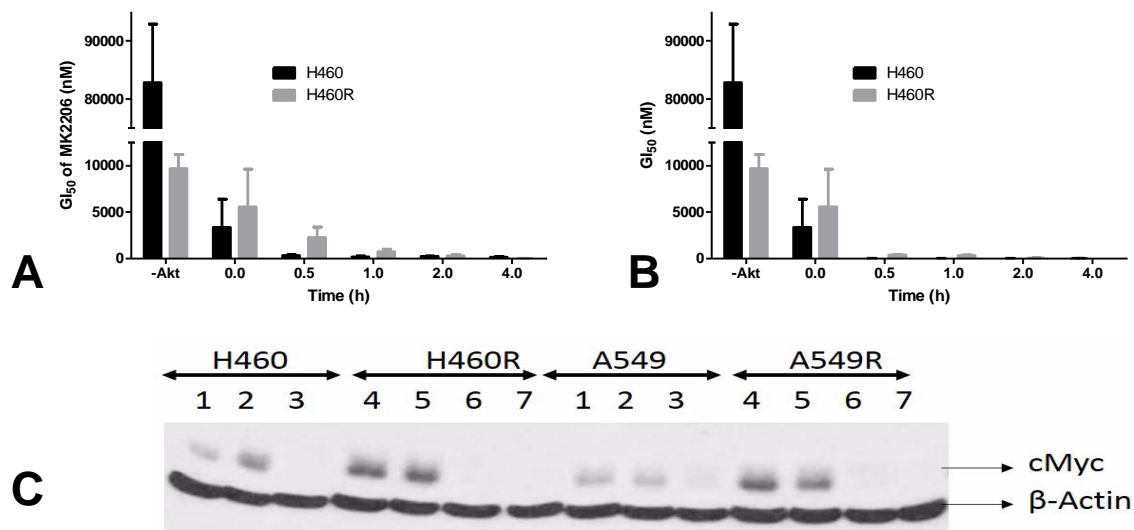
Figure 7.4: Time dependent treatment of combination of Akt and Myc inhibitors. H460 and H460R cells were first treated with MYCi and MK2206 was added at 1 μM after indicated time gap (A) or the vice versa (B). Since, addition of MYCi 4 h after addition of MK2206 had better anti-proliferative effect in H460 cells, the same treatment strategy was used to estimate cMyc expression levels in H460 and A549 cells (C). Lanes representations: 1. Blank, 2. MK2206 1 μM, 3. MYCi 1 μM, 4. Blank, 5. MK2206 1 μM, 6. MYCi 1 μM and 7. MK2206 1 μM + MYCi 1 μM. Data (Mean ±SEM) were from wells plated in triplicate and were representative of three independent experiments. $*p<0.05$, $** p<0.01$, $***p<0.001$.

7.4 Overexpression of glutaminase in resistant cells

Myc activates the glutaminase pathway through miR23a/b. To check if the amplification of Myc had any subsequent effect on downstream Myc signaling, glutaminase expression was estimated in both sensitive and resistant cells. As shown in Figure **7.5A**, glutaminase was found to be overexpressed in both H460R and A549R compared to the sensitive cell lines. Addition of a glutaminase inhibitor (CB839) resulted in a 10-fold GI_{50} change in H460R when compared

to H460 (**Figure7.5B**). Endogenous concentrations of glutamine and glutamate were estimated in both H460 and H460R by LC/MS. As shown in **Figure 7.5C**, the endogenous concentrations of glutamate increased in H460R indicating an increase in the activity of glutaminase. Endogenous levels of glutamine were however not affected indicating that Akt resistance did not influence the glutamine transport system (**Figure7.5C**). CB839 (100 nM) increased glutamine concentration by 67% and decreased glutamate concentration by 37% respectively in both H460 cells and H460R cells (**Figure7.5D, 7.5E**). MK2206 and compound **6j** increased glutamate concentration in H460 cells without affecting glutamine concentration. However, in H460R, MK2206 had no significant effect (**Figure7.5F**).
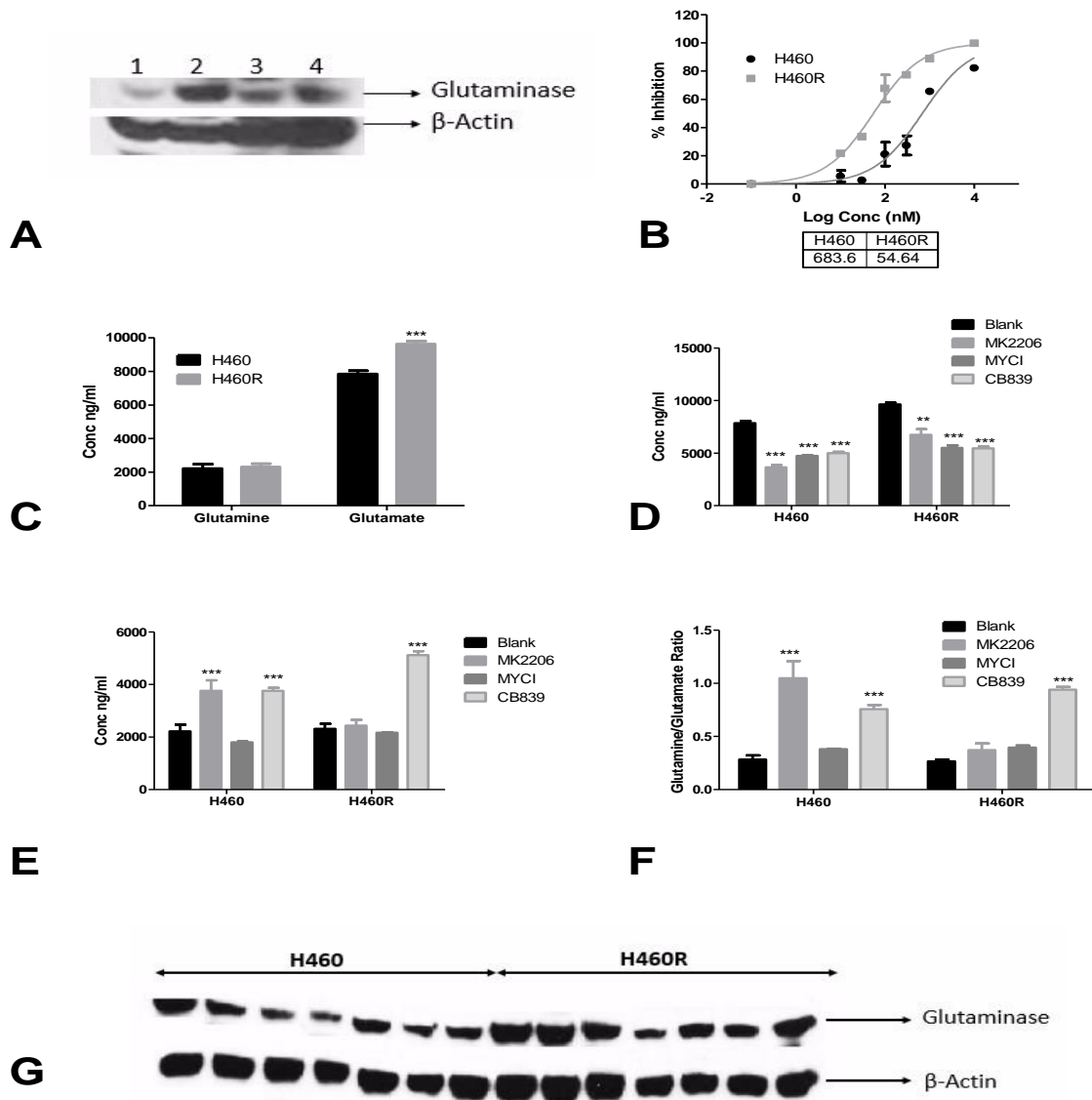
Figure 7.5: Glutaminase is over expressed in Akt resistant cell lines. Expression of glutaminase was estimated (A) in lanes: 1.H460, 2. H460R, 3. A549, 4. A549R. Dose response for CB839 in H460 (B) along with its effect on endogenous levels (C) of glutamine (D), glutamate (E) concentrations in H460 cells were estimated. Along with their ratio (F). Also, the effect of compounds on glutaminase were expressed (G). Lane representations: 1. MK2206 1 μM, 2. MK2206 10 μM, 3. MYCi 1 μM, 4. MYCi 10 μM, 5. CB839 100 nM, 6. CB839 1 μM, 7. DMSO Blank. Data (Mean ±SEM) were from wells plated in triplicate and were representative of three independent experiments. $*p<0.05$, $** p<0.01$, $***p<0.001$.

7.5 Triple combination of MK2206, CB839 and MYCi.

To determine if a triple combination of MK2206, MYCi and CB839 was more beneficial than a combination of CB839 alone, GI_{50} were obtained in H460 and H460R cells for CB839 in combination with 1 μM MK2206 or compound **6j** and 1 μM of MYCi. A significant reduction in GI_{50} was observed in both H460 and H460R compared to CB839 alone indicating that the triple combination was more effective (**Figure 7.6A**). Glutamine/glutamate ratio indicated that the triple combination was more effective compared to the single agent or the dual combinations of compounds tested (**Figure 7.6B**). Thus the overall mechanism for Akt resistance could be proposed as presented in **Figure 7.7**.
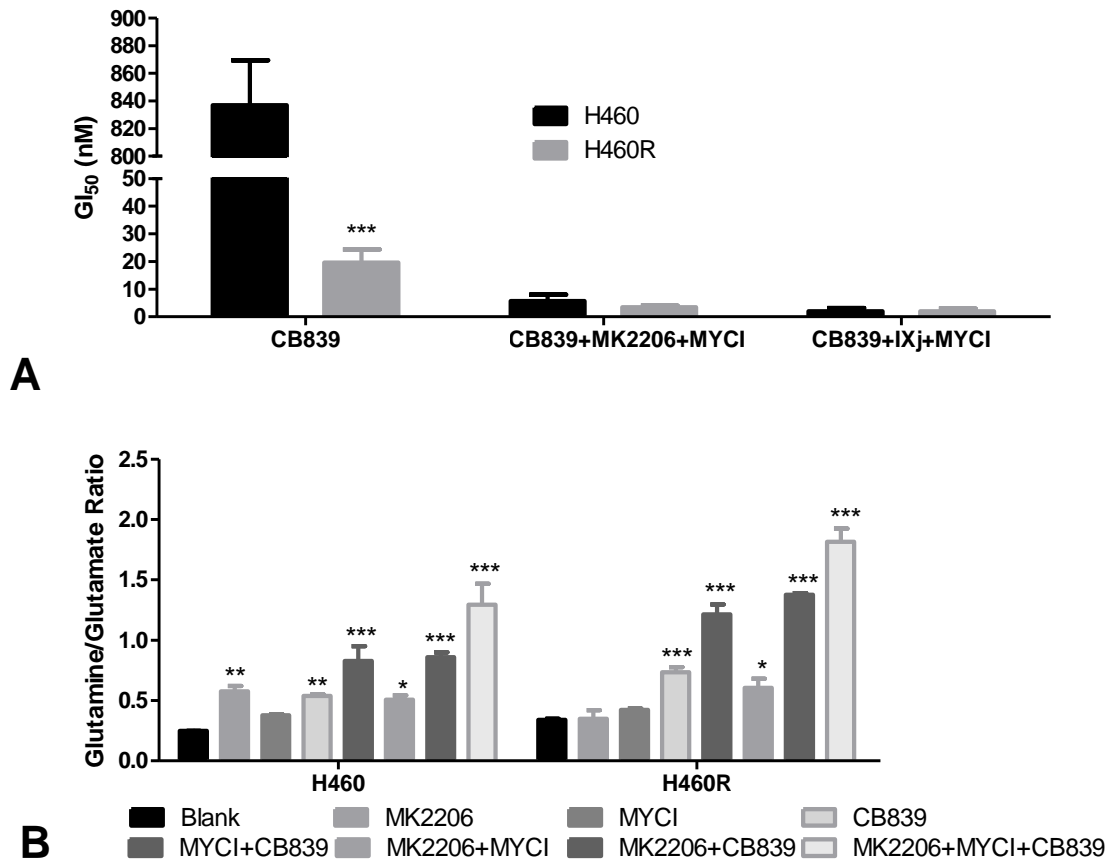
Figure 7.6: Combination of Akt, Myc and Glutaminase inhibitors is more beneficial in both Akt sensitive and resistant cell lines. Dose response of CB839 was calculated in presence or absence of 1 μM MK2206 or compound **6j** + 1 μM MYCi (A) along with concentration of glutamine/glutamate ratios in H460 cells (B). Data (Mean ±SEM) are from wells plated in triplicate and are representative of three independent experiments. $*p<0.05$, $** p<0.01$, $***p<0.001$.
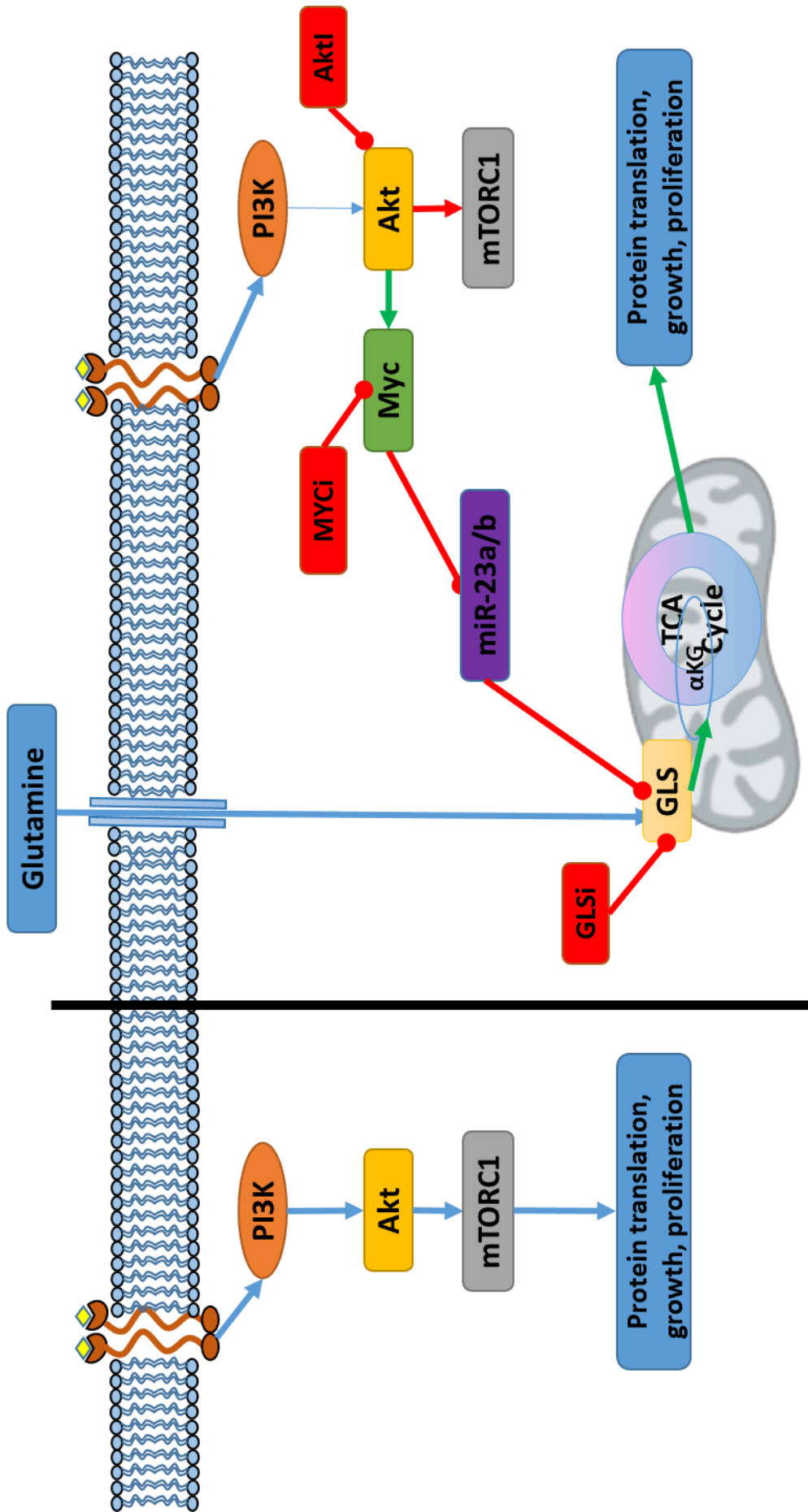
Figure 7.7: Proposed pathway for resistance to Akt inhibitors in lung cancer cell lines.

7.6 Summary and conclusion

Despite tumoral complexity, evolving knowledge on the molecular characteristics of cancer provided hope for the development of better drugs. Targeted therapies, however, had a mixed response in terms of successes and failures. Even with the successful therapies such as erlotinib, secondary mutations were reported that contributed to acquired resistance in lung cancer patients. In addition to secondary mutations in target protein, acquired resistance may also be due to alternative pathways. It is therefore clear that combination therapy would perhaps be beneficial compared to single agent alone.

The current study demonstrated that p-Akt expression was diminished after sustained treatment of MK-2206 in both H460 and A549 cells. Resistance was also observed with other allosteric inhibitors such as lead **6** and compound **6j** as well as competitive and isoform selective inhibitors of Akt such as A674563 (Akt1) and CCT128930 (Akt2). Results, therefore indicated that the resistance due to MK2206 was target specific rather than compound or binding-site specific. To better understand the mechanism of Akt inhibitor resistance, H460 and A549 cell lines were treated with MK2206 and the effect on downstream events were investigated. Data indicated that cMyc mediated sensitivity to MK2206 in NSCLC while sustained treatment with MK2206 resulted in amplification of cMyc and its associated pathway. Importantly, the lack of growth in resistant cells when treated with MYCi and potentiation of the effect of MK2206 in sensitive cell lines suggested that cMyc might be an important mediator of NSCLC response to Akt inhibitors. Conversely, since it was reported that the effect of cMyc on apoptosis and survival pathways were antagonised under hypoxic conditions, sensitive cell lines were treated with cobalt chloride, a known hypoxia mimetic agent. Results indicated that reduced cMyc concentration potentiates the effect of Akt inhibitors under hypoxic conditions. However, a

similar effect was not observed in resistant cell lines (at least at the lower concentrations of cobalt chloride) owing to the already amplified cMyc pathway.

For cancer cells to survive under hypoxic conditions, cells tend to rely more on glutamine rather than glucose metabolism for energy. The altered metabolism of cancer cells known as Warburg effect, was mediated through the cMyc pathway. Since cMyc expression was increased in resistant cells, its effect on downstream glutamine metabolism was also determined. Data suggested that, in addition to an increased cMyc expression, Akt resistant cells also had increased glutamine utilization as indicated by an increase in glutamate concentration in cells without affecting in glutamine levels. Resistant cells also had an overexpression of glutaminase, an enzyme required for the conversion of glutamine to glutamate in cells. Sustained high levels of expression of glutaminase was known to drive the growth of cancer cells with increased concentrations of cellular ATP. Importantly, the lack of growth in resistant cells when treated with CB839, a specific glutaminase inhibitor and potentiation of the effect of MK2206 or compound **6j** in sensitive cell lines suggested that glutaminase might also be an important mediator of NSCLC response to Akt inhibitors. In addition, MK2206 increased the ratio of glutamine to glutamate in sensitive cells with no effect on resistant cells. Data, therefore, strongly suggested that cMyc might play an important role as a tumour oncogene and contributed to a glutaminase dependent Akt inhibitor resistance in cells. High levels of cMyc in tumours suggest that the use of Myc inhibitors or glutaminase inhibitors might be a rational therapeutic strategy for Akt resistant lung cancer treatment.

The aforementioned hypothesis was supported in the two MK2206 resistant cells where specific Myc inhibitor (10058-F4) and glutaminase inhibitor (CB839) were more effective in inhibiting cell growth in resistant cells compare to sensitive cells. In addition, protein levels of cMyc were reduced by Myc inhibitor and glutaminase levels by CB839. Although, glutamate concentration was reduced by both MYCi and CB839, glutamine concentration was increased

only by CB839 indicating that the Akt inhibitor resistant cell were more sensitive to glutaminase inhibitors compared to Myc inhibitors. Results also indicate that MK2206, when used in combination with either MYCi or CB839, displayed synergistic growth inhibition of both Akt inhibitor sensitive and resistant cells. However, a triple combination (MK2206/ compound **6j** + MYCi + CB839) was even more beneficial in both sensitive and resistant cells as evident from the proliferation data and the ratio of glutamine/glutamate concentrations. To our knowledge, there were no studies till date that reported Akt inhibitors affecting the expression of cMyc/glutaminase pathway. In addition to cMyc or glutaminase expression, other pathways might also be involved for the combination effects of MK2206/compound **6j** and MYCi/CB839. The exact mechanism for synergism, however, for the combination remains unclear and further studies are needed.

Findings from this study may have important clinical implications for NSCLC patients who develop acquired resistance for Akt inhibitors. Our findings also suggested that Akt inhibitors were ineffective in subset of cancers with amplified Myc expression even if they harbour Akt activating mutations. Therefore glutaminase inhibitor therapy should be considered in patients whose tumours have become resistant to Akt inhibitors. Alternatively, to prevent Akt resistance, a combination of glutaminase inhibitors and Akt inhibitors could provide a rational treatment strategy for NSCLC patients.

Further studies using study lung cancer primary tumours and cell lines with acquired resistance to Akt inhibitors is warranted for obtaining insights into additional resistance mechanisms. Possible strategies include treatment with combinations to enhance initial tumour cell killing or prolonged an anti-tumour response. Our findings illustrated the relationship between Myc amplification and glutamine catabolism in presence of persistent Akt resistance in lung cancer. Thus, the use of glutaminase/Myc inhibitors in conjunction with Akt inhibitors could be a potential anti-tumour therapy.

In addition to NSCLC, it would be important to determine if Myc amplification contributed to resistance in other Akt dependent cancers such as prostate, breast and gastric cancers.

CHAPTER 8

RECAPTULATION AND FUTURE PERSPECTIVES

CHAPTER 8
RECAPTULATION AND FUTURE PERSPECTIVES

Given the incidences and mortality related to lung cancer among global population, development of novel treatment strategies is of utmost importance. Initial preclinical and early clinical data identified that targeting Akt kinase provided a rational and effective treatment option. Akt inhibitors in clinical phase such as MK2206 and perifosine, indicated that allosteric Akt inhibitors were more selective with less dose related toxicities. However, there was a dearth need of novel, potent and selective Akt inhibitors. In the present study, we focused on identification of novel scaffolds of Akt inhibitors along with characterisation of a lead molecule.

Major limitation for targeted therapies in cancer is the emergence of acquired resistance upon prolonged treatment. Major mechanisms of acquired resistance include the development of secondary mutations in the oncogenic pathway or amplification of compensatory pathways to promote survival and growth of cancer cells. Identification of molecular mechanisms for resistance provide insights for rational combination treatments and hence either prevent the formation of acquired resistance or prolong the sensitivity towards the targeted therapies. This study also focused on the identification of mechanisms for acquired resistance to Akt inhibitors and the ways to overcome the same.

In summary,

> ➢ In a high throughput screening against human Akt1 using a library of compounds, we successfully identified a novel scaffold of inhibitors of Akt *viz*., benzthienopyrimidines.

127

➢ Akt enzyme activity and anti-cancer activity of the lead was evaluated, both against the enzyme and in cell based assays.

➢ Based on the substructure analysis of the lead identified, we synthesized and characterized 18 compounds as analogues of lead **6** to improve the potency.

➢ Of the molecules synthesised, compound **6j** was found to be the most active in cellular assays. IC_{50} in Akt enzyme assay for compound **6j** was 0.327 μM while the GI_{50} in H460 and A549 cells were 0.9 μM and 1.6 μM respectively.

➢ In addition to the anti-proliferative activity, compound **6j** induced ROS concentration and caspase-3 activity in cancer cells thereby inducing apoptosis.

➢ Cell cycle analysis indicated that compound **6j** caused a G0/G1 arrest in cells when treated at a concentration of 1 μM. Compound **6j** also reduced downstream Akt pathway in a dose dependent manner.

➢ Metabolic and plasma stability studies with compound **6j** indicated that it could be administered by parenteral route for its optimal activity.

➢ Simultaneously, by incremental exposure to MK2206, an allosteric Akt inhibitor, stable Akt inhibitor resistant lung cancer cell lines were developed.

➢ Prolonged treatment with Akt inhibitors resulted in elevated cMyc expression levels along with a concomitant increase in glutaminase expression along with increased glutamine metabolism.

➢ Combinations of MK2206 with c-Myc and glutaminase were found to be beneficial compared to that of single agents alone in the treatment of lung cancer cell lines.

In conclusion, novel scaffolds of allosteric Akt inhibitors were designed, synthesized and a lead molecule was characterised. Resistance to targeted therapies of Akt was identified and the methods to overcome the same was demonstrated.

Figure 8.1: Graphical representation
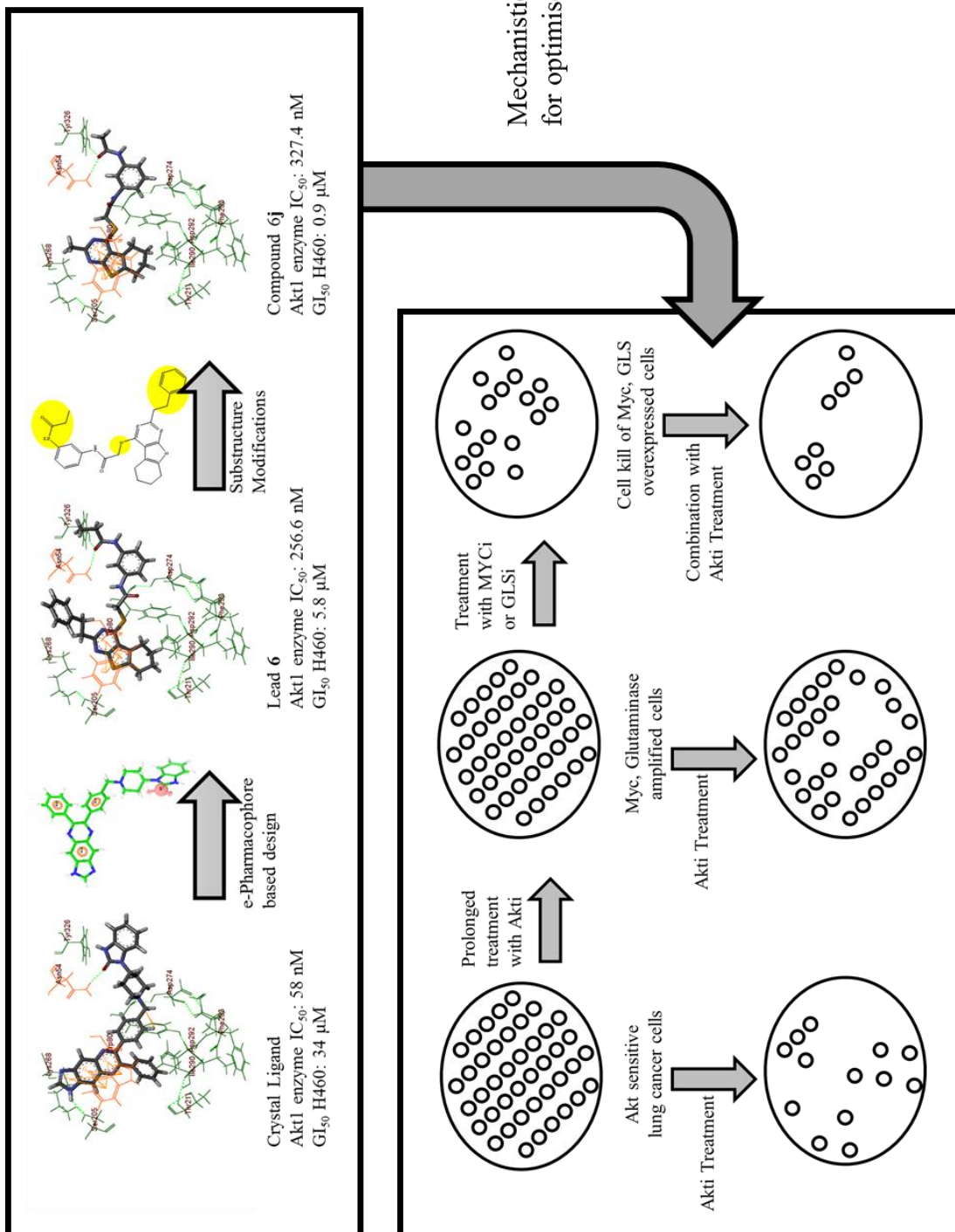
Future perspectives of this study include

➢ Recent studies demonstrated the crucial role of Akt in the development of various cancers along with certain inflammatory disorders. The present study could be extended to various other cancers along with the identification of several other biomarkers to predict a stable disease condition.

➢ Activities of these Akt inhibitors could be evaluated in inflammatory disorders such as asthma and arthritis.

➢ Correlation between the activity of Akt inhibitors and mutations such as PIK3CA and KRAS have been established. This correlation could further be extended to other mutations that amplify Akt activity.

➢ Mechanism for resistance to Akt inhibitors was identified to mediate through cMyc pathway in H460 and A549 cell lines. However, other mechanisms might also play a crucial role in this resistance which are yet to be identified.

➢ Correlating cMyc mechanism with other cell lines in lung cancer along with other cancers could also be evaluated in order to have a better understanding of the resistance pathways.

This study thus directs the scientific community to discover novel scaffolds of Akt inhibitors along with identification of novel mechanisms for Akt resistance thereby providing an upgraded ammunition to tackle the war on cancer.

REFERENCES

REFERENCES

Akamine P., Madhusudan., Brunton L.L., Ou H.D., Canaves J.M., Xuong N.H., Taylor S.S. Balanol analogues probe specificity determinants and the conformational malleability of the cyclic 3',5'-adenosine monophosphate-dependent protein kinase catalytic subunit. *Biochemistry.* 2004, 43: 85-96.

Alessi D.R., Caudwell F.B., Andjelkovic M., Hemmings B.A., Cohen P. Molecular basis for the substrate specificity of protein kinase B; comparison with MAPKAP kinase-1 and p70 S6 kinase. *FEBS Lett.* 1996, 399: 333-8.

Altomare D.A., Wang H.Q., Skele K.L., De Rienzo A., Szanto A.J.K., Godwin A.K., Testa J.R. AKT and mTOR phosphorylation is frequently detected in ovarian cancer and can be targeted to disrupt ovarian tumor cell growth. *Oncogene.* 2004, 23: 5853-7.

Altomare D.A., Testa J.R. Perturbations of the AKT signaling pathway in human cancer. *Oncogene.* 2005, 24: 7455-64.

Arboleda M.J., Lyons J.F., Kabbinavar F.F., Bray M.R., Snow B.E., Ayala R., Danino M., Karlan B.Y., Slamon D.J. Overexpression of AKT2/protein kinase Bbeta leads to up-regulation of beta1integrins, increased invasion, and metastasis of human breast and ovarian cancer cells. *Cancer Res.* 2003, 63: 196–206.

Arranz E., Robledo M., Martínez B., Gallego J., Roman A., Rivas C., Benitez J. Incidence of homogeneously staining regions in non-Hodgkin lymphomas. *Cancer Genet Cytogenet*. 1996, 87:1-3.

Arteaga C.L. EGF receptor mutations in lung cancer: from humans to mice and maybe back to humans. *Cancer Cell.* 2006, 9: 421-23.

Askham J.M., Platt F., Chambers P.A., Snowden H., Taylor C.F., Knowles M.A. AKT1 mutations in bladder cancer: identification of a novel oncogenic mutation that can cooperate with E17K. *Oncogene*. 2010, 29: 150–5.

Barnett S.F., Bilodeau M.T., Lindsley C.W. The Akt/PKB family of protein kinases: a review of small molecule inhibitors and progress towards target validation. *Curr Top Med Chem.* 2005, 5: 109-25.

Bellacosa A., de Feo D., Godwin A.K., Bell D.W., Cheng J.Q., Altomare D.A., Wan M., Dubeau L., Scambia G., Masciullo V., Ferrandina G., Benedetti Panici P., Mancuso S., Neri G., Testa J.R. Molecular alterations of the AKT2 oncogene in ovarian and breast carcinomas. *Int J Cancer*. 1995, 64: 280–285.

Bellacosa A., Kumar C.C., Di Cristofano A., Testa J.R. Activation of AKT kinases in cancer: implications for therapeutic targeting. *Adv. Cancer Res.* 2005, 94: 29-86.

Bjornsti M.A., Houghton P.J. Lost in translation: dysregulation of cap-dependent translation and cancer. *Cancer Cell.* 2004, 5: 519-23.

Bleeker F.E., Felicioni L., Buttitta F., Lamba S., Cardone L., Rodolfo M., Scarpa A., Leenstra S., Frattini M., Barbareschi M., Grammastro M.D., Sciarrotta M.G., Zanon C., Marchetti A., Bardelli A. AKT1(E17K) in human solid tumours. *Oncogene*. 2008, 27: 5648–50.

Boormans J.L., Korsten H., Ziel-van der Made A.C., van Leenders G.J., Verhagen P.C., Trapman J. E17K substitution in AKT1 in prostate cancer. *Br J Cancer*. 2010, 102: 1491–4.

Bozulic L., Surucu B., Hynx D., Hemmings B.A. PKBalpha/Akt1 acts downstream of DNA-PK in the DNA double-strand break response and promotes survival. *Mol Cell* 2008, 30: 203-13.

Breitenlechner C.B., Wegge T., Berillon L., Graul K., Marzenell K., Friebe W.G., Thomas U., Schumacher R., Huber R., Engh R.A., Masjost B. Structure-based optimization of novel azepane derivatives as PKB inhibitors. *J Med Chem.* 2004, 47: 1375-90.

Brognard J., Clark A.S., Ni Y., Dennis P.A. Akt/protein kinase B is constitutively active in non-small cell lung cancer cells and promotes cellular survival and resistance to chemotherapy and radiation. *Cancer Res.* 2001, 61: 3986-97.

Byun D.S., Cho K., Ryu B.K., Lee M.G., Park J.I., Chae K.S., Kim H.J., Chi S.G. Frequent monoallelic deletion of PTEN and its reciprocal associatioin with PIK3CA amplification in gastric carcinoma. *Int J Cancer*. 2003, 104: 318–27.

Cancer Genome Atlas Research Network. Comprehensive genomic characterization defines human glioblastoma genes and core pathways. *Nature*. 2008, 455: 1061–8.

Cappuzzo F., Magrini E., Ceresoli G.L., Bartolini S., Rossi E., Ludovini V., Gregorc V., Ligorio C., Cancellieri A., Damiani S., Spreafico A., Paties C.T., Lombardo L., Calandri C., Bellezza G., Tonato M., Crino L. Akt phosphorylation and gefitinib efficacy in patients with advanced non-small-cell lung cancer. *J Natl Cancer Inst.* 2004, 96: 1133-41.

Cardone M.H., Roy N., Stennicke H.R., Salvesen G.S., Franke T.F., Stanbridge E., Frisch S., Reed J.C. Regulation of cell death protease caspase-9 by phosphorylation. *Science.* 1998, 282: 1318-21.

Carnero A. The PKB/AKT pathway in cancer. *Curr Pharm Des.*, 2010, 16: 34-44.

Carracedo A. Pandolfi P.P. The PTEN-PI3K pathway: of feedbacks and cross-talks. *Oncogene.* 2008, 27: 5527-41.

Castillo S.S. Brognard J., Petukhov P.A., Zhang C., Tsurutani J., Granville C.A., Li M., Jung M., West K.A., Gills J.G., Kozikowski A.P., Dennis P.A. Preferential inhibition of Akt and killing of Akt-dependent cancer cells by rationally designed phosphatidylinositol ether lipid analogues. *Cancer Res.* 2004, 64: 2782-92.

Chalhoub N. Baker S.J., PTEN and the PI3-kinase pathway in cancer. *Annu Rev Pathol.* 2009, 4: 127–50.

Cheng J.Q., Godwin A.K., Bellacosa A., Taguchi T., Franke T.F., Hamilton T.C., Tsichlis P.N., Testa J.R. AKT2, a putative oncogene encoding a member of a subfamily of protein-serine/threonine kinases,is amplified in human ovarian carcinomas. *Proc Natl Acad Sci U S A.* 1992, 89: 9267–71.

Cheng J.Q., Ruggeri B., Klein W.M., Sonoda G., Altomare D.A., Watson D.K., Testa J.R. Amplification of AKT2 in human pancreatic cells and inhibition of AKT2 expression and tumorigenicity by antisense RNA. *Proc Natl Acad Sci U S A.* 1996, 93: 3636–41.

Cohen Y., Shalmon B., Korach J., Barshack I., Fridman E., Rechavi G. AKT1 pleckstrin homology domain E17K activating mutation in endometrial carcinoma. *Gynecol Oncol.* 2010, 116: 88–91.

Cristiano B.E., Chan J.C., Hannan K.M., Lundie N.A., Marmy-Conus N.J., Campbell I.G., Phillips W.A., Robbie M., Hannan R.D., Pearson R.B. A specific role for AKT3 in the genesis of ovarian cancer through modulation of G(2)-M phase transition. *Cancer Res.* 2006, 66: 11718–25.

Dahia P.L. PTEN, a unique tumor suppressor gene. *Endocr Relat Cancer.* 2000, 7: 115-29.

Datta S.R., Dudek H., Tao X., Masters S., Fu H., Gotoh Y., Greenberg M.E. Akt phosphorylation of BAD couples survival signals to the cellintrinsic death machinery. *Cell*. 1997, 91: 231-41.

Davies M.A., Stemke-Hale K., Tellez C., Calderone T.L., Deng W., Prieto V.G., Lazar A.J., Gershenwald J.E., Mills G.B. A novel AKT3 mutation in melanoma tumours and cell lines. *Br J Cancer*. 2008, 99: 1265–8.

Davies T.G., Verdonk M.L., Graham B., Saalau-Bethell S., Hamlett C.C., McHardy T., Collins I., Garrett M.D., Workman P., Woodhead S.J., Jhoti H., Barford D. A structural comparison of inhibitor binding to PKB, PKA and PKA-PKB chimera. *J Mol Biol*. 2007, 367: 882-94.

DeFeo-Jones D., Barnett S.F., Fu S., Hancock P.J., Haskell K.M., Leander K.R., McAvoy E., Robinson R.G., Duggan M.E., Lindsley C.W., Zhao Z., Huber H.E., Jones R.E. Tumor cell sensitization to apoptotic stimuli by selective inhibition of specific Akt/PKB family members. *Mol Cancer Ther*. 2005, 4: 271-79.

deGraffenried L.A., Friedrichs W.E., Russell D.H., Donzis E.J., Middleton A.K., Silva J.M., Roth R.A., Hidalgo M. Inhibition of mTOR activity restores tamoxifen response in breast cancer cells with aberrant Akt Activity. *Clin Cancer Res*. 2004, 10: 8059-67.

Dijkers P.F., Birkenkamp K.U., Lam E.W., Thomas N.S., Lammers J.W., Koenderman L., Coffer P.J. FKHR-L1 can act as a critical effector of cell death induced by cytokine withdrawal: protein kinase B-enhanced cell survival through maintenance of mitochondrial integrity. *J Cell Biol*. 2002, 156: 531-42.

Downward J. Targeting RAS signalling pathways in cancer therapy. *Nat Rev Cancer*. 2003, 3: 11-22.

Downward J. PI 3-kinase, Akt and cell survival. *Semin Cell Dev Biol*. 2004, 15:177-82.

Dumble M., Crouthamel M.C., Zhang S.Y., Schaber M., Levy D., Robell K., Liu Q., Figueroa D.J., Minthorn E.A, Seefeld M.A., Rouse M.B., Rabindran S.K., Heerding D.A., Kumar R. Discovery of novel AKT inhibitors with enhanced anti-tumor effects in combination with the MEK inhibitor. *PLoS One.* 2014, 9:e100880.

Dummler B., Tschopp O., Hynx D., Yang Z.Z., Dirnhofer S., Hemmings B.A. Life with a single isoform of Akt: mice lacking Akt2 and Akt3 are viable but display impaired glucose homeostasis and growth deficiencies. *Mol Cell Biol.* 2006, 26: 8042-51.

Dummler B., Hemmings B.A. Physiological roles of PKB/Akt isoforms in development and disease. *Biochem Soc Trans*. 2007, 35: 231-5.

Ekert P.G., Silke J., Vaux D.L. Caspase inhibitors. *Cell Death and Differ*. 1999, 6: 1081-6.

Engelman J.A., Janne P.A., Mermel C., Pearlberg J., Mukohara T., Fleet C., Cichowski K., Johnson B.E., Cantley L.C. ErbB-3 mediates phosphoinositide 3-kinase activity in gefitinib-sensitive non-small cell lung cancer cell lines. *Proc Natl Acad Sci U S A*. 2005, 102: 3788-93.

Engelman JA. The role of phosphoinositide 3-kinase pathway inhibitors in the treatment of lung cancer. *Clin Cancer Res.* 2007, 13: 4637-40.

Eruslanov E., Kusmartsev S. Identification of ROS using oxidized DCFDA and flow-cytometry. *Adv Prot Oxidative Stress II*. 2010, 594: 57-72.

Friesner, R.A., Banks, J.L.; Murphy, R.B., Halgren, T.A., Klicic, J.J., Mainz, D.T., Repasky, M.P., Knoll, E.H., Shaw, D.E., Shelley, M., Perry, J.K., Francis, P., Shenkin, P.S. Glide: A New Approach for Rapid, Accurate Docking and Scoring. 1. Method and Assessment of Docking Accuracy. *J Med Chem.* 2004, 47: 1739-49.

Govindan R., Page N., Morgensztern D., Read W., Tierney R., Vlahiotis A., Spitznagel E.L., Piccirillo J. Changing epidemiology of small-cell lung cancer in the United States over the last

30 years: analysis of the surveillance, epidemiologic, and end results database. *J Clin Oncol.* 2006, 24: 4539-44.

Greenwood J.R., Calkins D., Sullivan A.P., Shelley J.C. Towards the comprehensive, rapid, and accurate prediction of the favorable tautomeric states of drug-like molecules in aqueous solution. *J Comput Aided Mol Des.* 2010, 24: 591-604.

Gustafsson A.B., Brunton L.L. Differential and selective inhibition of protein kinase A and protein kinase C in intact cells by balanol congeners. *Mol Pharmacol.* 1999, 56: 377-82.

Hanahan D., Weinberg R.A. The hallmarks of cancer. *Cell.* 2000, 100: 57-70.

Hartnett J.C., Barnett S.F., Bilodeau M.T., Defeo-Jones D., Hartman G.D., Huber H.E., Jones R.E., Kral A.M., Robinson R.G., Wu Z. Optimization of 2,3,5-trisubstituted pyridine derivatives as potent allosteric Akt1 and Akt2 inhibitors. *Bioorg Med Chem Lett.* 2008, 18: 2194-97.

Hashimoto K., Mori N., Tamesa T., Okada T., Kawauchi S., Oga A., Furuya T., Tangoku A., Oka M., Sasaki K. Analysis of DNA copy number aberrations in hepatitis C virus-associated hepatocellular carcinomas by conventional CGH and array CGH. *Mol Pathol.* 2004, 17: 617–22.

Heerding D.A., Clark T.J. Leber J.D., Safonov I. WO07058850, 2007a.

Heerding D.A., Clark T.J. Leber J.D., Safonov I. WO07058852, 2007b.

Heerding D.A., Clark T.J. Leber J.D., Safonov I. WO07058879, 2007c.

Helmericks R.C.M., Grimes H.L., Bellacosa A., Malstrom S.E., Tsichlis P.N., Rosen N. Cyclin D expression is controlled post-transcriptionally via a phosphatidylinositol 3-kinase/Akt-dependent pathway. *J Biol Chem.* 1998, 273: 29864-72.

Hirai H., Sootome H., Nakatsuru Y., Miyama K., Taguchi S., Tsujioka K. An allosteric Akt inhibitor, MK-2206 enhanced anti-tumor efficacy by standard of care agents or molecular targeted drugs in vitro and in vivo; AACR Meeting Abstracts; 2009. p. 3707.

Hirata A., Hosoi F., Miyagawa M., Ueda S., Naito S., Fujii T., Kuwano M., Ono M. HER2 overexpression increases sensitivity to gefitinib, an epidermal growth factor receptor tyrosine kinase inhibitor, through inhibition of HER2/HER3 heterodimer formation in lung cancer cells. *Cancer Res.* 2005, 65: 4253-60.

Hu L., Hofmann J., Lu Y., Mills G.B., Jaffe R.B. Inhibition of phosphatidylinositol 3'-kinase increases efficacy of paclitaxel in in vitro and in vivo ovarian cancer models. *Cancer Res.* 2002, 62: 1087-92.

Kandel E.S., Hay N. The regulation and activities of the multifunctional serine/threonine kinase Akt/PKB. *Exp Cell Res.* 1999, 253: 210-29.

Kang S., Bader A.G., Vogt P.K. Phosphatidylinositol 3-kinase mutations identified in human cancer are oncogenic. *Proc Natl Acad Sci U S A*. 2005, 102: 802–07.

Kau T.R., Schroeder F., Ramaswamy S., Wojciechowski C.L., Zhao J.J., Roberts T.M., Clardy J., Sellers W.R., Silver P.A. A chemical genetic screen identifies inhibitors of regulated nuclear export of a Forkhead transcription factor in PTEN-deficient tumor cells. *Cancer Cell.* 2003, 4: 463-76.

Klempner S.J., Myers A.P., Cantley L.C. What a tangled web we weave: emerging resistance mechanisms to inhibition of the phosphoinositide 3-kinase pathway. *Cancer Discov.* 2013, *3*: 1345-54.

Kovacina K.S., Park G.Y., Bae S.S., Guzzetta A.W., Schaefer E., Birnbaum M.J., Roth R.A. Identification of a proline-rich Akt substrate as a 14-3-3 binding partner. *J Biol Chem.* 2003, 278: 10189-94.

Kozikowski A.P., Kiddle J.J., Frew T., Berggren M., Powis G. Synthesis and biology of 1D-3-deoxyphosphatidylinositol: a putative antimetabolite of phosphatidylinositol-3-phosphate and an inhibitor of cancer cell colony formation. *J Med Chem.* 1995, 38: 1053-56.

Krishan, A. Rapid flow cytofluorometric analysis of mammalian cell cycle by propidium iodide staining. *J Cell Biol.* 1975, 66: 188-93.

Kumar C.C., Madison V. AKT crystal structure and AKT-specific inhibitors. *Oncogene*. 2005, 24: 7493-501.

Kumar R, Rhodes N, Knick VB. GSK690693, a pan-Akt kinase inhibitor has potent anti-tumor activity and shows additive effect with lapatinib. *Annual Meeting of AACR*. 2007, 279.

Kuo K.T., Mao T.L., Jones S., Veras E., Ayhan A., Wang T.L., Glas R., Slamon D., Velculescu V.E., Kuman R.J., Shih Ie M. Frequent activating mutations of PIK3CA in ovarian clear cell carcinoma. *Am J Pathol.* 2009, 174: 1597–601.

Larue L., Bellacosa A. Epithelial-mesenchymal transition in development and cancer: role of phosphatidylinositol 3' kinase/AKT pathways. *Oncogene.* 2005, 24: 7443-54.

Lefranc F., Brotchi J., Kiss R. Possible future issues in the treatment of glioblastomas: special emphasis on cell migration and the resistance of migrating glioblastoma cells to apoptosis. *J Clin Oncol.* 2005, 23: 2411-22.

Liang J., Zubovitz J., Petrocelli T., Kotchetkov R., Connor M.K., Han K., Lee J.H., Ciarallo S., Catzavelos C., Beniston R., Franssen E., Slingerland J.M. PKB/Akt phosphorylates p27,

impairs nuclear import of p27 and opposes p27-mediated G1 arrest. *Nat Med.* 2002, 8: 1153-60.

Liang J., Slingerland J.M. Multiple roles of the PI3K/PKB (Akt) pathway in cell cycle progression. *Cell Cycle.* 2003, 2: 339-45.

Lindsley C.W., Zhao Z., Leister W.H., Robinson R.G., Barnett S.F., Defeo-Jones D., Jones R.E., Hartman G.D., Huff J.R., Huber H.E. Duggan M.E. Allosteric Akt (PKB) inhibitors: discovery and SAR of isozyme selective inhibitors. *Bioorg Med Chem Lett.* 2005, 15:761-64.

Lowe S.W., Lin A.W. Apoptosis in cancer. *Carcinogenesis.* 2000, 21: 485–95.

Lu W., Defeo-Jones D., Davis L.J., Hang G., Tammam J.G., Hatch H. *In vitro* and *in vivo* antitumor activities of MK-2206, a new allosteric Akt inhibitor; *Annual Meeting of AACR.* 2009, 3714.

Luo Y., Shoemaker A.R., Liu X., Woods K.W., Thomas S.A., de Jong R., Han E.K., Li T., Stoll V.S., Powlas J.A., Oleksijew A., Mitten M.J., Shi Y., Guan R., McGonigal T.P., Klinghofer V., Johnson E.F., Leverson J.D., Bouska J.J., Mamo M., Smith R.A., Gramling-Evans E.E., Zinker B.A., Mika A.K., Nguyen P.T., Oltersdorf T., Rosenberg S.H., Li Q., Giranda V.L. Potent and selective inhibitors of Akt kinases slow the progress of tumors in vivo. *Mol Cancer Ther.* 2005, 4: 977-86.

Maehama T., Dixon J.E. The tumor suppressor, PTEN/MMAC1, dephosphorylates the lipid second messenger, phosphatidylinositol 3,4,5-trisphosphate. *J Biol Chem.* 1998, 273: 13375-78.

Manning B.D., Cantley L.C. AKT/PKB signaling: navigating downstream. *Cell.* 2007, 129: 1261-74.

Mayo L.D., Donner D.B. A phosphatidylinositol 3-kinase/Akt pathway promotes translocation of Mdm2 from the cytoplasm to the nucleus. *Proc Natl Acad Sci USA.* 2001, 98: 11598-603.

Meuillet E.J., Ihle N., Baker A.F., Gard J.M., Stamper C., Williams R., Coon A., Mahadevan D., George B.L., Kirkpatrick L., Powis G. In vivo molecular pharmacology and antitumor activity of the targeted Akt inhibitor PX-316. *Oncol Res.* 2004, 14: 513-27.

Miwa W., Yasuda J., Murakami Y., Yashima K., Sugano K., Sekine T., Kono A., Egawa S., Yamaguchi K., Hayashizaki Y., Sekiya T. Isolation of DNA sequences amplified at chromosome 19q13.1-q13.2 including the AKT2 locus in human pancreatic cancer. *Biochem Biophys Res Commun.* 1996, 225: 968–74.

Nagler A., Ben-Yehuda D., Badros A., Hari P., Hajek R., Spicka I., Anderson K.C. Randomized placebo-controlled phase III study of perifosine combined with bortezomib and dexamethasone in relapsed, refractory multiple myeloma patients previously treated with bortezomib. *Blood.* 2013, 122: 3189-89.

Narayana N., Diller T.C., Koide K., Bunnage M.E., Nicolaou K.C., Brunton L.L., Xuong N.H., Ten Eyck L.F., Taylor S.S. Crystal structure of the potent natural product inhibitor balanol in complex with the catalytic subunit of cAMP-dependent protein kinase. *Biochemistry.* 1999, 38: 2367-76.

Narita Y., Nagane M., Mishima K., Huang H.J., Furnari F.B., Cavenee W.K. Mutant epidermal growth factor receptor signaling down-regulates p27 through activation of the phosphatidylinositol 3-kinase/Akt pathway in glioblastomas. *Cancer Res.* 2002, 62: 6764-9.

Noske A., Kaszubiak A., Weichert W., Sers C., Niesporek S., Koch I., Schaefer B., Sehouli J., Dietel M., Lage H., Denkert C. Specific inhibition of AKT2 by RNA interference results in reduction of ovarian cancer cell proliferation: increased expression of AKT in advanced ovarian cancer. *Cancer Lett.* 2007, 246: 190–200.

Ozes O.N., Mayo L.D., Gustin J.A., Pfeffer S.R., Pfeffer L.M., Donner D.B. NF-kappaB activation by tumour necrosis factor requires the Akt serine-threonine kinase. *Nature.* 1999, 401: 82-5.

Page C., Lin H.J., Jin Y., Castle V.P., Nunez G., Huang M., Lin J. Overexpression of Akt/AKT can modulate chemotherapy-induced apoptosis. *Anticancer Res.* 2000, 20: 407-16.

Pedrero J.M., Carracedo D.G., Pinto C.M., Zapatero A.H., Rodrigo J.P., Nieto C.S. Gonzalez M.V., Frequent genetic and biochemical alterations of the PI 3-K/AKT/PTEN pathway in head and neck squamous cell carcinoma. *Int J Cancer.* 2005, 114: 242–8.

Philp A.J., Campbell I.G., Leet C., Vincan E., Rockman S.P., Whitehead R.H., Thomas R.J., Phillips W.A. The phosphatidylinositol 3′-kinase p85alpha gene is an oncogene in human ovarian and colon tumors. *Cancer Res.* 2001, 61: 7426–29.

Plas D.R., Thompson C.B. Akt-dependent transformation: there is more to growth than just surviving. *Oncogene.* 2005. 24: 7435-42.

Powis G., Aksoy I.A., Melder D.C., Aksoy S., Eichinger H., Fauq A.H., Kozikowski A.P. D-3-deoxy-3-substituted myo-inositol analogues as inhibitors of cell growth. *Cancer Chemother Pharmacol.* 1991, 29: 95-104.

Reuveni H., Livnah N., Geiger T., Klein S., Ohne O., Cohen I., Benhar M., Gellerman G., Levitzki A. Toward a PKB inhibitor: modification of a selective PKA inhibitor by rational design. *Biochemistry.* 2002, 41: 10304-14.

Rhodes N., Knick V.B., McConnell R. GSK690693, a pan-Akt kinase inhibitor with potent pharmacodynamic and antitumor activity in vivo (abstract). Los Angeles, CA. Annual Meeting of AACR; 2007, p. 277.

Robey R.B., Hay N. Mitochondrial hexokinases, novel mediators of the antiapoptotic effects of growth factors and Akt. *Oncogene.* 2006, 25: 4683-96.

Ruggeri B.A., Huang L., Wood M., Cheng J.Q., Testa J.R. Amplification and overexpression of the AKT2 oncogene in a subset of human pancreatic ductal adenocarcinomas. *Mol Carcinog.* 1998, 21: 81–6.

Ruggero D., Pandolfi P.P. Does the ribosome translate cancer? *Nat Rev Cancer.* 2003. 3: 179-92.

Sabatini DM. mTOR and cancer: insights into a complex relationship. *Nat Rev Cancer.* 2006, 6: 729-34.

Salam N.K., Nuti R., Sherman W. Novel Method for Generating Structure-Based Pharmacophores Using Energetic Analysis. *J Chem Inf Model* 2009, 49: 2356–68.

Salvesen H.B., Carter S.L., Mannelqvist M., Dutt A., Getz G., Stefansson I.M., Raeder M.B., Sos M.L., Engelsen I.B., Trovik J., Wik E., Greulich H., Bo T.H., Jonassen I., Thomas R.K., Zander T., Garraway L.A., Oyan A.M., Sellers W.R., Kalland K.H., Meyerson M., Akslen L.A., Beroukhim R. Integrated genomic profiling of endometrial carcinoma associates aggressive tumors with indicators of PI3 kinase activation. *Proc Natl Acad Sci U S A.* 2009, 106: 4834–9.

Sancak Y., Thoreen C.C., Peterson T.R., Lindquist R.A., Kang S.A., Spooner E., Carr S.A., Sabitini D.M. PRAS40 is an insulin-regulated inhibitor of the mTORC1 protein kinase. *Mol Cell.* 2007, 25: 903-15.

Sangai T., Akcakanat A., Chen H., Tarco E., Wu Y., Do K.A., Miller T.W., Arteaga C.L., Mills G.B., Gonzalez-Angulo A.M., Meric-Bernstam F. Biomarkers of response to Akt inhibitor MK-2206 in breast cancer. *Clin Cancer Res.* 2012, 18: 5816-28.

Sansal I., Sellers W.R. The biology and clinical relevance of the PTEN tumor suppressor pathway. *J Clin Oncol.* 2004, 22: 2954-63.

Shayesteh L., Lu Y., Kuo W.L., Baldocchi R., Godfrey T., Collins C., Pinkel D., Powell B., Mills G.B., Gray J.W. PIK3CA is implicated as an oncogene in ovarian cancer. *Nat Genet.* 1999, 21: 99– 102.

Shi J., Yao D., Liu W., Wang N., Lv H., Zhang G., Ji M., Xu L., He N., Shi B., Hou P. Highly frequent PIK3CA amplification is associated with poor prognosis in gastric cancer. *BMC Cancer.* 2012, 12: 50.

Shin I., Yakes F.M., Rojo F., Shin N.Y., Bakin A.V., Baselga J., Artaega C.L. PKB/Akt mediates cell-cycle progression by phosphorylation of p27(Kip1) at threonine 157 and modulation of its cellular localization. *Nat Med.* 2002, 8: 1145-52.

Shivakumar D., Williams J., Wu Y., Damm W., Shelley J., Sherman W. Prediction of Absolute Solvation Free Energies using Molecular Dynamics Free Energy Perturbation and the OPLS Force Field. *J Chem Theory Comput.* 2010, 6: 1509–19.

Shoji K., Oda K., Nakagawa S., Hosokawa S., Nagae G., Uehara Y., Sone K., Miyamoto Y., Hiraike H., Hiraike-Wada O., Nei T., Kawana K., Kuramoto H., Aburatani H., Yano T., Taketani Y. The oncogenic mutation in the pleckstrin homology domain of AKT1 in endometrial carcinomas. *Br J Cancer.* 2009, 101: 145–8.

Soltoff S.P., Carraway III K.L., Prigent S.A., Gullick W.G., Cantley L.C. ErbB3 is involved in activation of phosphatidylinositol 3-kinase by epidermal growth factor. *Mol Cell Biol.* 1994, 14: 3550-58.

Stahl J.M., Sharma A., Cheung M., Zimmerman M., Cheng J.Q., Bosenberg M.W., Kester M., Sandirasegarane L., Robertson G.P. Deregulated Akt3 activity promotes development of malignant melanoma. *Cancer Res.* 2004, 64: 7002–10.

Stokoe D. PTEN. *Curr Biol.* 2001, 11: R502.

Surucu B., Bozulic L., Hynx D., Parcellier A., Hemmings B.A. In vivo analysis of protein kinase B (PKB)/Akt regulation in DNA-PKcsnull mice reveals a role for PKB/Akt in DNA damage response and tumorigenesis. *J Biol Chem.* 2008, 283: 30025-33.

Taniguchi C.M., Winnay J., Kondo T., Bronson R.T., Guimaraes A.R., Aleman J.O., Luo J., Stephanopoulos G., Weissleder R., Cantley L.C., Kahn C.R. The phosphoinositide 3-kinase regulatory subunit p85alpha can exert tumor suppressor properties through negative regulation of growth factor signaling. *Cancer Res.* 2010, 70: 5305–15.

Testa J.R., Bellacosa A. AKT plays a central role in tumorigenesis. *Proc Natl Acad Sci U S A.* 2001, 98: 10983-85.

Thant A.A., Nawa A., Kikkawa F., Ichigotani Y., Zhang Y., Sein T.T., Amin A.R., Hamaguchi M. Fibronectin activates matrix metalloproteinase-9 secretion via the MEK1-MAPK and the PI3K-Akt pathways in ovarian cancer cells. *Clin Exp Metastasis.* 2000, 18: 423-28.

Therese P.J., Manvar D., Kondepudi S., Battu M.B., Sriram D., Basu A., Yogeeswari P., Kaushik-Basu N. Multiple e-Pharmacophore Modeling, 3D-QSAR, and High-Throughput Virtual Screening of Hepatitis C Virus NS5B Polymerase Inhibitors. *J Chem Inform Modell.* 2014, 54: 539-52.

Thompson F.H, Nelson M.A., Trent J.M., Guan X.Y., Liu Y., Yang J.M., Emerson J., Adair L., Wymer J., Balfour C., Massey K., Weinstein R., Alberts D.S., Taetle R. Amplification of

19q13.1-q13.2 sequences in ovarian cancer. G-band, FISH, and molecular studies. *Cancer Genet Cytogenet.* 1996, 87: 55-62.

Tornillo L., Terracciano LM. An update on molecular genetics of gastrointestinal stromal tumours. J Clin Pathol. 2006, 59: 557-63.

Vermes I., Haanen C., Steffens-Nakken H., Reutellingsperger C. A novel assay for apoptosis flow cytometric detection of phosphatidylserine expression on early apoptotic cells using fluorescein labelled annexin V. *J Immunol Methods*. 1995, 184: 39-51.

Viglietto G., Motti M.L., Bruni P., Melillo R.M., D'Alessio A., Califano D., Vinci F., Chiappetta G., Tsichlis P., Bellacosa A., Fusco A., Santoro M. Cytoplasmic relocalization and inhibition of the cyclin dependent kinase inhibitor p27(Kip1) by PKB/Akt-mediated phosphorylation in breast cancer. *Nat Med.* 2002, 8: 1136-44.

Villunger A., Michalak E.M., Coultas L., Mullauer F., Bock G., Ausserlechner M.J., Adams J.M., Strasser A. p53- and drug-induced apoptotic responses mediated by BH3-only proteins puma and noxa. *Science.* 2003, 302: 1036-8.

Vivanco I., Sawyers C.L. The phosphatidylinositol 3-Kinase AKT pathway in human cancer. *Nat Rev Cancer.* 2002, 2: 489-501.

Weigelt B., Downward J. Genomic determinants of PI3K pathway inhibitor response in cancer. *Front Oncol.* 2012, 2: 109

Weng D., Song X., Xing H., Ma X., Xia X., Weng Y., Zhou J., Xu G., Meng L., Zhu T., Wang S., Ma D. Implication of the Akt2/survivin pathway as a critical target in paclitaxel treatment in humanovarian cancer cells. *Cancer Lett.* 2009, 273: 257–65.

Williams R., Baker A.F., Ihle N.T., Winkler A.R., Kirkpatrick L., Powis G. The skin and hair as surrogate tissues for measuring the target effect of inhibitors of phosphoinositide-3-kinase signaling. *Cancer Chemother Pharmacol.* 2006, 58: 444-50.

Wullschleger S., Loewith R., Hall M.N. TOR signaling in growth and metabolism. *Cell* 2006, 124: 471-84.

Wu W.I., Voegtli W.C., Sturgis H.L., Dizon F.P., Vigers G.P., Brandhuber B.J. Crystal structure of human AKT1 with an allosteric inhibitor reveals a new mode of kinase inhibition. *PLoS One*. 2010, 5: e12913.

Xing H., Weng D., Chen G., Tao W., Zhu T., Yang X., Meng L., Wang S., Lu Y., Ma D. Activation of fibronectin/PI-3K/Akt2 leads to chemoresistance to docetaxel by regulating survivin protein expression in ovarian and breast cancer cells. *Cancer Lett.* 2008, 261: 108–19.

Yap T.A., Li Yan, Patnaik A., Fearen I., Olmos D., Papadopoulos K., Baird D.R., Delgado L., Taylor A. Lupinacci L., Riisnaes R., Pope L.L., Heaton P.S, Thomas G., Garrett D.M., Sullivan D.M., de Bono J.S, Tolcher A.W. First-in-man clinical trial of the oral pan-AKT inhibitor MK-2206 in patients with advanced solid tumors. *Journal of Clinical Oncology*, 2011a, 29: 4688-95.

Yap T.A., Walton M.I., Hunter L.J., Valenti M., de Haven Brandon A., Eve P.D., Ruddle R., Heaton S.P., Henley A., Pickard L., Vijayaraghavan G., Caldwell J.J., Thompson N.T., Aherne W., Raynaud F.I., Eccles S.A., Workman P., Collins I., Garrett M.D. Preclinical pharmacology, antitumor activity, and development of pharmacodynamic markers for the novel, potent AKT inhibitor CCT128930. *Mol Cancer Ther.* 2011b, 10:360-71.

Yuan T.L., Cantley L.C. PI3K pathway alterations in cancer: variations on a theme. *Oncogene.* 2008, 27: 5497-510.

Zanella F., Rosado A., Garcia B., Carnero A., Link W. Chemical genetic analysis of FOXO nuclear-cytoplasmic shuttling by using image-based cell screening. *ChemBioChem* 2008, 9: 2229-37.

Zhao Z., Leister W.H., Robinson R.G., Barnett S.F., Defeo-Jones D., Jones R.E., Hartman G.D., Huff J.R., Huber H.E., Duggan M.E., Lindsley C.W. Discovery of 2,3,5-trisubstituted pyridine derivatives as potent Akt1 and Akt2 dual inhibitors. *Bioorg Med Chem Lett.* 2005, 15: 905-09.

Zhou B.P., Hung M.C. Novel targets of Akt, p21(Cipl/WAF1), and MDM2. *Semin Oncol.* 2002, 29: 62-70.

Zhou M., Gu L., Findley H.W., Jiang R., Woods W.G. PTEN reverses MDM2-mediated chemotherapy resistance by interacting with p53 in acute lymphoblastic leukemia cells. *Cancer Res.* 2003, 63: 6357-62.

Zimmermann S., Moelling K. Phosphorylation and regulation of Raf by Akt (protein kinase B). *Science.* 1999, 286: 1741-4.

APPENDIX

APPENDIX

LIST OF PUBLICATIONS

FROM THIS THESIS WORK

1. **Dinavahi S.S.,** Prasanna R., Viswanadha S., Sriram D., Yogeeswari D. A novel, potent, small molecule AKT inhibitor, exhibits efficacy against lung cancer cells in vitro. *Cancer Res Treat*. 2014, In print.

2. **Dinavahi S.S.,** Prasanna R., Viswanadha S., Sriram D., Yogeeswari D. Novel Akt inhibitors for cancer therapy. Indian patent application 5707/CHE/2014.

3. **Dinavahi S.S.,** Nallangi R., Alokam R., Veeraraghavan S., Viswanadha S., Sriram D., Yogeeswari D. Design, Synthesis and development of novel allosteric Akt inhibitors for lung cancer therapy. (To be communicated).

4. **Dinavahi S.S.,** Veeraraghavan S., Viswanadha S., Sriram D., Yogeeswari D. Acquired resistance to Akt inhibitors in lung cancer cell lines require amplification of cMyc and upregulation of glutamine metabolism (To be communicated).

OTHER PUBLICATIONS

1. Bolla N.R., Muthuppalaniappan M., **Dinavahi S.S.**, Viswanadha S., Bagul C., Kolupula S., Vakkalanka S.K., Atcha K.R., Kamal A. Synthesis of 1,5-Diarylpyrazoles as Potential COX-2 Inhibitors with Nitric Oxide Releasing Ability. *Lett Drug Des Discov*. 2013, 10: 594-603.

2. **Dinavahi S.S.**, Nyayapathy S., Sriram D., Yogeeswari D., Viswanadha S. Combined inhibition of PDE4 and PI3Kδ modulates the inflammatory component involved in the progression of Chronic Obstructive Pulmonary Disease. *Drug Res* 2014, 64: 214-9.

3. Pulla V.K., Alvala M., **Dinavahi S.S.**, Viswanadha S., Sriram D., Yogeeswari P. Structure-based drug design of small molecule SIRT1 modulators to treat cancer and metabolic disorders. *J Mol Graphics and Modell*. 2014;52:46-56.

4. Pulla V.K., **Dinavahi S.S.**, Viswanadha S., Sriram D., Yogeeswari P.. Targeting NAD production involved in SIRT-1 pathway for therapeutic intervention of cancer and inflammation: Structure-based drug design and biological screening. (In communication).

PAPERS PRESENTED AT NATIONAL/ INTERNATIONAL CONFERENCES

1. **Dinavahi S.S.,** Prasanna R., Viswanadha S., Sriram D., Yogeeswari P. BIA-6: A novel Akt inhibitor with potent activity in lung cancer**. 14th World Conference on Lung Cancer,** Sydney 27-30th Oct, 2013.

2. **Dinavahi S.S.,** Prasanna R., Viswanadha S., Sriram D., Yogeeswari P. Discovery of novel Akt inhibitors for cancer**. 5th International Conference on Stem Cells and Cancer,** Mumbai 19-21st Oct, 2013.

3. **Dinavahi S.S.,** Nyayapathy S., Viswanadha S., Sriram D., Yogeeswari P.. Combined inhibition of PDE4 and PI3Kδ inhibitors in COPD. **44th Indian Pharmacological Society,** Manipal 19-21st Dec, 2011.

4. Bhavar P.K., Yadav M.R., **Dinavahi S.S.**, Nyayapathy S. A novel, small molecule inhibitor, MSU-1001, in androgen-sensitive prostate cancer cell lines. **6th Asian Oncology Summit and 10th Annual Conference of the Organisation for Oncology and Translational Research**, Kuala Lampur 11-13th Apr, 2014.

BIOGRAPHY OF VENKATA SAKETH SRIRAM D

Venkata Saketh Sriram D completed his Bachelor of Pharmacy from University college of Pharmaceutical Sciences (UCPSc); Kakatiya University in the year 2009 and M. Pharmacy from Birla Institute of Technology and Science-Pilani, Hyderabad campus in the year 2011. He has been appointed as a PhD student in the department of pharmacy, for a collaborative research project between BITS-Pilani, Hyderabad campus and Incozen Therapeutics Pvt. Ltd., Hyderabad from 2012-2014 under the supervision of Prof. P. Yogeeswari. He has four scientific publications in well-renowned international journals and an Indian patent. He had presented papers at various national and international conferences.

<u>BIOGRAPHY OF PROF. P. YOGEESWARI</u>

Prof. P. Yogeeswari is presently working in the capacity of Professor and Associate Dean (Sponsored Research and Consultancy Division), Department of Pharmacy, Birla Institute of Technology and Science, Pilani, Hyderabad Campus. She received he Ph.D. degree in the year 2001 from Banaras Hindu University; Varanasi. She has been involved in research for the last 14 years and in teaching for 13 years. APTI honoured her with YOUNG PHARMACY TEACHER AWARD for the year 2007. In 2010, ICMR honoured her by awarding "Shakuntala Amir Chand Award" for her excellent biomedical research. She has also been granted IASP 2014 award for "Excellence in Pain Research and Management in Developing Countries" under the basic science research category received at the "15th World Congress on Pain" at Argentina in October 2014. She has collaborations with various national and international organizations that include National Institute of Mental Health and Neurosciences, Bangalore, Karolinska Institute, Stockholm, Sweden, National Institute of Immunology, New Delhi, India, Pastuer Institute, University of Lille, France, Bogomoletz Institute of Physiology National Academy of Science, Ukraine and Faculty of Medicine of Porto, Portugal,. She has to her credit more than 200 research publications and three Indian Patents. She is an expert reviewer of many international journals like Journal of Medicinal Chemistry (ACS), Journal of Chemical Information & Modelling (ACS, USA), Bioorganic Medicinal Chemistry (Elsevier), Recent Patents on CNS Drug Discovery (Bentham), etc. She has also co-authored a textbook on organic medicinal chemistry with Prof. D. Sriram titled "Medicinal Chemistry" published by Pearson Education and one book chapter in Jan 2013 by IGI Global. She is a life time member of Association of Pharmacy Teachers of India and Indian Pharmaceutical Society. She has successively completed many sponsored projects and currently on projects sponsored by DST, DBT, INDO-BRAZIL, ICMR-INSERM, and CSIR. She has guided seven PhD students and currently thirteen students are pursuing their PhD work.

<u>BIOGRAPHY OF Dr. SRIKANT VISWANADHA</u>

Dr. Srikant Viswanadha is presently working as Vice president, Drug Discovery, Incozen Therapeutics Pvt. Ltd. Hyderabad. He received his Ph.D. degree in nutritional biochemistry in the year 2003 from Virginia Polytechnic Institute and State Univerity; Blacksburg, VA, USA. He has a post-doctoral training in National Institute of Diabetes, Digestive, and Kidney Diseases (NIDDK), National Institutes of Health (NIH), USA. He received a NIDDK travel award in 2006 for 'Research Excellence' and John Lee Pratt Fellowship in 2000 at Virginia Tech. He has been involved in research for the last 12 years. He has 10 research papers, 1 book chapter, 11 international poster presentations and 6 international patents to his credit.